Shallow landslides triggered by rainfall: integration between ground-based weather radar and slope stability models in near-real time.

Università degli Studi di Firenze

Facoltà di Scienze Matematiche, Fisiche e Naturali
2008

Lorenzo Leoni

Tutor: Filippo Catani

Dottorato di ricerca in Scienze Geologiche
XXI ciclo
Settore disciplinare GEO 05

Contents

List of Figures

List of Tables

Chapter 1

Introduction and objectives

1.1 Introduction

Although the term "shallow landslides" is not included in landslide classification (Cruden & Varnes, 1996; Varnes, 1978) it is widely used in literature to describe slope movements of limited size that mainly develop in soils up to 5m in depth. Typical slope movements that can be described as shallow landslides are soil slips, soil slumps and debris flows.

Even though the size of these landslides is usually quite limited, they are very dangerous for people and buildings because of many intrinsic features. First of all they are very frequent in time and space in areas prone to this kind of phenomena. Moreover the triggering usually occurs without any significant premonitory signals. Shallow landslides are a huge hazard for the community even because they can evolve into debris flows, landslide characterized by a high velocity and the capability to be channelized and to increase their volume during the run out.

Many researches have shown that the main triggering factor for shallow slope failure is the infiltration of water after heavy rainfalls (Campbell, 1975; Pierson, 1980; Rulon & Freeze, 1985; Buchanan & Savigny, 1990; Johnson & Sitar, 1990; Reid, 1994; Crozier & Glade, 1999; Iverson, 2000). In fact when the water starts to infiltrate in the soil the pore-water pressure increases so as the shear strength of the soil is reduced leading to slope failure. For this work only landslide triggered by rainfall have been studied, excluding all the other minor triggering factors like earthquakes, rapid snow melt etc. It is important to distinguish between saturated and unsaturated soils because they have different behaviour with respect to the shear strength. In saturated soils, according to the principles of effective stress, when infiltration occurs shear strength reduces with the increasing pore pressures. In unsaturated soils instead it is necessary to take into account the additional strength given by the matric suction (Fredlund & Rahardjo, 1993).

There are many factors that control the hydrological response of a slope and its stability. These factors can be divided in two major groups (Wu & Sidle, 1995): the almost-static variables and the dynamic variables. The almost static variables are those that show very small or not visible variations in short temporal scale. In this group we can include all the soil properties (mechanical

properties, depth, permeability) and the topographic features (elevation, slope, curvature). The static variables are very important to define the probability of occurrence of landslides in each areas and to define the susceptibility of the slopes to failure. The dynamic variables are instead those that can change very quickly in time and that control the triggering of failures along the slopes, like the amount of rainwater infiltration and the degree of saturation.

In this work we use ground-based weather data as an input for the dynamic variables and data collected during field work for the almost-static ones. The rainfall maps obtained from ground-based weather radars are used to evaluate the degree of saturation and, coupled with the mechanical characteristic of the soil, to evaluate the distributed slope stability.

The research described here is partly the result of the work carried out within the PREVIEW (PREVention, Information and Early Warning, pre-operational services to support the management of risks) project, an initiative approved within the EU Sixth Framework Programme (FP6) with the aim of developing innovative geo-information prototype services for atmospheric, geophysical and man-made risks to be applied at a European scale. The Landslides Platform is part of the Geophysical Cluster and comprises two prototype services: Monitoring of deep-seated, slow-moving landslides (Service 1) and; Prediction of shallow rapid slope movements (Service 2). This work focuses on the results achieved within the development of Service 2.

1.2 Abstract

This PhD thesis treats the problem of rainfall-triggered landslides modeling and landslides hazard assessment. During this study I have tried to integrate innovative methodologies like weather radar measurements with physically based models to build up a system able to alert and eventually forecast the occurrence of shallow landslides when triggered by heavy rains.

Two test sites have been chosen, the Armea basin and the Island of Ischia, characterized by different lithological and geomorphological features but both definitely prone to the development of shallow landslides. During the fieldwork in these areas many data have been collected to build a data set of geotechnical and geomorphological properties to be used as input for the slope stability models. Following the landslides occurrence in December 2006 in the Armea basin, a multispectral, Quickbird satellite imagery was acquired. With the aid of this new satellite imagery it was possible to recognise all the landslides triggered by the event and to build up a database in order to be used for the validation of the slope stability models.

The meteorological data needed as an input for the slope stability models, recorded by ground-based weather radars, have been provided by the CIMA (Centro di ricerca Interuniversitario in Monitoraggio Ambientale, University of Genova) for the Armea basin and by the Italian Air Force for the Island of Ischia.

To evaluate the slope stability within the test areas two different models are proposed: the first uses as an input the soil moisture maps calculated with an independent hydrologic model (C-DRIFT) and than applies, pixel by pixel, the infinite slope stability model to obtain a distributed map of the factor of safety. The second model developed is based on the Iverson (2000) method for

landslides triggered by rain infiltration but with some modifications and adds-on needed to make it more proficient evaluating slope stability. These modifications include the capabilities to take into account the effect of suction in unsaturated soils and an algorithm that makes it possible for the model to be used in near-real time. Moreover this model is designed to evaluate the factor of safety at different depths and to record the lowest value in the final output file.

To use these physically based models with spatially distributed input data two command line softwares have been developed. These softwares have been then tested with rainfall data regarding past events actually occurred in order to provide a validation for both the test sites. The results are quite good but the modified Iverson model achieves better performance, with both low false positive and low false negative percentage.

Since the meteorological data needed by these models are elaborated in different research structures, a network is needed to move the data from the server where they are produced and stored to the server where the slope stability models are installed. The results of the computation, that is a set of maps of the factor of safety, need then to be moved to another server to be published on the web using a Web-GIS interface. This result has been achieved using system scripts and synchronization tools running on the central node of the network represented by the server of the Department of Earth Sciences in Florence.

Since the aim of this study was to build a warning system that should work in near-real time, all the chain, starting from the radar measurement of the rainfall until the computation of the factor of safety, has been projected to run automatically, using the capabilities of the Linux servers to work with scripts and with scheduled events. The near-real time factor of safety computation is already active for the Armea basin and the result can be viewed and downloaded through a Web-GIS interfaces. The automatic network would be active even for the Island of Ischia if it were available the real time radar data.

1.3 Objectives

The final objective of this PhD thesis was to develop an integrated procedure for the forecasting and warning of shallow landslides at basin scale to be used for civil protection purposes. The study should blend advanced techniques and tools from different fields including meteorology, hydrology, geological and geotechnical modelling, remote sensing and GIS.

One by one, the main objectives to be reached in order to build the warning system are:

- Chose almost two test sites where the warning system could be applied and tested.
- Within these areas, collect data regarding soil properties, geomorphological characteristics and topographic features of the area. Even data regarding past landslides events need to be collected to be used for the validation of the stability model in the case that any new occurrence was lacking during the development of this thesis.
- Collect radar rainfall data for the test sites. This data should be available for both the real time computations of the model and for the validation phase using past occurrences.

- Elaborate a slope stability model that should be used to assess the occurrence of shallow landslides triggered by rainfall. This model should take into account the different spatial distributions of rainfall intensity and for the slope normal redistribution of groundwater associated with transient infiltration of rain. This model should even take into account the different behaviour between saturated and unsaturated soils.

- Since this model should work for wide areas and calculate the factor of safety for each discrete landscape cells it is necessary to develop a software to run the model quickly and efficiently.

- The final results of the model should be easily and immediately available by local authorities that should be able to take decisions on the basis of these results.

- Make the hole process almost automatic, from the capture of the radar data to the transmission and the communication of the results.

1.4 Methodologies and innovations

The main objectives of this study have been reached thanks to a close interaction between many different fields including meteorology, hydrology, geological and geotechnical modelling, remote sensing and GIS. The most advanced techniques from all these research fields have been coupled together to build the shallow landslides warning system.

Thanks to the collaboration with CIMA, it has been possible to access advanced meteorological data recorded in near-real time by the ground based weather radar of Monte Settepani, near Savona. The use of real time radar data within a slope stability model can be considered as a great innovation since the majority of the warning systems uses values coming from rain gauges and rainfall thresholds to issue an alert. The system developed during this study uses instead distributed maps of rainfall intensity and is therefore able to take into account the spatial variability of a rainstorm and thus to better infer the effects of this variability on the distributed slope stability.

Another goal of this work is represented by the software developed for the computation of the factor of safety using a modified version of the Iverson (2000) model. The major improvement to the original model is the introduction of the effect of suction on the soil strength in order to consider the different behaviour between saturated and unsaturated soil. The other improvement is the algorithm that represents the core of the software. This algorithm has been designed to apply the modified Iverson model in near-real time instead of after the occurrence of landslides. All the other slope stability software already existing in literature, like TRIGRS (Baum et al., 2002), SEEP/W (Krahn, 2004), SHALSTAB (Dietrich & Montgomery, 1998) or GEO-topFS (Simoni et al., 2008), can only be used after the occurrence of the events, when the history of the rainfall pattern in space and time is already available. In that case these softwares can be very useful for back analysis and for many other scientific reasons but cannot be used within an automatic forecasting chain. The software developed during this study is instead designed to run every time step or every time it receives, in near-real time, the present or forecasted rainfall conditions. After the first

run it remembers the previous soil conditions and updates them during the next run as soon as a new rainfall intensity map is available.

The entire work takes many advantages of the use of computer science and open source software (i.e. Mapserver Web-GIS and many synchronization tools), especially for the building of the automatic network needed to obtain radar rainfall data, transmit them from server to server, compute the factor of safety and publish the results on the Web-GIS platform.

1.5 Thesis Organization

The structure of the thesis is as follows:

- **Chapters 2** provide a description of the background about landslide classification and landslides triggering factors. Here the data needed for landslides modeling and the different approaches to landslide hazard assessment are described as well.
- **Chapter 3** includes general knowledge about the triggering mechanisms for shallow landslides and a summary of the most important slope stability models already existing with particular attention for the Iverson's model.
- **Chapter 4** briefly outlines general knowledge about radar meteorology and weather data used for this thesis.
- **Chapter 5** contains a description of both the test sites (Armea basin and Island of Ischia) where the models developed during this study have been tested, the description of the major recent landslides occurred and outlines the field work conducted in both the areas.
- **Chapter 6** provide a description of the models proposed for shallow landslide stability assessment and a description of the softwares developed for the real time computation of the factor of safety using the weather radar data.
- **Chapter 7** is intended to focus on the input data used for the two models briefly describing both the stationary and the dynamic data.
- **Chapter 8** describes the warning system that has been built up, how the model and the system can work in near-real time and the publication of the results on a Web-GIS platform.
- **Chapter 9** presents practical applications and the result of the developed models on both the test areas. The two model have been validated using two past landslide event occurred in April 2006 and in December 2006.
- **Chapter 10** draws conclusions and contains a summary of the contributions of the work.
- **Appendix A** contains the C++ source code of the infinite slope stability model.
- **Appendix B** contains the C++ source code of the modified Iverson's model.

1.6 Original contributions

The original contributions of this PhD thesis are included in chapters 5, 6, 8, 9 and can be summarized as follows:

- **Chapter 5:** field work data collection in both the test site, photointerpretation of the satellite image in a GIS environment and building of the new landslide inventory for the 2006 rainfall event in the Armea basin.
- **Chapter 6:** development of the two slope stability model and the C++ computer codes in order to apply the models automatically for large areas. The first model is a standard version of the infinite slope solution while the second one (Section 6.1.2) include original solution for transient rainfall infiltration (modified from the original Iverson model) and for the slope stability computation which takes into account the effect of soil suction.
- **Chapter 8:** planning and building of the automatic warning system. This task includes the building of the automatic chain for the synchronization of different servers, the computation of the factor of safety with the two developed softwares and the publication of the results on the Web-GIS platform.
- **Chapter 9:** simulation of the near-real time functionality of the warning system using meteorological data regarding past event that have recently triggered landslides in both the test sites. Validation of the results using the data collected during the field work and the original landslide inventory map.

Chapters 2, 3, and 4 are a summary of the knowledges needed to perform this study and a state of the art of slope stability models

Chapter 2

General knowledge and definitions

2.1 Definition and classification of landslides

Landslides with floods, earthquakes and volcanoe eruptions are phenomena known as "natural disasters". Even though the cost in term of casualties and damages to infrastructures can be very high for earthquakes or floods, overall costs related to landslides can be even higher. That is because landslides are characterized by a high temporal frequency and spatial diffusion so as in the long term the amount of damage due to landslides occurrence overtake that due to other natural disasters (Guzzetti, 2000).

A landslide is a soil or rock mass moving under the force of gravity along a slope and with a downward direction of propagation (Cruden, 1991). This definition includes both mass movements along natural slopes and artificial slopes or dumps and even deep creep movements in rock slopes.

Landslide classification is quite difficult because the phenomena are not perfectly repeatable so it is not possible to develop a taxonomic classification. Landslides are thus usually characterized by different morphology, type of movements, triggering factors and involve genetically different material. For this reason, landslide classifications are based on different discriminating factors, like type of movement or type of involved material.

2.1.1 Landslides classification

The most widely used classification of slope movement was proposed by Varnes in 1958 and than modified by the same author in 1978 (table 2.1). This classification is based mainly on the type of movement but takes into account even the type of material involved. There are five basic considered type of movements: falls, topples, slides (rotational and translational), lateral spreads and flows. A sixth type, the complex movement, is defined as a combination of two or more basic types of movement. The involved material is divided in two classes: rocks and soils. The latter are subdivided in other two classes: predominantly fine soils and predominantly coarse soils (Varnes, 1978).

As already said in the introduction, the main subject of this thesis are the

Type of movement		Type of material		
		Bedrock	Soils	
			Predominantly fine	Predominantly coarse
Falls		Rock fall	Earth fall	Debris fall
Topples		Rock topple	Earth topple	Debris topple
Slides	Rotational	Rock slump	Earth slump	Debris slump
	Traslational	Rock slide	Earth slide	Debris slide
Lateral spreads		Rock spread	Earth spread	Debris spread
Flows		Rock flow	Earth flow	Debris flow
Complex		Combination in time or space of two or more principal types of movement		

Table 2.1: Landslides classification of Varnes

shallow landslides. According to the classification of Varnes, the landslide types that in presence of soil depth less than a few meters can be ascribed to the shallow landslides group are slides, flows and complex landslides.

2.1.2 Slides

A slide is characterized by a sliding movement along one or more planes. There are two types of slides: rotational slides and traslational slides. The rotational slides develop along a curved surface of sliding and are typical in homogeneous materials. The traslational slides occur instead along planar or slightly wavy plans. Usually this plan is controlled by structural or stratigraphic discontinuities like the boundary between bedrock and soil.

Translational slides in shallow soils are usually called soil-slips (Campbell, 1975; Moser & Hohensinn, 1983; Ellen, 1988; Crosta & Frattini, 2002).

2.1.3 Flows

A flow can be described as a "spatially continuous movement in which surfaces of shear are short-lived, closely spaced, and usually not preserved" (Cruden & Varnes, 1996). The distribution of velocities within the moving mass is similar to that in a viscous liquid. This type of propagation cause a huge amount of deformation within the entire sliding mass. This feature differentiates flows from the other types of landslides like slides where usually the landslide body moves rigidly along a slip surface.

The term "debris flow" has been used as general term to describe a rapid mass movement, gravity controlled of a mixture of granular solids, water and air (Costa, 1984). Following Costa (1984) the term debris flow can be broadly interpreted as a general term, to include many other types of flow like mudflows, wet grain flows, lahars, tillflows, wet rock avalanches, debris avalanches and debris torrents. Debris flows may include a wide range of sediment size, from boulders to clay, and their mechanical characteristics may vary significantly with differences in water and clay content and sediment size and sorting.

It is then important to distinguish between flows that involve different types

of materials. That is because the involved material deeply affect the morphology and the velocity of the displacing mass.

In this work we have adopted the classification of flows proposed by Hungr et al. (2001) that takes into account the type of involved material and the degree of saturation. They distinguish between five main class:

- *Earth flows* are from slow to rapid or intermittent movement of plastic clayey earth (Hungr et al., 2001). They usually have a tongue-shaped mass with a hummocky surface and lobed ends. They develop where water-rich unconsolidated material moves by slumping and plastic flow.

- *Debris flows* are "very rapid to extremely rapid flows of saturated non-plastic debris in a steep channel" (Hungr et al., 2001). The plasticity index is lower than 5. The granulometry of the sliding mass can be from sandy to gravely. One of the key features of debris flows is that they develop within a channel or in a regular confined path. These channels can be a first or second order drainage channel but even an established gully. The presence of these confined channels is very important because they control the direction of flows and deeply affect the type of movement and morphology of the flows. The presence of water in the channels can lead to an increase of water content in the sliding mass thus affecting the type of movement. The lateral confinement typical of channelized slides can even affect the depth of the body, the vertical velocity gradient and thus the vertical and longitudinal sorting of the material.

- *Mud flows* are "very rapid to extremely rapid flows of saturated plastic debris in a channel, involving significantly greater water content relative to the source material" (Hungr et al., 2001). The plasticity index is higher than 5. The main difference between a mud flow and a debris flow is the presence of the clay rich plastic component in mud flows. This clay can lead to longer runout due to the delay in dilution by water and drainage (Scott et al., 1992).

- *Debris floods* are "very rapid, surging flows of water, heavily charged with debris in a steep channel" (Hungr et al., 2001). These flows, even called "hyperconcentrated flows", can be told apart from a debris flow for the amount of solid concentration. As suggested by Costa (1984), when a flow exceed the threshold of 80 percent of solid concentration it can be classified as a debris flow. For the same reason, in a single debris flow, a part can be diluted downstream and assume the character of a debris flood.

- *Debris avalanches* are "very rapid to extremely rapid shallow flows of partially or fully saturated debris on a steep slope, without confinement in an established chanel" (Hungr et al., 2001).

2.1.4 Complex landslides

A complex landslide is defined as a combination of two or more basic types of movements (falls, topples, slides, spreads and flows) (Varnes, 1978). Many large landslides are complex, although one type of movement dominates over

the other types in certain areas of a slide or at a particular time. One of the most important cases for the study of shallow landslides is the soil slip-debris flows complex landslide. This slope movement starts as a traslational slide and evolve in a flow due to the increase in saturation (Campbell, 1975).

2.2 Debris flow and "shallow landslides"

One of the main targets of this thesis is the study of the triggering of shallow landslides due to heavy rainfall. As already said, a shallow landslide can be described as a slope movement of limited size that mainly develops in soils up to a maximum of a few meters. One of the most dangerous landslides that can be described as a shallow landslides are debris flows. The danger of these phenomena can be related to the high velocity that they can reach during the runout and even with the nearly totally absence of premonitory signals. Moreover debris flows from different sources can combine in channels, and their destructive power may be greatly increased. The triggering of debris flow, usually related with heavy rainfall, happens suddenly and during the runout they can reach velocities up to 20 m/s (Hungr et al., 2001). Due to this high velocities they acquire very high kinetic energy thus becoming dangerous for buildings and infrastructures.

The development of shallow landslides and debris flows can be divided in two stages: the triggering and the propagation of the mass along the slope.

2.2.1 Triggering

Debris flows usually develop on steep terrain and in areas with no woodland or with brushes and small trees. The triggering usually occurs in the upper part of the slope, often in correspondence of an abrupt change in slope angle or along the edge of a natural or artificial escarpment.

There are many factors that can lead to the triggering of a debris flow. First of all a change in the interstitial water pressure system due to rainfall. As the soil gradually saturates, pore-water pressures increase and shear strengths decrease (Sidle & Swanston, 1982). They can even be triggered during intense rainfall by the loss of the component of apparent cohesion (Fredlund, 1987). Other causes can be a variation to the external force system due to an earthquake or to natural erosion or to anthropic activity. In this work, only landslides triggered by rainfall will be studied.

The factors that deeply affect the triggering of a shallow landslide can be divided in three main groups:

- Lithology and geology: soil properties like cohesion, internal friction angle and soil unit weight can affect the slope stability because they directly influence the mechanical failure strength. Permeability is then one of the major factors that control the hydraulic circulation both in surface and underground. The time needed to completely saturate a soil is strictly related to the permeability thus affecting the probability of reaching the critical pore pressure (Iverson & LaHusen, 1989; Iverson et al., 1997; Iverson, 1997; Iverson et al., 2000; Takahashi, 1981). Also the stratigraphy of

a terrain is very important because the presence of one or more impermeable layers can cause a rapid saturation of the upper layers so as to reach the critical pore pressure and trigger the landslide.

- Morphology and topography: morphological features like the slope gradient deeply affect the stability of a slope (Pierson, 1980; Renau & Dietrich, 1997; Montgomery & Dietrich, 1994). A particular topography can control the superficial and graundwater flow concentration.

- Hydrology: the initial moisture condition of a soil can affect the slope stability. Hydrological factors that can lead to the triggering of a shallow landslide are the rise of the water table, variations in groundwater seepage or change in flow direction from recharge to discharge areas (Zêzere et al., 1999; Tsai & Yang, 2006; Tsai, 2008).

2.2.2 Propagation and effect

The behaviour of a flow after the triggering phase and during the propagation along a slope has been analysed by many authors using in situ analysis, laboratory models and simulations (Costa, 1984; Hungr, 1996; Iverson, 1997; Johnson & Rodine, 1984; Takahashi, 1978, 1981).

The first phase of the propagation is characterized by high energy and erosion power. During this phase the thickness of the frontal part of the flow starts to rise due to the eroded material that is included in the sliding mass. Subsequently the volume remains more or less constant along the erosion channel created by the passage of the landslide.

The frontal part of the debris flow is generally characterized by a high concentration of big clasts and gravel while in the middle part materials became finer and the tail of the flow is characterized by the finest granulometries (Takahashi, 1981). The presence of the coarsest clasts in the frontal part of the flow is the main reason, in conjunction with the high velocity reached, of the great destructive power of this type of landslide.

The stopping phase of a flow generally occurs when the slope angle becames lower than 3°. Usually this decrease in slope angle is reached together with an abrupt increase of the available transversal section (Takahashi, 1981). During this phase the frontal coarse part of the flow slows down until stopping and it is overlayed by the materials from the main body so that the thickness of the flow increases. The diluted material from the tail of the flow usually bypasses the main body opening an erosion channel within the deposition area.

2.3 Data needed for landslide modeling

Many kinds of data are needed for landslide modeling and risk assessment. Some methods are based on the study of past landslide events to infer a relation between the event and the factors that control the triggering and the evolution of the landslide. This relation, that can be reduced to a deterministic or statistic equation, can be used to forecast the future distribution of landslides on the basis of the present conditions and the behaviour of the controlling factors. So for models that use past events to calibrate a threshold or to infer an equation is very important to have a deep and updated knowledge of historical landslides

occurred in the studied area. This record of landsliding, if including the time and date of occurrence, can be very useful even for the validation of the results of physically-based models.

For methods based on a physical simulation of the landslides, the most important kind of data are those related with the topographic and physical properties of the terrains. These models, even known as physically-based models, use topographic and geotechnical properties to simulate the infiltration of water within the soil and to compute the slope stability using a geometrically simplified representation of the slope. Obviously, for distributed models all the input data need to be distributed, that is for each cell or pixel where the slope stability is computed the value of each input dataset is needed (cell by cell computation).

2.3.1 Topographic data

The gravity force is the main reason that makes a slope instable and deeply affect the final computation of the slope stability. The most important topographic data is thus the slope angle, the angle between the horizontal plane and the slope itself. To obtain a distributed map of the slope angle, a digital elevation model (DEM) is needed.

A digital elevation model or digital terrain model (DTM) is a topographic surface arranged in a data file as a set of regularly spaced x, y, z coordinates where z represents elevation. The distributed slope angle can be derived from the DEM with the aid of a software or a GIS tool. These tools are build on different algorithms but all calculate the rate of maximum change in z-value from each cell to its neighbors. The maximum change in elevation over the distance between each cell and its neighbors identifies the steepest downhill descent. Other minor DEM-derived topographic features that could play a role in slope stability are the orientation of the slope, its length and curvature.

2.3.2 Geological and geotechnical data

For physically-based slope stability models the parameters related with the physical behaviour of a soil have obviously a key role. In particular geotechnical data like coeshion, internal friction angle and soil unit weight deeply affect the stability balance between shear strength and destabilizing forces. It is very important to have a robust dataset of geotechnical data to describe as best as possible the spatial variations of soil properties. These variations in fact take place quite abruptly and it is nearly impossible to have a hold on them in detail. For distributed models, it is quite usual to extend a value of a certain soil property to an entire area that is expected to have similar features (Iverson, 2000; Wu & Sidle, 1995; Baum et al., 2005; Salciarini et al., 2006; Crosta & Frattini, 2003). For example, if a detailed geologic map is available, it is possible to assign an average value of a certain soil property to each cell included in the same geologic or lithologic formation.

2.3.3 Rainfall data

A slope can become unstable when the water table rises due to rainfall infiltration since pore-water pressure increases and shear strength decreases. The total amount and intensity of rainfall is thus very important because it is the

main triggering factor for shallow landslide. All the other data like slope and cohesion contribute to the define the spatial distribution of shallow landslides because they can define how easily a slope can become unstable thus resulting very useful for shallow landslides susceptibility assessment. Rainfall data are instead the fundamental input that make possible for the system to overcome the threshold and trigger a new slope movement.

When computing the slope stability for a large area or basin it is very important to have an accurate distributed representation of the rainfall intensity. A storm is often characterized by a high spatial and temporal variability so that it is quite difficult to obtain an good quality representation of the rainfall event. One of the more proficient tools to obtain a distributed map of rainfall are satellite and radar detected data. With the aid of this tools it is possible to greatly improve a simulation and to explain the usual non-uniform distribution of landslides (Crosta & Frattini, 2003). This argument will be deeply treated in chapter 4.

2.4 Hazard evaluation and assessment

Landslide hazard for a given area is defined as the probability of occurrence of a destructive event characterized by a certain intensity and during a defined time period (Varnes, 1984).

For the hazard evaluation it is very important to distinguish between predisposing factors, that are the features of a slope that make it prone to instability, and those factors that can lead to the triggering. In the group of the predisposing factors are enclosed all the geological, structural, geomorphological and hydrological features like the soil properties, the slope angle, the soil depth and the potential presence of faults. This group of features represent the quasi-static variables of the slope stability balance (Wu & Sidle, 1995) because they don't show significant changes in time. The predisposing factors have a deep influence in the spatial distribution of landslides and in susceptibility evaluation.

The triggering factors are instead those which modify the natural equilibrium and change dynamically with time leading to the triggering of a landslide. In the category of these dynamic variables it is possible to include rainfall events, earthquakes and volcano eruptions. The dynamic variables are of great importance for the temporal forecasting of landslides. The analysis of the predisposing factors is thus useful for the spatial forecast of hazard and landslides susceptibility while the triggering factors are useful also for the temporal forecast.

2.4.1 Spatial prediction

The spatial forecast of hazard is the estimation of the relative stability of a particular slope by comparison with another one. It represent the spatial probability of occurrence of a landslide in different zone of a fixed area or basin.

It is possible to distinguish between two main approaches for spatial prediction of landslide hazard:

- A qualitative approach that provides a descriptive and qualitative evaluation of the hazard.

- A quantitative approach that provides a numerical estimate (in terms of probability of occurrence or factor of safety) of the spatial hazard.

In the first group are enclosed the methods based on an empirical evaluation of susceptibility to instability on the basis of geomorphological evidences, like those proposed by Kienholz (1978),Brundsen et al. (1975) or Humbert (1977). Other quantitative approaches to hazard evaluation are those that attribute a weight to each factor responsible for slope instability and organize them within a ranking to obtain an index of landslide susceptibility. This ranking of factor can be subjective if the weights are decided a priori (Gee, 1992; Anbalagan & Singh, 1996; Pareschi et al., 2002) or objective if it is possible to quantify the relative importance of each factor (Brabb, 1984; Lee et al., 2002). Others proposed method for landslide susceptibility assessment are based on bivariate or multivariate statistical analysis (Yin & Yan, 1988; Bonham-Carter et al., 1989; Baeza & Corominas, 2001), on stochastic hydrological simulations (Hammond et al., 1992) or on neural network analysis(Lee et al., 2003, 2004; Ermini et al., 2005) in order to obtain the probability of failure of a slope.

A quantitative approach is that used by physically based models. These models can achieve a probabilistic output (probability of failure) or a deterministic result (factor of safety) and use physical laws to describe the triggering and propagation of landslides (Crosta & Frattini, 2003; Dhakal & Sidle, 2004; Dietrich et al., 1995; Wu & Sidle, 1995; Iverson, 2000). The main benefit of using physically based models is that they can take into account the dynamic variables of the system and control the long-time and short-time behaviour. But to reach these results they need as input data a detailed characterization of the soil and this is not always possible to achieve, especially when data are scanty or not representative of the whole area.

2.4.2 Temporal prediction

Temporal forecast should give the probability of occurrence of landslides in terms of an absolute value of hazard (H) that could be expressed as

$$H(N) = 1 - (1 - P)^N \tag{2.1}$$

where P is the probability of occurrence of an event during a time period of N years.

Typical approach to temporal forecast of landslide hazard are (Canuti & Casagli, 1996):

- Analysis of temporal series related to the effect of landslides to obtain directly the return periods.
- Analysis of temporal series related to the causes of landslides. With this approach the return periods are calculated using the temporal series of natural hazard like rainfall and earthquake that are recognized as the triggering factors.
- Use of in situ or remote monitoring systems.

The first approach is useful for the study of singular recurrent phenomena or for limited areas where landslide occurrence is quite uniform and homogeneous.

Unfortunately this approach requires to be applied to a quite long and statistically significant temporal series of landslides. That is why it is not useful for large areas where it is quite difficult to obtain an homogeneous and highly populated landslide database.

For large areas it is better to use the temporal series of the causes of landslides. In this case it is necessary to collect and analyze historical data related to the triggering factors like rainfalls, earthquake, erosion and anthropic activity. The most important factor, especially for shallow landslides, are rainfalls while earthquakes must be taken into account only in seismic areas . Erosion could be important along riverbanks and escarpments. The anthropic activity is instead not related with hazard forecast but with prevention and must be taken into account during urban planning and risk assessment.

Chapter 3

Slope stability models

To simulate or eventually forecast the triggering of landslides due to heavy rainfall it is necessary to take into account at least three fundamental processes (Crozier & Glade, 1999):

- The spatial and temporal rainfall intensity pattern. It is important to have an high quality registration (and eventually forecast) of the rainfall event; how the rainfall intensity has changed moving from a zone to another one and how the intensity has changed during time from one moment to another. One of the most useful techniques to obtain a high quality registration of rainfall is the use of ground-based weather radars. This argument will be discussed in chapter 4.

- The rainfall infiltration in the soil and the variations in the groundwater pressure distribution. The interaction between the soil and the hydrologic processes at a given depth is very important because it controls which part of the slope is most prone to landsliding.

- The mechanical balance between destabilizing forces and shear strength of the soil. Changes in groundwater pressures and in soil wetness changes the strengths and stresses of the soil. When the destabilizing forces became larger than the strength the soil became unstable.

In literature many physically based models for spatially distributed assessment of shallow landslide hazard have been proposed in the last years (Montgomery & Dietrich, 1994; Hsu, 1994; Wu & Sidle, 1995; Borga et al., 1998; Burton & Bathurst, 1998; Cho & Lee, 2001; Baum et al., 2002; Casadei et al., 2003; Crosta & Frattini, 2003; Montrasio & Valentino, 2003; Frattini et al., 2004; Tsai et al., 2007; Simoni et al., 2008). Usually these models are based on the coupling of an hydrological model and a slope stability model like, for instance, the infinite slope model.

The applicability of these models hinges on many factors. First of all the knowledge of the area to be studied and the presence of data regarding the soil properties and topography. If a detailed characterization of the soil is available or if it is possible to derive it in some way, is than possible to evaluate the distributed stability of the area. Once a rainfall occurs the hydrological part of the model computes the groundwater pressure distribution. These pressures are

than used in the slope stability model to obtain a probabilistic output (probability of failure) (Simoni et al., 2008; Schmidt et al., 2008) or a deterministic result (factor of safety) (Iverson, 2000; Crosta & Frattini, 2003).

3.1 Instability and development of shallow landslides

A soil mass can became unstable and eventually evolve in a flow mainly in two ways: for a Coulomb-type failure within the soil or bedrock along a steep slope, or for liquefaction of the soil mass due to the high interstitial water pressures (Iverson et al., 1997). These behaviours can occur independently but in many cases they appear to operate simultaneously and synergistically. Physically based models build as the coupling of an hydrological model and a slope stability model can take into account both this conditions and infer how a variation in the water pressure distribution can affect the passage between Coulomb failure and liquefaction.

To understand where and when a shallow landslide could be triggered it is necessary not only to have a sufficiently deep knowledge of the area in terms of morphology and soil properties, but even to know the physical and mechanical processes that can lead a slope to instability. All the proposed models are based on physical laws and on some rational approximations to develop a theoretical model that should represent the geomechanical changes that occur in the slope during infiltration.

3.1.1 Failure criterion, effective tension and interstitial water pressures

To provide a framework for assessing shallow landslide triggering it is necessary to introduce here some principles of soil mechanics and grain-flow mechanics. First of all the Coulomb failure rule. This rule describes the criterion for slip along a surface in soils of many types (Iverson et al., 1997). The shear failure along a surface in granular material or in unlithified regolith is driven by the equation:

$$\tau = \sigma^{'} \tan\phi + c^{'} \tag{3.1}$$

where τ is the shear stress acting on the surface, $\sigma^{'}$ is effective normal stress (for convention the normal stress is positive when in compression), ϕ is the internal friction angle of the material and $c^{'}$ is the effective cohesion.

The internal friction angle is affected by the intrinsic friction between the clasts of a soil and by the way in which clasts interlock geometrically each other. The product $\sigma^{'} \tan\phi$ represent the frictional component of the soil strength. The cohesion is instead the component of the shear strength of the soil that is independent of interparticle friction. It depends mainly on electrostatic forces and on cementation between the clasts due to secondary mineralization (Mitchell & Soga, 2005). Even the cohesion given by secondary causes such as vegetation roots can add some strength to the soil. The contributes of cohesion to the total amount of strength can be little but it becomes important and exceeds the

frictional strength at shallow depths on steep slope where the effective stress is relatively low (Iverson et al., 1997).

The effective stress of the equation 3.1 include implicitly the effects of pore-fluid pressure (u_w) witch is isotropic and affect the total effective stress as in the equation:

$$\sigma^{'} = \sigma - u_w \tag{3.2}$$

where σ is the total normal stress (Terzaghi, 1936). This equation, in the Mohr two-dimensional representation of the stress state, is graphically represented by a line that separates the stable part to the unstable part. This line represent the failure envelope, a linear model with two parameters, also known as Mohr-Coulomb failure criterion. The stress state within a plane that contains the major (σ^1) and minor (σ^3) principal stress, plotted on a graph of shear stress vs normal stress, can be represented by means of a graphical construction known as the Mohr circle of stress. A stress condition represented by a Mohr circle that touches the line of the Coulomb failure envelope is known as limiting stress state. In this stress state the failure occurs.

Pore pressures may change with depth so it is fundamental to model the spatial distribution of pore pressure $p(x, y, z)$ where x, y, z are space coordinates. The groundwater flow is driven by the pressure head distribution $h(x, y, z)$ defined as the measurement of water pressure per unit weight above a certain depth and it is usually measured as a water surface elevation expressed in meters. The pore pressure distribution is related with the pressure head with this simple equation:

$$p = \gamma_w(h + z) \tag{3.3}$$

where γ_w is the unit weight of the water and z is a space coordinate oriented vertically downward. The origin of z, here and in the next paragraphs, is fixed at a point on the ground surface.

The Darcian specific discharge $\overrightarrow{q}$ that controls the groundwater flux is represented by the equation:

$$\overrightarrow{q} = K\nabla h \tag{3.4}$$

where K is tensor of the hydraulic conductivity of the soil and ∇h is the gradient of the pressure head distribution.

The equations 3.1-3.4 show that the knowledge of the pore pressure distribution is absolutely fundamental for the assessment of Coulomb slope failure.

3.1.2 Apparent cohesion in unsaturated soils

The effective stress of the equations 3.1 and 3.2 has been defined by Terzaghi (1936) as "that part of the total stress which produces measurable effects such as compaction or an increase in shearing resistance". But equation 3.1 doesn't take into account the effect of the compressibilty of the singular grains (c_s). In fact, if c_s represent a considerable fraction of the total compressibility of the soil (c) thus the effective stress should be defined as:

$$\sigma' = \sigma - (1 - \frac{c_s}{c})u_w \tag{3.5}$$

(Skempton, 1960). This equation clarifies that "Terzaghi's equation does not give the true effective stress, but gives an excellent approximation for the case of saturated soils" (Mitchell & Soga, 2005).

There are many forces in soil that are not included in the effective stress equation 3.1 and that can produce measurable effects on deformation and strength. One of these are the Van Der Waals forces, attractive or repulsive physicochemical forces between molecules that can play an important role especially in fine grained soils (Bolt, 1956). Another important force, especially in unsaturated soils, are the capillary forces (Bishop, 1959; Mitchell & Soga, 2005). This force is associated with a sometimes macroscopic increase in shear and tensile strength so that it needs to be taken into account when describing the stress state in unsaturated soils. This force is negative by convention and is called matric suction.

There are various approaches for describing the state of the stress in unsaturated soil (Lu et al., 2006):

- The modified effective stress approach proposed by Bishop (1959) with a modified form of the classic effective stress equation

$$\sigma' = \sigma - u_a + \chi(u_a - u_w) \tag{3.6}$$

  where u_a is the air pressure and χ is a parameter varying between zero and 1 as a function of the degree of pore-water saturation. The difference between u_a and u_w represents the matric suction. The classical Mohr-Coulomb criterion for the case of unsaturated soils can then be written as:

$$\tau_f = c' + [(\sigma - u_a) + \chi(u_a - u_w)]tan\phi' \tag{3.7}$$

  where c' is the effective cohesion (the intercept of the extended Mohr-Coulomb failure envelope where the net normal stress and the matric suction are equal to zero) and ϕ' is the effective angle of internal friction.

- The independent stress state variable approach proposed by Fredlund & Rahardjo (1993) where the net normal stress and the matric suction are treated independently within the shear strength equation:

$$\tau_f = c' + (\sigma - u_a)\tan\phi' + (u_a - u_w)\tan\phi^b \tag{3.8}$$

  where the first two terms represent the classical Mohr-Coulomb criterion and the last term uses an additional friction angle ϕ^b to account for the contribution of the matric suction to shear strength. The effective cohesion indicates an increase in strength as matric suction increases. This increase can be defined using the ϕ^b angle as follows:

$$c = c' + (u_a - u_w)\tan\phi^b \tag{3.9}$$

  where c is the total cohesion intercept, measured as the intercept of the extended Mohr-Coulomb failure envelope with the shear stress axis at a specific matric suction.

- Many other authors have proposed different approach in the form of modified stress variables like Alonso et al. (1990) that include volumetric strain due to matric suction in the critical state soil mechanics or Gallipoli et al. (2003) that introduces a dependence between a stress variable and the degree of saturation and the matric suction.

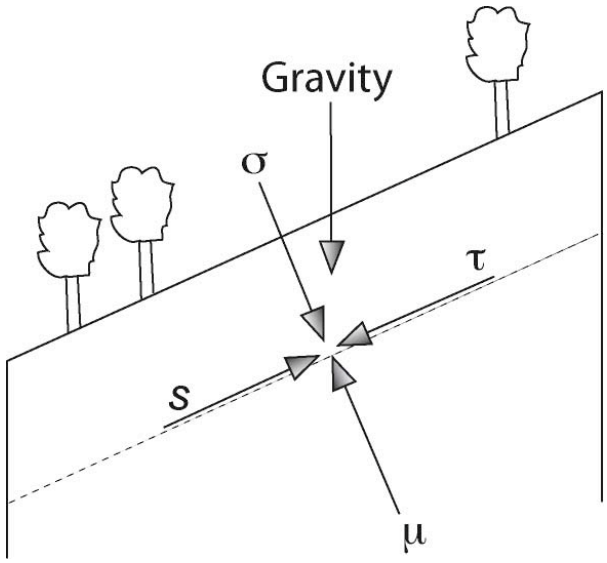

Figure 3.1: Force diagram for the infinite slope model. S is the shear strength, τ the shear stress, μ is the pore-fluid pressure and σ is the normal stress.

Equations 3.6-3.9 show that when computing the stability analysis for unsaturated soils it is fundamental to take into account the increase in strength and cohesion due to matric suction. Using the simple form of the shear failure equation, valid just for saturated conditions, would result in an underestimated value of the factor of safety.

3.1.3 Infinite slope model for stability analysis

Many models for slope stability analysis have been proposed for different types of simulation and for different types of landslides (Bishop, 1955; Spencer, 1967; Janbu, 1973; Morgenstern & Price, 1965). All this methods are quite tricky and need a large amount of data to be successfully applied. But if a few simplifications are made it is possible to obtain a model that is more simple to use and needs less input data.

For shallow landsliding we can observe that it is usually characterized by an elongate shape and that the influence of the toe and head portion is usually negligible so as it can be represented as a single slice with the slide surface approximately parallel to the ground surface. If the landslide has a small depth in comparison to length and width, as it usually occurs for shallow landslides, it is possible to assume a simplified geometry of the slide characterized by a planar slip surface on an infinitely extended planar slope, both laterally and distally. This approach is known as infinite slope (Skempton & DeLory, 1957). It assumes that the failure is the result of translational sliding, that the failure plane and the water table are parallel to the ground surface and that the failure occurs along a single layer of infinite length.

The forces acting at a point along the potential failure plane are those illustrated in figure 3.2 .The resisting force of earth materials is the shear strength

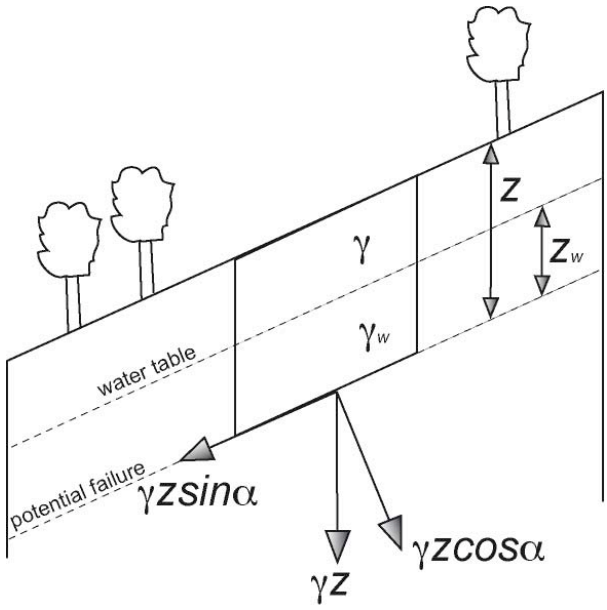

Figure 3.2: Vector components of gravity and position of the water table. γ is the soil unit weight, γ_w is the unit weight of water, Z the thickness of slope material above the slide plane, Z_w is the water table depth and α is the slope angle.

S, described by the Terzaghi's equation:

$$S = (\sigma - u_w) \tan \phi + c \tag{3.10}$$

The slope normal component of gravity, resisting to downslope movement, is the normal stress σ that can be described as:

$$\sigma = \gamma z \cos \alpha \cos \alpha \tag{3.11}$$

where γ is the soil unit weight, z is the thickness of slope material above the slide plane and α is the slope angle.

The pore-fluid pressure that reduces the resisting forces and the shear strength of the material can be represented as follows:

$$\mu = \gamma_w m z \cos \alpha \cos \alpha \tag{3.12}$$

where γ_w is the unit weight of water and m is the vertical height of water table above the slide plane expressed as a fraction of total tickness ($m = z/z_w$). The slope parallel component of gravity is the shear stress τ:

$$\tau = \gamma z \cos \alpha \sin \alpha \tag{3.13}$$

The factor of safety (FS) is defined as the ratio between resisting and driving forces (Ritter, 2004) and in the case of the infinite slope model it assumes the form:

$$FS = \frac{ResistingForce}{DrivingForce} = \frac{ShearStrength(S)}{ShearStress(\tau)} \tag{3.14}$$

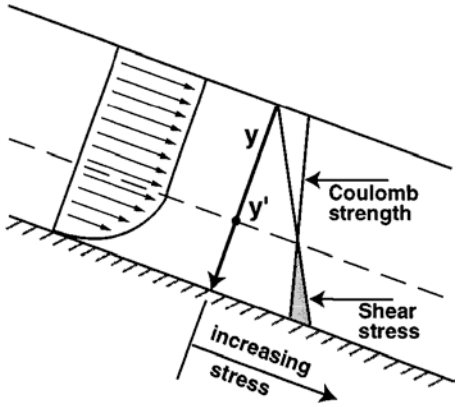

Figure 3.3: Bingham model on an infinite slope (from Iverson et al. 1997)

$$FS = \frac{C + (\gamma - m\gamma_w) z \cos\alpha \cos\alpha \tan\phi}{\gamma z \sin\alpha \cos\alpha} \tag{3.15}$$

When the shear strength is greater than the shear stress, the factor of safety has a value major than1 and the slope may be considered stable. If instead the shear strength is less than the shear stress the factor of safety has a value less than 1 and the slope should be considered unstable.

3.2 Slope stability models for shallow landslides

Many models have been proposed to explain the triggering of shallow landslides and debris flows. These models usually focus on failure and triggering of an infinite slope of isotropic and homogeneous soil.

One of the most known hypothesis for mobilization of debris flows and shallow landslides is that proposed by Johnson & Rodine (1984) and known as Bingham model. This model assumes that the triggering can occur only if the shear stress exceed the Coulomb strength defined by equation 3.1. In this case the strength, or yield strength, is assumed to be an intrinsic material property, and does not vary dynamically with the other soil properties. The main assumption of the Bingham model is that a failure can occur only when a soil with a particular water content exceeds a critical thickness. In such case the shear stress at the base of the slope is higher than the yield strength (figure 3.3). Below the failure plane, the Bingham model assumes that the yield strength is not fixed but changes as a function of variables like pore pressure and friction angle (Iverson et al., 1997).

An alternative hypothesis for shallow landslides mobilization has been proposed by Takahashi (1978). This model is based on the Bagnold (1954)'s concept of dispersive stress but is essentially a Coulomb failure model for a fully saturated and cohesionless soil with slope parallel seepage. This model assumes that the soil is fully saturated and that the water flows across the slope and accross the slope surface (figure 3.4). The presence of surface water allows the failure at an arbitrary soil depth and in slopes of varying steepness. Due to the presence of surface water, the angle of failing slopes is reduced to less than $\frac{\phi}{2}$

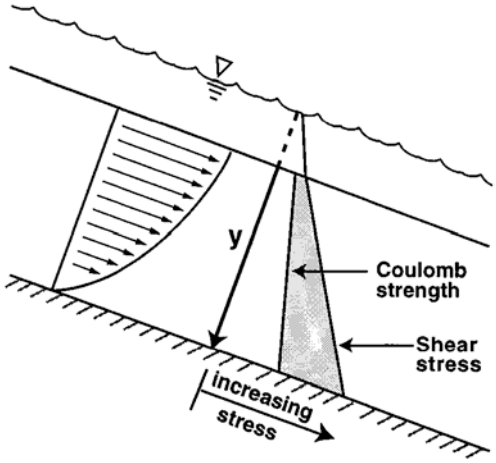

Figure 3.4: Takahashi model on an infinite slope (from Iverson et al. 1997)

so as Takahashi's model works best for debris flows triggered by flash floods in relatively gently slopes due to the surface-water surcharge (Iverson et al., 1997).

Other models consider the debris flows as a two-phase mixture of solid and fluid and assume that debris flows are triggered by the pore pressure growth beyond hydrostatic values. For some authors when the Coulomb failure occur and the cohesion bonds are broken, the pore pressure due to the groundwater flow can rise enough to liquefy the soil (Denlinger & Iverson, 1990). Others postulate that the mobilization of debris flows may occur only when the contraction of loose soils during a quasistatic failure increase pore pressure until a critical state (Casagrande, 1979; Sassa, 1984), a behaviour similar to that observed in undrained laboratory test cells. It is very important to consider how fast the porosity can change during soil contraction compared to the variation of the pore pressure. In fact if this variation is slow the pore pressure can change balancing the new porosity but if the porosity variation is too fast the pore pressure increase can lead to the liquefaction of the soil.

As already said in section 2.2 the main triggering factor for shallow landslides and debris flows is the increase in groundwater pore pressure in response to heavy rainfall. At the same time the infiltrating water adds weight that plays a mechanical role especially where the cohesion contributes significantly to the Coulomb soil strength (Iverson et al., 1997). The pore pressure increase in a slope can occur in two ways: by direct infiltration of water at the slope surface and by groundwater flow from adjacent portions of the slope. The direct infiltration usually involves a vertical flow from the surface to the deepest part of the soil while the groundwater flow usually is directed from a saturated area towards closest materials. The increase in in pore pressure in the soil can be obtained even when the infiltrating or flowing water elevates the regional water table until a shallow level within the soil. Usually the groundwater-flow models used for distributed slope stability analysis treat soils and rocks as continuous porous media that obey Darcy's law even though field evidence indicates that the flow distribution in natural slopes can be influenced by rock fractures, root channels and animal burrows (Pierson, 1983).

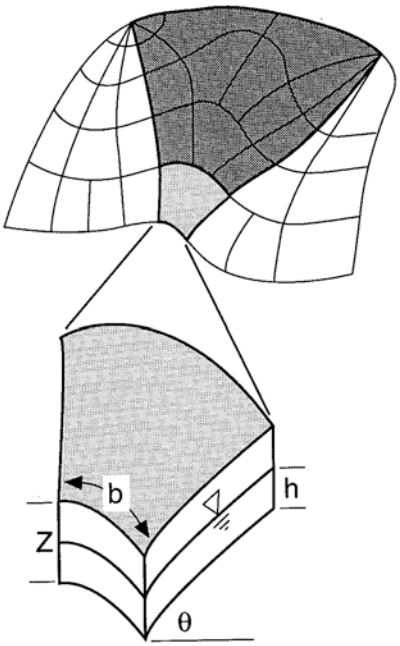

Figure 3.5: Topographic elements used in the TOPOG hydrologic model. Each element is defined by the intersections of contours lines and flow tube boundaries (from Montgomery & Dietrich, 1994)

Topography plays an important role in driving surface and groundwater flows. A model that explicitly takes into account the topographic influence on soil saturation and slope stability is that proposed by Montgomery & Dietrich (1994). They use the hydrologic model TOPOG (O'Loughlin, 1986) to predict the degree of soil saturation in response to a steady state rainfall for topographic elements defined by the intersection of contours and flow tube boundaries (figure 3.5). The flow tube approach used by TOPOG permits substantialy to include the topographic control on the pore pressure and this pore pressure is then used to estimate the slope stability with the infinite slope model while treating the subsurface flow in the steady state. Further developments of this model include the free software SHALSTAB (Dietrich & Montgomery, 1998). This topographic approach results very proficient in capturing the spatial variability of shallow landslides hazard even though there is a tendency for overprediction to occur, depending on the quality of topographic data (Dietrich et al., 2001). Another model that uses the flow tube approach has been proposed by Rosso et al. (2006). In their model the hillslope hydrology is modeled by coupling the Darcy's low for the seepage flow with the conservation of mass of soil water.

All the approaches derived from the Montgomery and Dietrich's model do not take into account transient movement of soil water and this simplification can negatively affect the results because the steady flow condition is unrealistic for the major part of natural slopes during and immediately after a rainfall event. Other models use unsteady flows like those proposed by Okimura & Ichikawa (1985) or Wu & Sidle (1995). The first uses a finite difference approach to model

the groundwater flow. The latter couple the infinite slope stability approach with a groundwater kinematic wave model, and a continuous change vegetation root strength model. This model allows for varying soil depth and hydraulic conductivity but totally neglect the unsaturated zone. Casadei et al. (2003) link a dynamic and spatially distributed shallow subsurface runoff model to an infinite slope model to predict the spatial distribution of shallow landslides even accounting for evapotraspiration and unsaturated zone storage.

The major part of the above authors consider the pore pressure as deriving uniquely from the rising of a saturated layer above a fixed slip surface. Others have proposed models that instead consider the pore pressure as generated by the advance of a wetting front coming from the top. Someone uses the Green-Ampt infiltration model (Green & Ampt, 1911) to infer the movements of the wetting front and to find out the critical depth of triggering within the soil (Pradel & Raad, 1993). Many other authors (Iverson, 2000; Crosta & Frattini, 2003; Simoni et al., 2008) have used different solutions to the Richards equation (Richards, 1931) to represent the movement of water in unsaturated soils and to assess the effect of transient rainfall on timing and location of landslides.

3.3 Rainfall triggered by heavy rainfall: Iverson's model

In literature many applications of the Montgomery and Dietrich model have shown that this approach works quite well for the spatial assessment of landslide hazard but it is not so proficient for the temporal forecast (Montgomery et al., 1998; Guimarães et al., 2003). The main reason is that it treats the subsurface flow as a steady state process thus it is not possible to represent the transient water flux due to the occurrence of short and high intensity rainstorms. As observed by Iverson (2000) the steady state approximation is valid just under the following conditions: very long rainfall duration, very low rainfall intensity, shallow soil depth and strongly anisotropic conductivity (slope normal component $>>$ slope parallel component). With this approximation is thus not possible to capture the effect of high intensity rainfall in the short time periods that often trigger shallow landslides and debris flows.

The model proposed by Iverson (2000) uses a particular solution of the Richards (1931) equation to predict the rainfall induced pore pressure and its response to different time and space. The use of the Richards equation, that describes the movement of water in porous soils, removes the need for the assumption of steady state conditions in subsurface flow so that it is possible to describe transient conditions and infiltration due to complex and high intensity rainfall events.

3.3.1 Hydrological model

The extended form of the Richards equations that governs the unsteady and variably saturated Darcian flow of groundwater in response to rainfall can be

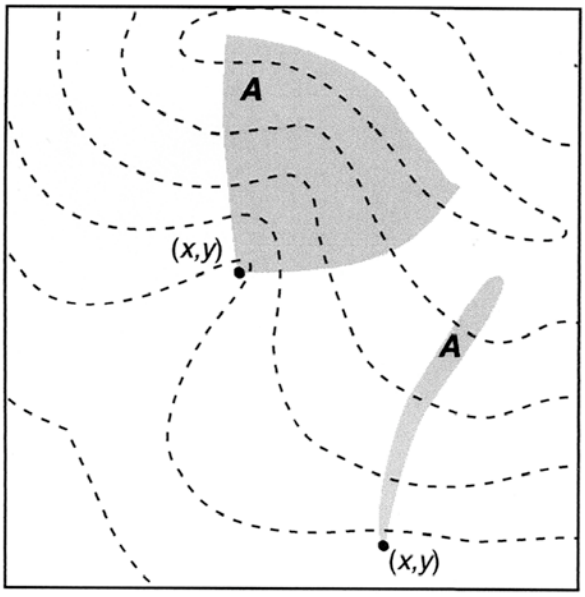

Figure 3.6: The planimetric contributing area A is defined as the area enclosed by the upslope topographic divide and hypothetical flow lines normal to topographic contours (from Iverson, 2000)

written as follows (Hurley & Pantelis, 1985; Iverson, 2000):

$$\frac{\partial \psi}{\partial t}\frac{\partial \theta}{\partial \psi} = \frac{\partial}{\partial x}\left[K_L(\psi)\left(\frac{\partial \psi}{\partial x} - \sin\alpha\right)\right] + \frac{\partial}{\partial y}\left[K_L(\psi)\left(\frac{\partial \psi}{\partial y}\right)\right] + \frac{\partial}{\partial z}\left[K_Z(\psi)\left(\frac{\partial \psi}{\partial z} - \cos\alpha\right)\right] \tag{3.16}$$

where x, y, and z are the axes of a reference coordinate system with z normal to the slope, x tangent to the local surface slope and y tangent to the local topographic contour. ψ is the groundwater pressure head. θ is the soil water volumetric content, t is time, α is the slope angle, K_L and K_Z are respectively the hydraulic conductivity in lateral directions (x and y) and the hydraulic conductivity in slope-normal direction (z).

Iverson investigates how the physical process leading to landslide triggering can operate on different timescales. The aim of this process is to find out a simple solution for the Richards equation to be applied in the hydrological model. First he observes that for times grater than A/D_0 (where $D_0\left[L^2T^{-1}\right]$ is the maximum hydraulic conductivity and $A\left[L^2\right]$, figure 3.6, is the catchment area that might influence the pressure head distribution in x, y, H) the groundwater pressure head get to a steady background distribution in response to a rainfall. A/D_0 represents the minimum time necessary for lateral pore pressure trasmission from the area A. This steady background distribution can affect the landsliding in the point x, y, H. The triggering of landslides is instead the result of a rainfall over a shorter timescale of H^2/D_0 (H is the depth from the slope surface) witch is associated to transient pore pressure transmission during and immediatly after a rainstorm. So it is possible to establish a length scale ratio ϵ between

the two timescales:

$$\epsilon = \sqrt{\frac{H^2 D_0}{A/D_0}} = \frac{H}{\sqrt{A}} \tag{3.17}$$

If $\epsilon << 1$ it is possible to use the simplified solution of Richards equation using the long term and short term pressure head responses.

For short time periods the dimensionless time is defined as $t^* = tD_0/A$. If the soil is initially dry the diffusion term can be neglected and the Richards equation becomes (Frattini & Crosta, 2005):

$$\frac{\partial \psi^*}{\partial t^*} + \frac{\partial \psi^*}{\partial Z^*}\left(\cos^2\alpha \frac{I_Z}{K_Z}\frac{C_0}{C(\psi)}\frac{dK_Z^*}{d\psi^*}\right) = 0 \tag{3.18}$$

where ψ^* is the normalized groundwater pressure head ($\psi^* = \psi/H$), t^* is the dimensionless time ($t^* = tD_0/H^2$), I_Z is the rainfall intensity, C_0 is the minimum value of $C(\psi) = d\theta/d\psi$, that is the change in volumetric water content per unit change in pressure head. This equation is now similar to that representing the "piston-flow" model described by Green & Ampt (1911). But if we consider wet initial conditions, the gravity flux can be neglected and the pressure head equation becomes:

$$\frac{\partial \psi}{\partial t} = D_0 \cos^2\alpha \frac{\partial^2 \psi}{\partial Z^2} \tag{3.19}$$

where D_0 is the maximum diffusivity. Equation 3.19 describes the response of $\psi(Z,t)$ to rainfall of fixed intensity and duration. If we find a solution of equation 3.19 and summing a series of response it is thus possible to describe the pressure head response in case of complicated rainfall series with varying intensity and duration. To find a solution to the differential equation 3.19 is necessary to fix the following boundary conditions:

$$\psi(Z,0) = (Z - d_Z)\beta \tag{3.20}$$

$$\frac{\partial \psi}{\partial Z}(\infty, t) = \beta \tag{3.21}$$

$$\frac{\partial \psi}{\partial Z}(0,t) = \begin{cases} -\frac{I_Z}{K_Z} + \beta & t \leq T \\ \beta & t > T \end{cases} \tag{3.22}$$

where T is the rainfall duration, d_Z is the water table depth in the vertical direction Z and β is the initial steady state pressure head distribution defined as $\beta = \cos^2\alpha - \left(\frac{I_Z}{K_Z}\right)_{steady}$. The boundary condition 3.20 assumes a steady state pressure head distribution, 3.21 assumes that at great depths below the water table the vertical groundwater became negligible but persist the steady state pressure head distribution. The last condition 3.22 states that Darcy's low governs the water entry at the ground surface and that the pressure head distribution is defined by β when it is not raining ($t > T$) and by β plus a short time infiltration rate during rainfall ($t \leq T$).

With these boundary condition the solution of the diffusive equation 3.19 suggested by Iverson (2000) is:

$$\frac{\psi}{Z}(Z, t \leq T) = \beta\left(1 - \frac{d}{Z}\right) + \frac{I_Z}{K_Z}\left[R(t^*)\right] \tag{3.23}$$

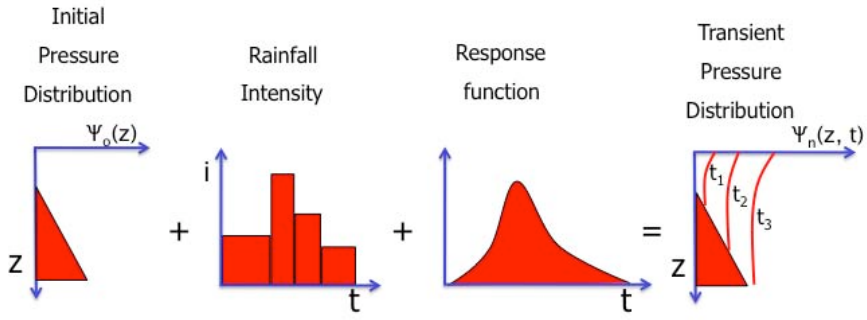

Figure 3.7: Schematic representation of the diffusive model (modified from Iverson, 2000)

$$\frac{\psi}{Z}(Z, t > T) = \beta\left(1 - \frac{d}{Z}\right) + \frac{I_Z}{K_Z}\left[R(t^*) - R(t^* - T^*)\right] \tag{3.24}$$

where $R(t^*)$ is a pressure head response function which depends only on normalized time and is defined as:

$$R(t^*) = \sqrt{\frac{t^*}{\pi}}\exp\left(-\frac{1}{t^*}\right) - erfc\left(\frac{1}{\sqrt{t^*}}\right) \tag{3.25}$$

The normalized times are:

$$t^* = \frac{t}{Z^2/\hat{D}} \tag{3.26}$$

$$T^* = \frac{T}{Z^2/\hat{D}} \tag{3.27}$$

where $\hat{D}$ is the effective hydraulic diffusivity defined as:

$$\hat{D} = 4D_0\cos^2\alpha \tag{3.28}$$

where D_0 is the maximum characteristic diffusivity.

As shown in figure 3.7 during every time step (t_1, t_2, t_3) the diffusive model, using the rainfall intensities and the response function, is applied to the initial steady state pressure head distribution to obtain the new transient groundwater pressure head for every depths.

3.3.2 Slope stability model

The slope stability model proposed by Iverson (2000) is based on a one dimension analysis and uses the equations 6.10-3.28 to compute the pore pressure distribution within the soil. The assumption needed for the infinite slope analysis (soil depth << length and width of the slice) is perfectly in agreement with the assumption ϵ<<1 made to develop the simplified solution of the Richards equation.

As specified in section 6.1.1, the infinite slope model is a balance at every depth between the downslope components of the stress and the resisting stress

due to basal friction. The dimensionless factor of safety (FS) varies as a function of depth and time so it is useful to divide the equation in a steady background component (FS_0) and a time varying component (FS'). The final equation used by Iverson (2000) to compute the slope stability is obtained by merging the classical infinite slope stability equation (3.15) with the solutions of the diffusive equation (6.10 and 6.11):

$$FS(Z,t) = \frac{\tan\varphi}{\tan\alpha} + \frac{c}{\gamma_S Z \sin\alpha\cos\alpha} - \frac{\psi_0(Z)\gamma_W \tan\varphi}{\gamma_S Z \sin\alpha\cos\alpha} - \frac{[\psi(Z,t) - \psi_0(Z)]\gamma_W \tan\varphi}{\gamma_S Z \sin\alpha\cos\alpha} \tag{3.29}$$

$$FS(Z,t) = \frac{\tan\varphi}{\tan\alpha} + \frac{c}{\gamma_S Z \sin\alpha\cos\alpha} - \frac{\psi_0(Z)\gamma_W \tan\varphi}{\gamma_S Z \sin\alpha\cos\alpha} - \\ - \frac{\gamma_W}{\gamma_S}\frac{\tan\varphi}{\sin\alpha\cos\alpha}\frac{I_Z}{K_Z}\begin{cases} [R(t^*)] & t^* \le T^* \\ [R(t^*) - R(t^* - T^*)] & t^* > T^* \end{cases} \tag{3.30}$$

where α is the slope angle, φ is the soil friction angle, c is the cohesion, γ_S is soil unit weight and γ_W is the unit weight of groundwater. These equations show that in addition to the soil and slope parameters, that are used for the computation of the steady state factor of safety (FS_0), to determine the time varying component (FS') only three more variables are necessary: the normalized time (t^*), the normalized rainfall duration (T^*) and the rainfall intensity (I_Z). The factor of safety can be calculated at every depth and the depth Z that determines the depth of landsliding is the first that yields a value equal to one.

3.4 Software for slope stability analysis

Distributed slope stability models supply algorithms and equations to be applied to every cell, or pixel of an extended area. Sometimes these equations must be applied at different depths for each pixel so that the computation can be extremely time consuming depending on the thickness of the soil, the extension of the studied area and the complexity of the equation. To overcome of this problem, since the early age of informatics and computer sciences, many softwares have been developed to make it easier to apply stability models at large scale and to visualize the results in many ways. All these softwares relics on codes that in some way introduces simplifictive hypothesis to the general forms of equations.

An example of a software for distributed slope stability analysis is SHALSTAB (SHAllow Landslide STABility model) (Dietrich & Montgomery, 1998). It uses a distributed steady state description of the hydrological fluxes coupled with an infinite slope analysis. The basic tool is a grid-based model, a combination of C++ programs and ARC/INFO AML scripts intended to be used within an ESRI-ArcGIS software environment. This model has been classified as spatially predictive because it is not suited to forecast the timing of landslide triggering (Simoni et al., 2008).

SINMAP (Stability Index MAPping) and SINMAP2 are other add-on tools for the ESRI-ArcGIS software. They have their theoretical basis in the infinite slope stability model with groundwater pore pressures obtained from a topographically based steady state model of hydrology (Pack et al., 1998, 2001).

The necessary input information (slope and specific catchment area) are obtained from the analysis of Digital elevation models (DEM). These parameters can be adjusted and calibrated with an interactive visual procedure that adjusts them based upon observed landslides. SINMAP allows uncertainty of the variables through the specification of lower and upper bounds that define uniform probability distributions. Between these bounds the parameters are assumed to vary at randomly respect to the probability distribution.

Other softwares have a more complex approach to the hydrological modelling of the groundwater flow. For example SEEP/W is a finite element software that resolve the Richards equations to account for transient groundwater flow within a slope. This software analyzes groundwater seepage and excess pore-water pressure dissipation within porous materials and can model both saturated and unsaturated flow (Krahn, 2004). SEEP/W is very proficient in resolving saturated-unsaturated and time-dependent problems. SEEP/W results are than used by the software SLOPE/W to perform the slope stability analysis adopting the limit equilibrium method. This software works very well for single slope stability analysis (Tofani et al., 2006) but is not suited to be applied for a distributed analysis.

TRIGRS (Transient Rainfall Infiltration and Grid based Regional Slope stability model) is a software developed for computing the transient pore pressure distribution due to rainfall infiltration using the method proposed by Iverson (Baum et al., 2002). It is a fortran program that supply as final result the distributed map of the factor of safety. This program, freely distributed both as source code and executable files, has been widely used by many authors for regional landslide hazard assessment (Baum et al., 2005; Salciarini et al., 2006; Chien-Yuan et al., 2005) and works under the assumptions of nearly saturated soil, presence of flow field and isotropic, homogeneous hydrologic properties (Baum et al., 2002). TRIGRS is very sensitive to initial conditions so, if the initial water table depth is poorly constrained, it may produce questionable results.

One of the more advanced models for distributed slope stability is the one recently proposed by Simoni et al. (2008) and called GEOtop-FS. This model uses the hydrological distributed model GEOtop (Rigon et al., 2006) to compute pore pressure distribution by solving the Richards equations and an infinite slope stability analysis to compute the distributed factor of safety. Even though they use the Richards equation to analyse the groundwater flow, the authors assume saturated conditions and doesn't deal with unsaturated soils. The main novelty of GEOtop-FS is that the factor of safety is computed with a probabilistic approach assigning statistical distributions to soil parameters instead of single deterministic value.

Chapter 4

Radar meteorology

RADAR (RAdio Detection And Ranging) was developed during World War II to detect aircraft while they where still out of visual range. They were widely used during the war but it became immediately clear that radars where so proficient in detecting rain and blobs of precipitations as they were in finding aircraft.

Between 1950 and 1980, reflectivity radars, which measure position and intensity of precipitation, were built by weather services all around the world. Between 1980 and 2000, weather radar networks became widespread in North America, Europe, Japan and other developed countries. Traditional radars were then replaced by Doppler radars, which track the relative velocity of the particles in the air in addition to position and intensity of could. Nowadays wheather services all around the world use radar data for weather forecast and for natural hazard assessment and mitigation. Radars are also used on aircrafts and satellites to look down at clouds and precipitation.

4.1 Meteorology with ground-based weather radar

A weather radar is a type of radar used to locate a precipitation, calculate its motion, estimate its type (rain, snow, hail, etc.), and forecast its future position and intensity (figure 4.1). It transmits a beam of radiation and receives an amount of radiation back depending on whatever the beam encounters. Ground based weather radars are used mainly for local registration of rainfall because the spatial range of action is limited to a few hundreds of kilometers.

The beam transmitted by a radar is characterised by three fundamentals properties: pulse repetition frequency (PRF), transmission time and beam width (figure 4.2). The pulse repetition frequency is the number of radiations transmitted per second, the transmission time is the duration of each pulse and the beam width is the angular width of the emitted beam (usually 1°). From the transmission time it is possible to calculate the pulse length that combined with the beam width permits the computation of the pulse volume. The pulse length defines the radial resolution while the beam width defines the angular resolution.

The detection of rain with the radar occur when the beam hits a raindrop in the atmosphere. The processes that take place in this case are *scattering* and *absorption*. The energy of the beam is scattered in all direction but a small amount of energy is sent back to the radar; at the same time the raindrop

Figure 4.1: The weather radar of Monte Settepani, located near the Colle del Melogno, Savona, Italy at 1387 m a.s.l.

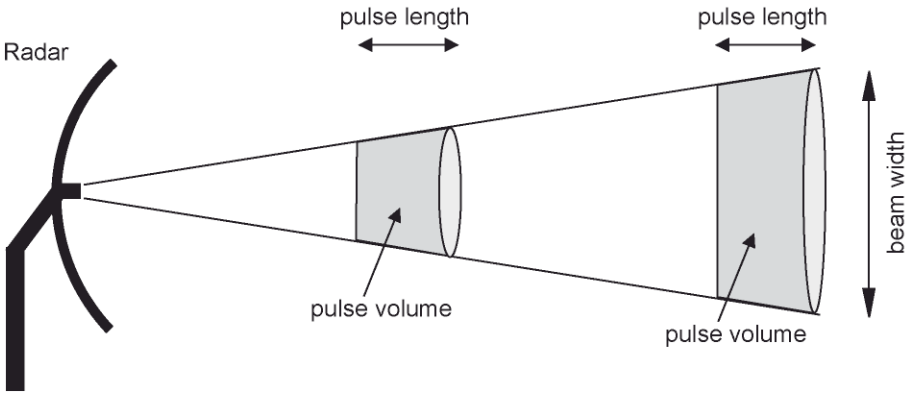

Figure 4.2: Schematic representation of the properties of the emitted beam

Weather radar bands		
Frequency (GHz)	Wavelength (cm)	Band
90	0.1	W (clouds)
30	1.0	K (clouds)
10	3.0	X (rainfall)
5	6.0	C (rainfall)
3	10.0	S (rainfall)
1.5	20.0	L (rainfall)

Table 4.1: Radar frequencies used for rain detection

absorb a small amount of energy. This two processes are even known together as *attenuation*. The problem is that not only raindrops can produce attenuation but even atmospheric gases, aerosols, hail, snow and insects. In some cases is possible to distinguish between a different type of target thanks to the different amount of absorption end/or scattering. For example hail can be easily detected because it is characterized by a very high reflectivity.

Radars may use different frequencies for different reasons. The high-frequency, short-wavelength bands are very useful for detecting clouds and aerosols because they are easily attenuated by very small amounts of gases. With a longer wavelength the beam is less attenuated but at the same time it cannot discriminate small target. The more used bands are the S-bands because they are a good compromise between high sensitivity and minimal attenuation. In table 4.1 the variety of radar frequencies used for clouds and rain detection are shown. The images generated by a radar are not flat maps of precipitation because the beam is usually inclined at an angle not lower than 0.5° above horizontal. This is done to keep the beam away from object on the ground like buildings and mountains. When a radar record the signal after hitting a target (echo), firstly it analyzes the reflectivity, where high values indicate rain and extremely high values indicate hail. Then, using the time variation of reflectivity, it is possible to infer how the target moves measuring its radial velocity. Finally, the radar measures the turbulence using the spectrum width, that is obtained measuring the time variation of radial velocity.

The most known radar products are reflectivity maps that represent a measure of how much energy has been scattered back to the radar from the target (figure 4.3). Different reflectivities correspond to different types of targets like, in order of increasing reflectivity, light snow, moderate rain, heavy rain, hail. Another important product is the radial velocity image. From this image is possible to gather the rotation of a mass or more precisely the components of the movement, toward or away from the radar. With the radial velocity is even possible to infer a vertical profile of the precipitation and wind.

Meteorological radars are very proficient in reliably detect the spatial-temporal pattern of the observed precipitation field. Sometimes however they are not completely satisfactory in estimating the correct precipitation amounts. The only instruments that, due to direct measurements, can provide a good estimate of precipitation amounts are rain gauges but they totally lack information on precipitation organization. Thus to have a distributed spatial pattern characterized by a better estimate of rainfall amount it is possible to use radar measured rainfall maps that takes into account the precipitation measured by

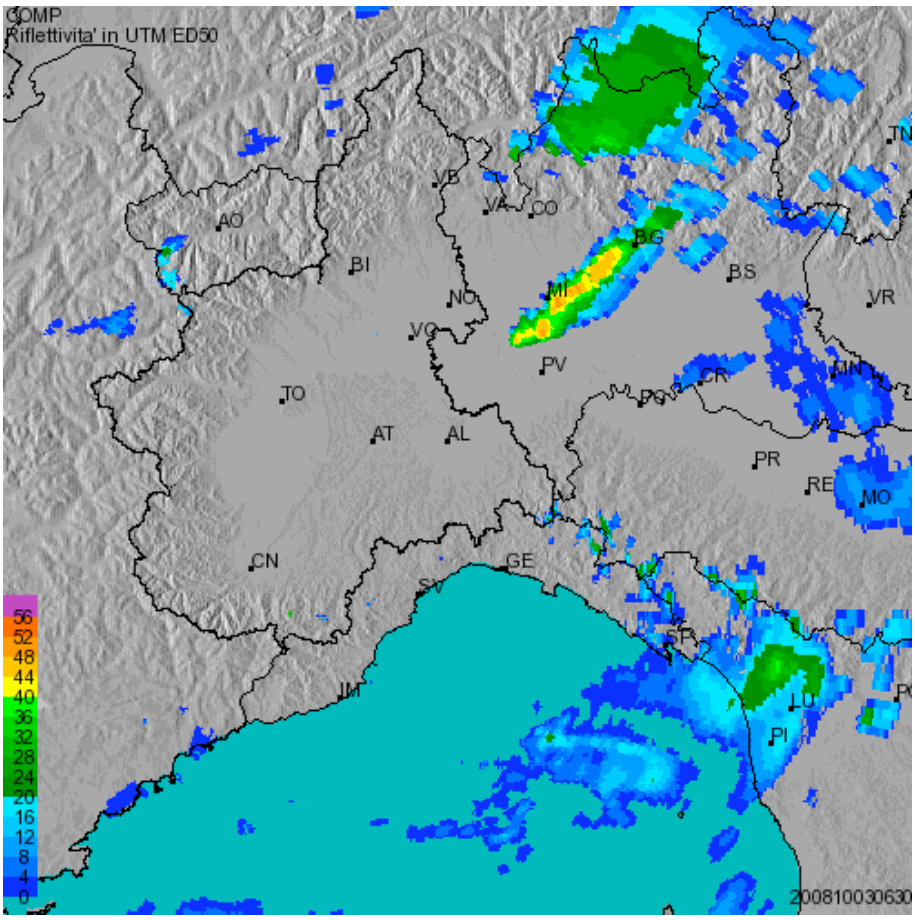

Figure 4.3: Example of reflectivity map registered by the weather radar located in Monte Settepani (near Savona, Italy).

rain gauges networks. This process of calibration is done through an algorithm that allows for correcting radar-measured precipitation fields by using rain gauge measurements.

4.2 High resolution radar rainfall maps

Observation of intense precipitation events at small spatial-temporal scales is a crucial element both for developing procedures for stochastic downscaling and for providing high resolution fields for deriving soil conditions and to compute the groundwater pressure head distribution.

As said in the previous section, the rainfall amount measured by radar need to be corrected using specific algorithm to take into account precipitation measured by rain gauges. For this work an algorithm has been used that combines the uniform range dependent adjustment, by which the bias is removed from radar estimates, and the spatially varying adjusting method by which radar measurements can be adjusted to fit individual gauge observations (Alberoni & Nanni, 1992).

This algorithm consist in defining an anisotropic adjustment factor A^{ANA} for each precipitation structure observed by the radar. This factor is composed by:

- A range-dependent factor $A(r)$ that depends on the distance between precipitation structure and radar.
- A rain-gauge dependent factor A^G that depends on each rain-gauge observation that constraints the radar measured precipitation field.

In the first step an adjustment factor (the ratio between the gauge and the radar value in the same location) A_K is computed. Then a regression analysis is performed, by which the range dependence of $\log A_K$ is determined. As a result, a symmetrical range dependent adjustment factor field $A(r)$is obtained. For each cell ij of the radar field, the adjustment factor A^G is determined as follows:

$$A_{ij}^G = \frac{\sum^n W_{ijk} A_k}{\sum^n W_{ijk}} \tag{4.1}$$

where n is the number of raingauges considered and W_{ijk} is the weight factor for the k-th raingauge et the ij radar cell and is defined as

$$W_{ijk} = \exp\left(-\frac{r_{ijk}^2}{4\bar{r}_{ijk}^2}\right) \tag{4.2}$$

where $\bar{r}_{ijk}^2$indicates the average distance between the radar cells and the raingauges and r_{ijk}^2 indicates the distance between the radar cell ij and the k-th raingauge. The final step computes the anisotropic adjustment factor A^{ANA} by combining the isotropic range-dependent function to an additional term, which takes into account the density of the gauge network:

$$A_{ij}^{ANA} = A(r) + \exp\left(-\frac{\bar{r}_{ij}}{1.5\rho}\right)\left[A_{ij}^G - A(r)\right] \tag{4.3}$$

where ρ represents the average density of the raingauge network defined as the ratio between the area covered by the network and the number of raingauges. Multiplication of the adjustment factor field with the original radar field produces the corrected radar field.

4.3 Weather forecast and the PREVIEW project

The PREVIEW (PREVention, Information and Early Warning, pre-operational services to support the management of risks) project is an R&D initiative funded within the EU Sixth Framework Programme (FP6) with the aim of developing innovative geo-information prototype services for atmospheric, geophysical and man-made risks to be applied at a European scale. Within this project the main objective was to develop an integrated procedure for the forecasting and warning of distributed shallow landsliding to be used for civil protection purposes. To achieve this aim it is necessary to use advanced meteorological forecasting techniques to overcome the limits of traditional approaches because traditional warning systems, based only on rainfall observations do not leave enough time to adopt appropriate protection measures against fast phenomena.

As said in the previous chapters, intense rainfall events are one of the main factors that trigger surface landslides. Procedures for issuing early warnings to the population require the knowledge of the precipitation field down to scales of a few square kilometers and tens of minutes. Current operational practice relies heavily on the use of limited-area meteorological models (LAMs) that provide precipitation forecasts on scales of about 100 km^2 and a few hours. A gap thus exists between the scales resolved by limited-area meteorological models and the scales required for properly modelling the landslide process. An option to fill the scale gap and to obtain small-scale rainfall estimates is based on the use of stochastic models for rainfall downscaling. A stochastic disaggregation algorithm is capable of generating a small-scale fluctuating field from a smoother rainfall distribution on larger scales. In principle, this approach provides precipitation fields that should simultaneously satisfy the large-scale constraints imposed by meteorological forecasts (e.g., the expected average rainfall intensity) and are consistent with the known statistical properties of the small-scale rainfall distribution (Rebora et al., 2006). A downscaling model suitable for operational use in a hydrometeorological forecasting chain should be simple, robust and computationally fast and linked in a clear way to the large-scale prediction. In past years, several stochastic models for rainfall downscaling have been proposed (for a review on disaggregation models type see Ferraris et al., 2003). All available disaggregation models have been proven to score fairly well in reproducing the small-scale statistical properties observed for precipitation (Ferraris et al., 2003). However, linking these models with the features of the large scale fields is not that easy. Many downscaling procedures currently available for operational purposes account only for the total precipitation predicted by the LAM, while some other models are based on CAPE predictions (Perica & Foufoula-Georgiou, 1996). Other information provided by the meteorological model is not preserved. For this study a downscaling procedure, able to account for the reliable features of the meteorological prediction, has been used. Its parameters can be directly derived from the large-scale field with no need for calibration. Ferraris et al. (2003) have shown that the multifractal proper-

ties of radar-measured rainfall fields are compatible with those obtained from a nonlinearly transformed autoregressive process. Starting from these results a new downscaling model has been developed. This procedure is called RainFARM, Rainfall Filtered AutoRegressive Model, and it was proposed by Rebora et al. (2006) to which we refer for a complete description and further details. The RainFARM belongs to the family of algorithms called metagaussian models (see, e.g. Guillot & Lebel, 1999) and it is based on a nonlinear transformation of a linearly correlated process. The model is able to generate small-scale rainfall fields that take into account not only the total amount of precipitation predicted by the meteorological model but also its (linear) correlation and the position of the main rainfall patterns. Here the model is used to produce an ensemble of high-resolution precipitation forecasts starting from the most recent precipitation prediction produced either by Ensemble Prediction Systems (EPS) or by Limited area Ensemble Precipitation System (LEPS) or deterministic LAM forecasts. For each forecast precipitation field, RainFARM provides 100 high-resolution fields on a spatial domain of 448 km by 448 km and for the whole temporal extension of the forecast run, at a resolution of 1.75 km in space and 10 minutes in time. The production and processing of all the meteorological products has been managed by the CIMA (Centro di ricerca Interuniversitario in Monitoraggio Ambientale, University of Genova) for the data regarding the test site located in the Liguria region and by the Italian Air Force Meteorological Service for the second test site.

4.4 Radar rainfall maps and soil moisture (C-DRIFT)

The radar rainfall maps can be used as an input for hydrogeological models to reproduce the soil moisture conditions of a hillslope that may lead to slope instability. Given the difficulties associated with estimating the spatial distribution of soil moisture from point measurements on one side and from satellite observations from the other, soil moisture is often estimated from hydrological models. It can be computed directly within a slope stability model that couples hydrological modelling with a stbility analysis (Iverson, 2000; Baum et al., 2002; Simoni et al., 2008) or in two different steps, firstly using a model to infer the groundwater distribution and then a slope stability model (Schmidt et al., 2008). In this work both the approaches will be investigated.

Published hydrologic models vary in the level of detail they use in representing the physical system and temporal variation of the driving forces. Some of the important differences between published hydrologic models are: the computation of evapotranspiration; the partitioning between infiltration and runoff; the temporal definition of evapotranspiration demand and precipitation; the computation of vertical and lateral redistribution; and the number of soil layers used (Schmugge et al., 1980). Among the most popular hydrological models able to reproduce soil moisture maps are SVAT (Soil Vegetation Atmosphere Transfer) models (Neitsch et al., 2001) and TOPMODEL (Beven et al., 1995). In this work a continuous distributed hydrological model has been used: the C-DRiFt (Continuous Discharge River Forecast) model (Gabellani, 2005; Gabellani et al., 2005). It is a semi-distributed hydrological model able to simulate the discharge

process, the evapotranspiration process and the hypodermic flow propogation within a basin, allowing a description of the soil moisture state in each pixel in which the basin is discretized (Gabellani, 2005). It is an extension of the event model DRiFt (Giannoni et al., 2000, 2005) in which the description of evapotranspiration and the sub-flow has been introduced to complete the hydrologic cycle. It takes into account the spatial variation of inputs such as meteorological input, morphologic, geological and anthropic characteristics of the basin, but it is lumped in parameters, the discharge can be obtained in a given location wherever in the catchment while soil moisture conditions are reproduced in each pixel. The input data, necessary to the application of the model, consist of a Digital Elevation Map of the studied area, the soil properties maps, meteorological data (rainfall, temperature, short wave radiation) and vegetation maps. The model solves explicitly both the continuity equation and the energy balance in a distributed way, using some simplifications. It uses a modified Horton method to simulate the infiltration process (Gabellani et al., 2008) and considers the soil a porous medium schematized as a reservoir with two parameters: Vmax and f0 (Gabellani, 2005). The first one represents the soil capacity expressed in millimiters (mm) and f0 is the initial infiltration capacity for a dry soil expressed in millimetres per hour (mm/h). They are a function of soil type and soil use. For the energy balance the model uses the approximation called "force-restore equation", this allows explicit computation of evaporation and transpiration without the need of empirical closure models. These schematization allows the quantification of the partitioning of precipitation water into infiltration and runoff and regulate the hypodermic flow and the recharge of deep water whose vertical and lateral distribution are managed in a distributed fashion. In this way a description of the soil moisture state is possible in each pixel in which the basin is discretized (Giannoni et al., 2000, 2005; Gabellani et al., 2005). Results of the simulations are hourly maps of soil moisture content for each pixel within the target area. Soil moisture content is expressed as degree of saturation defined as V(t)/Vmax where V is the actual soil water content at time t and Vmax is the soil retention capacity. This quantity in an essential input for the slope stability model. The stand alone hydrological model used here to determine the soil moisture conditions has been provided by the CIMA.

4.5 Weather forecast and rainfall data as an input for slope stability models

Advanced meteorological forecasting techniques can be employed to overcome the limits of traditional approaches and to develop an integrated procedure for the forecasting and warning of distributed shallow landsliding. Traditional warning systems, based only on rainfall observations do not leave enough time to adopt appropriate protection measures against fast phenomena. This concept has been elaborated by different authors (Ferraris et al., 2002; Siccardi, 1996; Siccardi et al., 2004) with reference to flash floods and holds even more strongly for rainfall induced shallow landslides. Therefore, the challenge is to develop tools able to anticipate what meteorological and hydrological conditions may trigger these landslides, before the precipitation event arrives. To succeed, two major sources of uncertainty have to be addressed: the uncertainty associ-

ated with the meteorological forecast and the uncertainty associated with the soil properties values. The uncertainty related to meteorological predictions of precipitation (meteorological uncertainty) can be dealt with by using meteorological ensemble forecasts. With this approach, for each forecasted event, an ensemble of possible scenarios of precipitation is produced as an input for the hydrological modelling (Siccardi et al., 2004). The probabilistic forecasts are based on the assumption that the initial conditions of the model and the physical parameterizations are affected by an intrinsic error which increases with the lead time of the forecast.

It is here important to understand that to evaluate the reliability of the slope stability model that has been developed during this study, we will use measured data of rainstorm actually occurred instead of forecasted ones. With this apporoach is possible to remove uncertainty associated with the meteorological forecast and to compare the results of the model with landslide actually triggered. This approach doesn't affect the final results of the stability model because the format of the rainfall input file is the same for both measured rainfall maps and forecasted rainfall maps. It is not among the aims of this phd thesis to evaluate the error related with weather forecast.

Chapter 5

Proposed prototype regions

5.1 The Armea basin

The test site is located in Liguria, a Region in NW Italy south of the Alps (Figure 5.1). Meteorological conditions change at a local and regional scale, due to localized storm cells or to regional cyclonic conditions. The latter is the case when moving from the Alpine–pre-Alpine sectors to the Tyrrhenian coast. Mean annual precipitation ranges from 750–1250 mm in the west to 1350–1850 mm in the central and eastern parts of the Region.

Due to the geographical location and to the morphological and geological setting, landslides are frequent in Liguria. According to Italian archive of historical information on landslides and floods, 1806 landslide events damaged 1233 localities during the period 1800–2001 in the four Provinces of the Liguria Region. The historical information reveals that damaging events are most frequent in the rainy season, during the period September through December, in all four Provinces. A strong control on soil slips is the presence of a shallow bedrock. A peculiarity of some failures is represented by the presence of old dry stone walls, completely covered by colluviated material, associated with the slide scar.

Landslides are a quite recurrent phenomenon: they are prevalently represented by soil slips, soil slumps and soil slip-debris flows. These landslides are cause of economical losses and sometimes of casualties. They damage cultivations, settlements and pose hazard to the safety of people. Soil slip-debris flows are gravity-induced mass movements and are one of the most hazardous natural phenomena. Their considerable hazard potential is related to the abundance of susceptible areas, the high areal density and the high velocity of the movements. These shallow landslides can be triggered by rainstorms of high intensity and short duration or by prolonged rainfall of moderate intensity. The area under investigation has been affected by several rainfall-induced landslide events in the last years. On November 2000, a high-intensity winter storm hit the coast of the Ligurian Sea. Damage was particularly severe in Imperia Province where landslides caused three fatalities and severely damaged the infrastructure, private homes, agriculture, and the flower industry. Landslides were most abundant at Ventimiglia, near San Remo, and in the Armea and Argentina valleys. Soil slips were also reported near Mentone, in France. After the event, 1024 rainfall induced landslides were inventoried in an area of about 500 km2.

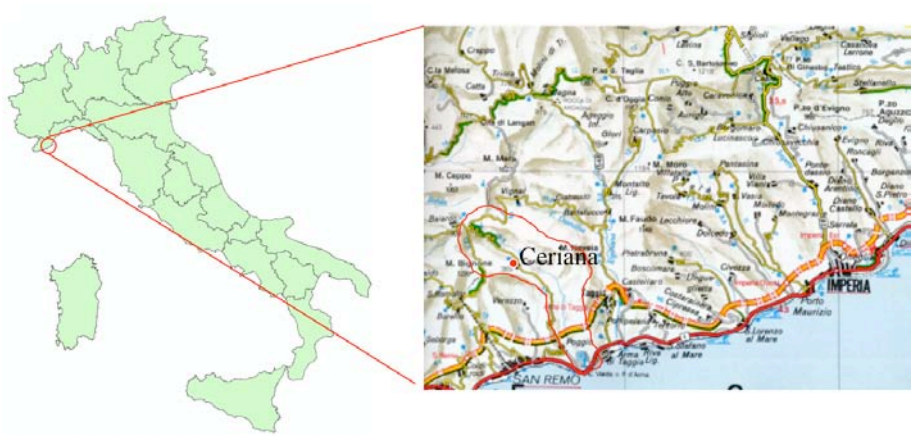

Figure 5.1: Geographic setting of the Armea basin

Landslides triggered by the high-intensity rainfall were both shallow and deep seated. Shallow landslides were mostly soil slips and debris flows. Most of the soil slips mobilized into debris flows. Debris flows travelled long distances (up to 1.5 km in the Armea valley), involving considerable volumes of material.

5.1.1 Geographic setting

The Armea basin is located in the western part of the Liguria region, in the province of Imperia, not far from the frontier between Italy and France.

This basin has an extension of 38 km^2 and it is entirely encompassed in the municipality of Ceriana and Arma di Taggia. The Armea stream begin in the Alpi Marittime and flows into the Mar Ligure with a total length of 16 km. In the northern part of the basin the watershed represented by the M. Colletazzo (1233m). M. Alpicella (1238), M. Merlo (10013) while in the western part there are the Punta Lodiro (1083), M. Bignone (1299) and M. Colma, and in the eastern part Punta Pistorin (483) and M. Santa Maria (463).

The studied area is not the entire basin, but just the middle and upper part for a total extension of 33 km^2. This part has been chosen because it is characterized by a mountainous morphology, consolidated bedrock and frequent occurrence of shallow landslides.

5.1.2 Geological setting and evolution

The geological evolution of this area is related with the Alpine orogenesis that occurred in this geographic setting between 90 and 40 million years ago (Late Cretaceous-Eocene). The area is usually subdivided in three paleogeographic domains: the Delfinese-Provenzale-Elvetico domain, the Brianzonese domain and the Piemontese domain (Menardi-Noguera, 1988).

The lithological succession that characterize the Armea basin is mainly constituted of turbidite deposits developed within a deep marine sedimentary basin, the Ligure-Piemontese Ocean, a branch of the Western Mediterranean Tethys. This ocean was located between the Insubric continent and the Paleoeuropean continent during the Late Jurassic-Early Cretaceous (Figure 5.2). When during

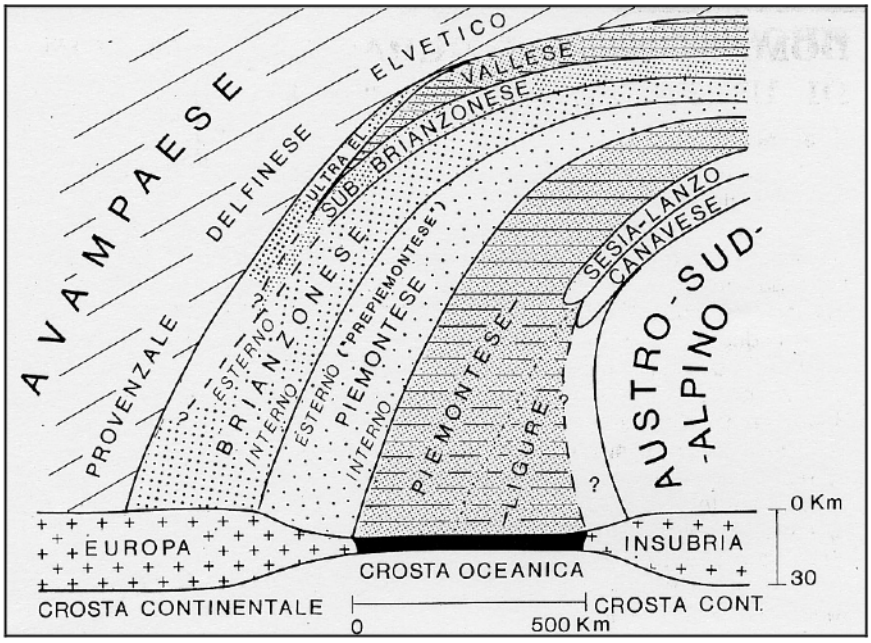

Figure 5.2: Paleogeographic scheme of the Alpi Liguri during Mddle-Late Jurassic (from Vanossi, 1991)

the Early Cretaceous the stress regime of the area became compressive, a fast relief growth occurred. The consequent rapid erosion of these reliefs provided the sediment mass for the turbidites deposition.

The closure of the Ligure-Piemontese Ocean and the Alpine orogenesis led to the building of a fold-and-thrust belt. The tectonic Unit of Sanremo-Monte Saccarello ovethrusted the Paleoeuropean continent. This unit was than overthrusted by Delfinese-Elvetico-Provenzale domain, represented in the Armea basin by the Ventimiglia Flysch and by the sedimentary melange (Complesso di Progressione della Falda del Flysch ad Elmintoidi).The southern part of the basin is characterized by Upper Pliocenic sediments, mainly sand, clay and gravel. These sediments are in contact with the lower turbidites with a trasgressive stratigraphic unconformity.

The major part of the studied area is occupied by formations included in the tectonic Unit of Sanremo-Monte Saccarello which represent the geometrically upper portion of the Alpi Liguri sedimentary wedge and is present in the Armea basin with all its geologic formations. These formations are, from bottom to top: Formazione di San Bartolomeo, Arenarie di Bordighera, Calcari di Monte Saccarello and Marne di Sanremo. The two last formations are sometimes combined together and called Flysch di Sanremo. The only formation present in the area which is related with the Delfinese-Provenzale-Elvetico domain is the Complesso di Progressione della Falda del Flysch ad Helmintoidi. This formation is divided within the geologic map in two different lithologic units: the sandy-pelitic flysch and the massive sandstones. The southern part of the test site area is occupied by plicenic sediments composed mainly by conglomerates,

sands and clays.

5.1.3 Geologic formations

This sector of the Alpi Liguri chain has been widely studied in the past and there exist many paper about the evolution of each single geologic formation. As a support during the field work and during the following parametrization of the soil properties, a geologic map (scale 1:10.000) has been used. This map was produced by researchers of the University of Pavia during the fieldwork for the basin planning named "Piano di Bacino del Torrente Armea e del Rio Fonti". This geologic map has been carefully checked during the fieldwork conducted for this PhD thesis and some minor changes to the exact position of few boundaries between formations have been added. The results are shown in figure 5.3.

In the **Unit of Sanremo-Monte Saccarello** are included from the bottom to the top the following geologic formations:

- *Formazione di San Bartolomeo*: this formation, even known as "Argilliti del Colle S. Bartolomeo", is composed of marine basin sediments characterized by a low sedimentation rate, mainly turbidites and hemipelagic sediments. The outcrops of this formation are located within the core of the anticline that characterize the structural setting of the middle Armea basin. This formation is in stratigraphic contact with the chaotic facies of the Ventimiglia flysch (Complesso di Progressione della Falda del Flysch ad Helmintoidi) on the bottom and with the Arenarie di Bordighera formation on the top. The lithologies are mainly quartzose-micaceous sandstones and brown-green pelites with manganese and iron oxides. In the upper part appear red and green clays, quartzose sandstone and thin layers of calcareous turbidites. The age is Late Campanian - Barremian. The exact thickness of this formation cannot be estimated due to the intense tectonic deformation.

- *Arenarie di Bordighera*: this formation has been divided in two different sedimentary facies, a distal facies and a channel facies. The first one represents the distal part of a turbiditic submarine conoid (Sagri, 1980). This facies crops out pervasively in the Armea basin with alternating thin turbidites and hemipelagites. The thickness of these layers varies between 5 cm and 30 cm. Lithologically it is composed of marnous limestone and calcareous marls with Helmintoides and Chondrites traces alternating with calcarenites, quartzose sandstone and micrites. The age can has been recognised as Late Campanian and the maximum thickness in this area is about 50m. The second facies of the Arenarie di Bordighera formation are sedimentary deposit that can be related with the proximal part of the submarine conoid. This facies is composed by coarse channelized deposit with sandstones, conglomeratic sandstones, conglomerates and massive sandstones. Turbidites of varying thickness can be found intercalated between the proximal fan deposit , especially in the upper part of the formation. The passage to the upper formation is gradual and signed by the progressive increase of the marnous-calcareous layers. The age of this second facies is Late Campanian - Maastrichtian and the total thickness is between 400m and 500m.

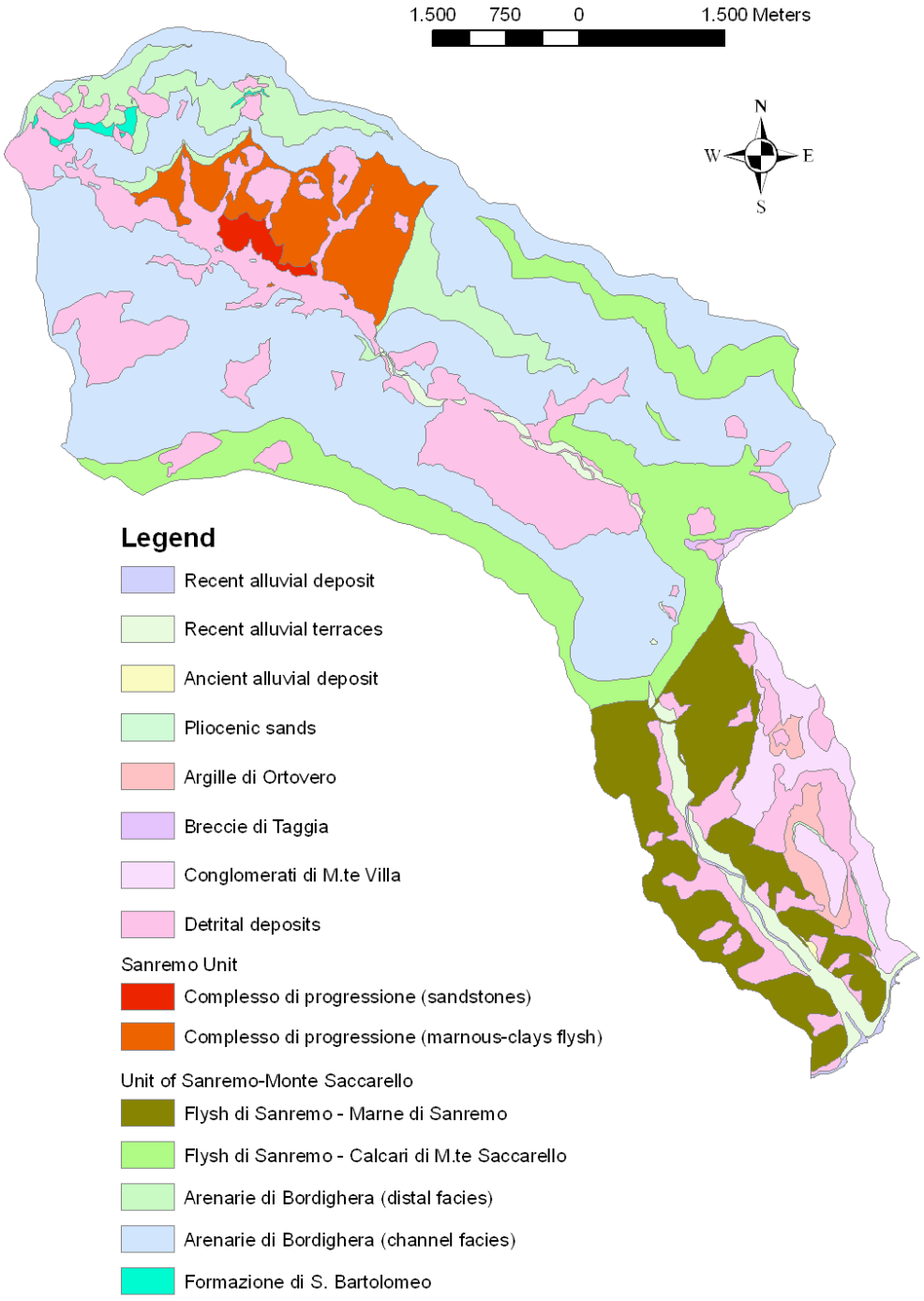

Figure 5.3: Geologic map of the Armea basin. See section 5.1.3 for a detailed description of the formations.

- *Calcari di Monte Saccarello*: this formation is included in the group of "Helmintoides Flysch". The depositional environment was a narrow basin with high sedimentation rates below the carbonate compensation depth (ccd). Lithologically it is composed by marls and calcareous sandstones (lithofacies "b" of Sagri, 1984) with minor calcilutites and arenaceous turbidites. The main outcrops are located along the ridge on the southwestern part of the basin. The passage to the upper formation is gradual and signed by the progressive increase of the marnous-calcareous layers. The age of the Calcari di Monte Saccarello formation is Late Campanian - Maastrichtian and the maximum thickness is about 300m.

- *Marne di Sanremo*: this formation is composed of arenaceous and clay layers (lithofacies "d" of Sagri, 1984) with minor intercalations of calcilutites and arenaceous-marnous layers. Interlayers are constituted of silt and clay with thickness up to few decimeters. The age is Maastrichtian.

In the **Delfinese-Elvetico-Provenzale Domain (Sanremo Unit)** is included only one formation:

- *Complesso di progressione della Falda del Flysch ad Helmintoidi*: this formation represents the chaotic facies and stratigraphically higher, of the Ventimiglia Flysch formation. It is composed by a marnous-clays olistostromes with sandstones and some detrital extra-basinal clasts included. The caotic appearance is due not only to synsedimentary reasons but even to the intense tectonic deformation occurred and especially to the final overthrusting of the Unit of Sanremo-Monte Saccarello. Outcrops of this formation are visible only in the tectonic window known as "Finestra tettonica di Ceriana". The total thickness in unknown and the age is Priabonian.

The **Quaternary Deposits** present the area are:

- *Alluvial terraces*: these deposits are terraced embankments of loose material adjacent to the sides of the river valley. The granulometry of these sediments is heterogeneous with gravels, sands and silts. The gravels lithotypes are mainly sandstones and limestones. These terraces are often occupied by anthropic activities and different type of infrastructures. In the southern part of the Armea basin, not far from the coastline, these deposits can reach thicknesses of more than 20m but in the studied area, in the middle and northern part of the basin, the thicknesses are usually limited to a maximum of a few meters.

- *Detrital deposits*: these deposit are widely present in the Armea basin especially in areas occupied by the Arenarie di Bordighera formation (channel facies) where they can reach the thickness of more than 3m. They are composed of incoherent deposits with varying granulometry and composition that can be classified as eluvial deposits, colluvial deposits, paleolandslides and talus-debris slope.

5.1.4 Tectonic and structural setting

Among the structural features that characterize the Armea basin one of the most important is the thrust fault that led to the superimposition of the Sanremo-Monte Saccarello Unit over Delfinese-Elvetico-Provenzale domain. This event, occurred between Late Cretaceous and Late Eocene consist of a tectonic translation of the entire unit from the basal complex to the more recent formations. This thrust fault is visible in correspondence of the Ceriana tectonic window.

The entire Sanremo-Monte Saccarello Unit shows a polyphase plicative deformations that can be related with the overthrusting and to the compressive stress regime occurred during the build up of the Alpi Liguri fold and thrust belt (Merizzi & Seno, 1991). In the formations were massive competent sandstones and limestones are prevalent, the main deformation pattern consists of a fracture cleavage instead of schistosity. The basal complex is instead characterized by a pervasive plastic deformation.

The main structural feature that dominate the area is the presence of syncline and antycline mega folds with sub-horizontal axial planes and South-West vergence. Sometimes faulting occurs along the hinges of these folds so as many zones of non-coaxial shear strain can be found within these formations. From North to South there are 4 main folds: the Monte Alpicella antycline, the Costa dei Frati syncline, the Ceriana antycline and the Monte Bignone syncline.

The last tectonic regime activated in the Armea basin is a distensive regime that has led to the development of near vertical normal faults (oriented North-West/South-East and North-East/South-West) and a regional fracture pattern. To these faults is associated the seismic activity registered in the area.

5.1.5 Geomorphological setting

The Armea basin is characterized by a high relief energy. There are mountains higher than 1200 m (the highest, Monte Bignone, is 1299m a.s.l.) with deep narrow valley. The slope angles are quite high with a mean slope gradient of 27% and a maximum of 50° calculated analysing a 5m resolution digital elevation model (Figure 5.4). These slopes lead to a widespread erosion due to the intense surface runoff. At the same time the high gradients make the slopes more prone to slope instability especially where there are bedding planes oriented in the direction of the slope and where the bedrock is pervasively fractured or deeply altered. The high erosion rates that characterize the Armea basin determine the widespread presence of detrital deposits classified as eluvial, colluvial and talus-debris slope deposits. The thickness of these deposit is often more than 3m. The granulometries are varied ranging from from silt to blocks up to more than on meter. The matric composition is deeply affected by the bedrock lithology and range between silt where there are fine grained lithotype to sands for coarser lithotype. The maximum thicknesses of the detrital deposits are reached along the slopes of the right side of the Armea basin. In these thick deposits there are many suspended groundwater bodies and on the boundaries, due to the high permeability contrast between the sandy-deposits and the lithoid bedrock, the groundwater level crops out as shown by the presence of many springs.

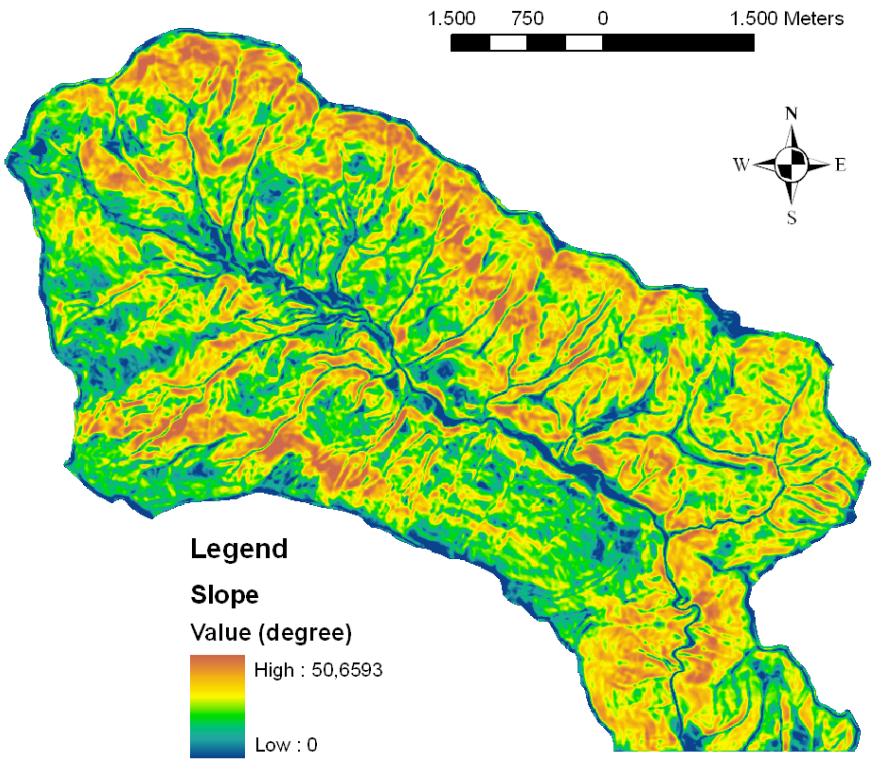

Figure 5.4: Slope map of the Armea basin obtained analysing a 5m resolution digital elevation model

5.1.6 Landslides type and occurrence

The Armea basin is characterized by a widespread slope instability. The presence of many type of landslides, quiescent and active, is due to many reasons: the high slope gradients, the poor conditions of the bedrock, widespread presence of detrital deposits and, especially in the northern part of the basin, to the bedding planes oriented in the direction of the slope.

The landslides occurred in the Armea basin are both deep and shallow but the second one are the most. The deep landslides are usually characterized by a rotational-translational movement and can be classified as complex. Shallow landslides of the Armea basin are soil slip, soil slump, earth flow end debris flow. The majority of these landslides are located in the northern and central part of the basin, usually triggered by heavy rainfall events like that occurred in November 2000 in December 2006. Shallow landslides occurrence is a widespread phenomena in all the basin and are usually located where the slopes are higher and the soil depth is between a few decimeters to one meter or something more, independently of the lithology of the bedrock. Deep landslides instead are located especially in correspondence of thick detrital deposit or where the bedrock alteration is quite deep and pervasive.

5.1.7 Event occurred on November 2000

Between October and November 2000 in the entire Liguria region heavy rainfalls occurred with a total cumulative for the 45-day period higher than 1000mm. In some places the cumulative rainfall exceeded 70% of the mean annual precipitation (Guzzetti et al., 2004). On November 23, at the end of this very wet period, an intense rainfall event hit the Imperia Province and the Armea basin. In proximity of the Armea basin, where the landslides where more abundant, only two rain gauges where available: the San Remo rain gauges, located along the coast and the San Romolo rain guge located about 5.5 km inland at an elevation of 795 m a.s.l.. By interpolating these data Guzzetti et al. (2004) obtained a spatial distribution of the rainfall event (Figure 5.5) that shows a high intensity rainfall centered on the Armea basin. According with the Sanremo rain gauge the cumulative rainfall was about 170 mm while at San Romolo was about 240 mm. Unfortunately no quantitative radar rainfall data were available for the Armea valley but witnesses suggest that the cumulative rainfall was very high, similar or higher than that recorded by the San Romolo rain gauge and with a very high intensity.

Landslides triggered by this rainfall event were a total of 1024 in the entire Imperia Province (Guzzetti et al., 2004). This result was obtained by the interpretation of 334 aerial photographs taken 45 days after the event. More than 300 of these landslides were located in the Armea valley, as confirmed by the landslide inventory provided by the Imperia Province in collaboration with the Università degli Studi di Firenze. These landslides were both shallow and deep. The major part of the shallow ones were classified as soil slip and debris flow. Debris flows, usually starting as soil slips and then mobilized into flows, reached distances up to more than 1 km during the runoff phase and involved considerable volumes of material (Figure 5.6 a). Numerically soil slips were the most abundant while the deep ones were those involving highest volumes of material. Among deep landslides two of these (Bestagno and Mainardo land-

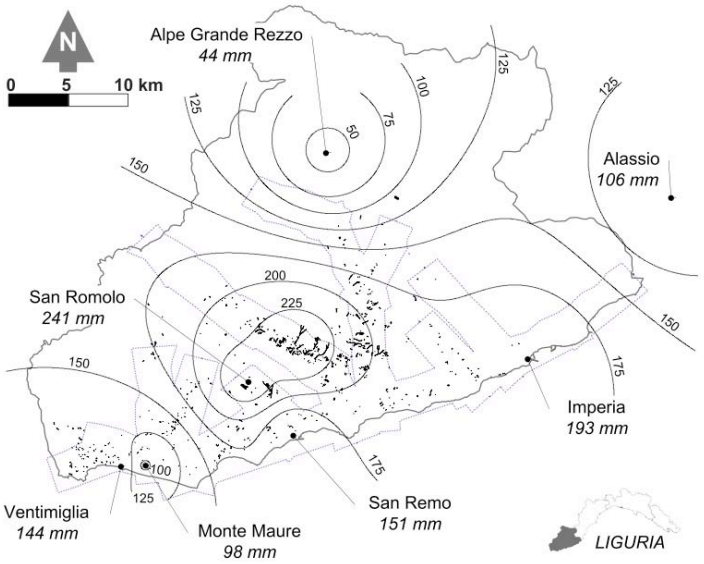

Figure 5.5: The spatial distribution of cumulative rainfall occurred on November 23 in the Imperia Province (from Guzzetti et al., 2004)

a) b)

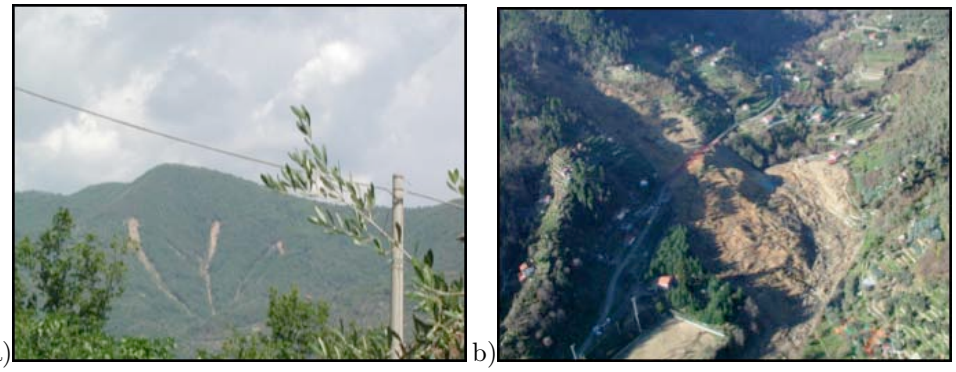

Figure 5.6: Landslides triggered by the rainfall event of 23th november 2000 in the Armea basin. a) Debris flows along which reached runoff distance of more than 1km. b)The Bestagno landslide which damaged the provincial road n°55 and killed two people.

a)  b) 

Figure 5.7: Landslides occurred in the Armea basin on 8 December 2006. a) Soil slip near Ceriana b)The landslides which damaged a main road, destroyed a car and injured the occupant.

slides), classified as complex slump-earth flows, resulted in many damages to infrastuctures. Moreover, the Bestagno landslide, occurred during the night of 23th of November, killed two people in their house (Figure 5.6 b).

5.1.8 Event occurred on December 2006

On 8 December 2006 a storm occurred in the Armea basin. Although it was significantly smaller than the 2000 event it nonetheless triggered several superficial landslides and caused a certain amount of damage. One landslide damaged a main road, destroyed a car and injured the occupant (Figure 5.7b). A field survey conducted in the week following the event confirmed the occurrence of several tens of landslides in the basin. For each landslide at least one photo was taken, the crown and toe coordinates were acquired by means of a GPS and a brief description indicating type, size and location have been drafted. Unfortunately the weather condition didn't allow to reach every part of the Armea Basin and in some cases it was possible to achieve only a visual description and a photo. For that reason a satellite image was ordered to complete the inventory map of the new landslides.

Differently from the 2000 rainfall event, for the rainstorm occurred on December 2006 it has been possible to achieve the radar rainfall map recorded by the Monte Settepani weather radar and elaborated by the CIMA as described in section 4.2.

5.1.8.1 High definition satellite image acquisition and orthorectification

Optical satellite remote sensing technology has recently been exploited for landslide hazard and risk assessment (Metternicht et al., 2005), since it is capable of providing reliable, cost-effective and repetitive information over wide areas. Very high resolution (VHR) satellite imagery (Ikonos, Quickbird, Orbview, Worldview) can provide a powerful tool for a quick reproduction of a map, up to a scale of 1:2000, of local events: they thus represent a viable tool in many fields, including landslides, to provide important observations that supplement traditional observations from field reconnaissance (Casagli et al., 2005). In fact, one benefit of obtaining satellite imagery is the ability to evaluate the extent of

damages even in areas where field surveys are difficult. Furthermore, because satellite imagery covers a large area, it allows one to consider fully the context of the environment and potential interactions between failures. These observations are difficult to formulate from the ground during traditional survey and can complement field reconnaissance observations. Following the landslides occurrence in December 2006, a multispectral, pan-sharpened Quickbird satellite imagery was acquired on 13th of March 2007, three months after the events, with a mean ground pixel size of 0.65 m; the average sun azimuth and elevation angles at the acquisition time were 160.82º and 41.62 º respectively while the off nadir angle was 14º. The image was orthorectified using the rational polynomial coefficients (RPC) model and selection of seventy distributed ground control points (GCP) retrieved from recent topographic maps at 1:5.000 scale. The elevations of the points were taken from a digital elevation model (DEM) with a grid resolution of 5m, produced from the digitized topographic maps with a contour interval of 5 m. Data have been processed through radiometric enhancement in order to produce the best false colour composites for visual interpretation. Simple red-green-blue colour composites were used as the most effective way for landforms interpretation; the image allowed to accurately identified new landslides as small as 2-3 m in width as well as relict landslides, in the whole basin. The photointerpretation of satellite image was performed in a GIS environment using the typical criteria of spectral reflectance and texture analysis. Main interpretation keys were gathered from the ancillary data, photos and observations collected during the field work.

5.1.8.2 New landslide database for the validation of the model

With the aid of the new VHR satellite imagery it was possible to recognise all the landslides triggered by the event of December 2006 (Figure 5.8). Comparing the new landslide database obtained by photointerpretation with the old landslide database, it was possible to find out if these new landslides were actually new or otherwise a reactivation of old ones, maybe those occurred in November 2000. The new geographic database is made of 148 entries. Each entries has four attributes: x coordinates, y coordinates, landslide area and a distinction between new landslides and reactivated ones. The results of this photointerpretation has been validated during the fieldwork when the most of these landslides has been recognised.

5.1.9 Field work and base data collection

The aim of the fieldwork was to collect data regarding various aspects of the Armea basin, with the main focus on soil parameters(e.g. thickness, hydraulic conductivity) in the areas where an exceptional storms triggered landslides in 2000 and 2006. The data gathered has been used for calibration and validation of the soil depth model (see section 5.1.11) and factor of safety models, as a part of the activities for the realization of the PREVIEW project.

Saturated hydraulic conductivity was measured with an Amoozemeter in several sites and at different depths (Figure 5.9). In particular, a superficial landslide next to the town of Ceriana was target of 4 measurements involving different lithologies present in the basin and, where possible in locations where landslides occurred in 2000.

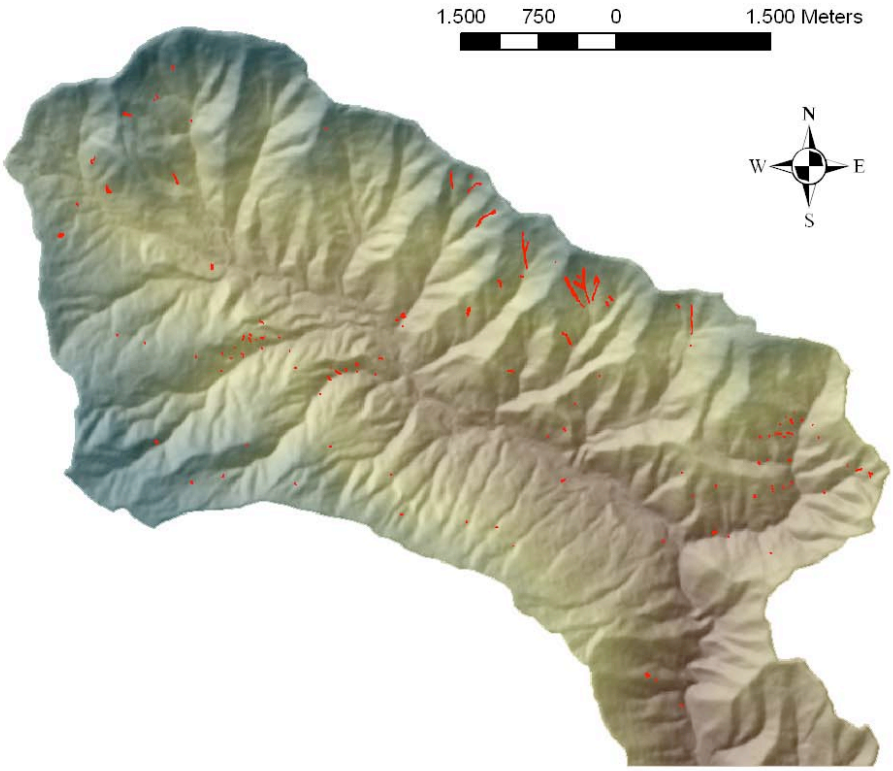

Figure 5.8: The new geographic database of landslides occurred on 8 December 2006 in the Armea basin

Figure 5.9: Measuring saturated hydraulic conductivity with the Amoozemeter

At all locations where hydraulic conductivity was measured soil were collected. Laboratory tests has been performed on the samples to determine grain size distribution, plasticity indexes, angle of internal friction, etc.

The largest amount of time was spent collecting soil depth data. At each location the depth of the soil to the bedrock was measured with a tape measure, where present the different soil layers were described, at least one photo was taken and the site coordinates and elevation were acquired by means of GPS. This data was collected in the proximity of landslides and also in as many portions of the basin as possible, including at low, intermediate and high elevations and in different geomorphic and geolithological settings. The aim was to acquire a spatially distributed data set representative of the different soil conditions present within the basin. It should be noted that the measurements were constrained by the availability of outcrops, mainly located along roads cuts.

5.1.10 The new digital elevation model

At the beginning of this study a good quality digital elevation model (DEM) was lacking for the Armea basin. The only DEM available was that developed by the Istituto Geografico Militare (IGM), characterized by a resolution of 20m and derived from a topograpic map (scale 1:25000) projected in the Gauss-Boaga coordinate system. It has been immediatly clear that this DEM was not suitable for the objective of this study for many reasons: first of all the 20m resolution was not enough to derive the topographic and geomorphological features needed for the stability model. Along each slope the spatial variability is very high so as a 20 meters DEM would fail to show important changes in slope angle and curvature. Moreover a careful inspection of the DEM showed the the presence of many errors (small valley that should be actually a hill and viceversa) probably due to the semi-automatic processes used during the conversion from the original vector format to the raster file.

In order to have a good base to use for slope stability modelling it was necessary to build ex novo a new digital elevation model. There was not a digital topographic map availabble better than that provided by IGM so it was necessary to digitalize a new topographic map provided by the Liguria region and characterized by as scale of 1:5000 (Cinti, 2007). The topographic map has been georeferenced in an UTM32 WGS84 coordinate system and then digitalized

obtaining e vector format. This file has been then treated with the tool named TOPOGRID within an ESRI ArcGIS 9 software environment to obtain as a final result a good quality, 5m resolution digital elevation model. This DEM has been used as a base for every topographic and morphometric analysis during this work.

5.1.11 Soil depth modeling (GIST)

A distinctive feature of this work is the attention paid to the use of soil thickness as an input data for landslides forecasting. Several studies have shown that soil thickness is one of the most important parameters controlling shallow landslide initiation (Johnson & Sitar, 1990; Wu & Sidle, 1995; Van Asch et al., 1999). Even if there are many methods to estimate soil depth at discrete measure-points or at least at the slope-scale, no effective models have been proposed so far to easily predict soil thickness over sites as large and as geologically heterogeneous as the Armea catchment. Therefore at present when this parameter is needed in basin scale modelling, a constant value (inferred from a few in situ measurements) is often used. This is an extreme simplification, since soil thickness shows a very high spatial variability (Birkeland, 1984; Taylor & Eggleton, 2001; Selby, 1993). To take this variability into account, sometimes spatially distributed soil thickness maps are obtained by means of mathematical correlations with a simple morphometric attribute (slope gradient or elevation are the most used) (Salciarini et al., 2006; Saulnier et al., 1997). Anyway this method is mainly employed because it grants a simple and quick application; if we consider that soil thickness patterns are the result of complex interactions between many interplaying factors (topography, lithology, vegetation, climate, human activity...) it's clear that such a simple technique is fated to fail whenever applied at large scale (Segoni, 2008). For the landslide forecasting tool presented here I utilize an empirical model developed at the Department of Earth Sience in Florence and known as GIST (Segoni, 2008; Segoni & Catani, 2008). The model is based on three morphometric attributes (slope gradient, slope curvature and position within the hillslope profile) and on geomorphological and lithological criteria. GIST model hasn't been used uncritically, as it has been tested and validated in the Armea catchment before being used in this work. It is an empirical model that can produce distributed soil thickness maps at catchment scale with an high spatial resolution (5m in this work); it uses cheap and easily available data and gives a major importance to geomorphological and geological factors (Segoni, 2008; Segoni & Catani, 2008). The model links soil thickness to gradient, curvature and relative position within the hillslope profile. While the relationship with gradient and curvature should reflect the kinematic stability of the regolith cover, allowing greater thicknesses of soil over flat and concave areas (Braun et al., 2001; Heimsath et al., 1999), the distance from the hill crest (or from the valley bottom) should instead account for the position of the considered soil unit within the soil catena (Carson & Kirkby, 1972; Conacher & Dalrymple, 1977; Moore et al., 1993). This last parameter is fundamental: points having equal gradient and curvature can have very different soil thickness due to their different position along the hillslope profile. To be applied, this newly developed model requires a few computations to be carried out in a GIS system and a geomorphological survey aimed to recognize the soil catena typical of the hillslopes and to acquire soil thickness measures needed

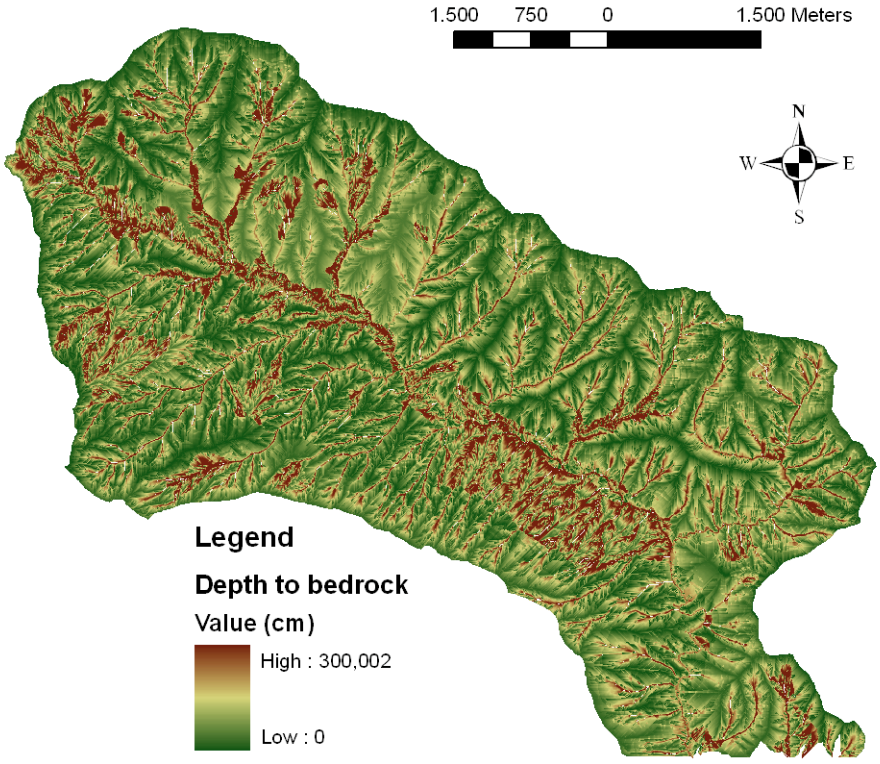

Figure 5.10: Depth to bedrock map of the Armea basin obtained with the GIST model

for the model calibration (Segoni, 2008). The obtained soil thickness map (5m resolution) is shown in Figure 5.10 and a high dependence on bedrock lithology and on the relative position is clearly detectable. In fact a general tendency of the soil to thicken towards the valleys is noticeably and sharp discontinuities are met at the boundaries between very different geological units. Both trends match with field observations. In particular, shallowest soils are met in the calcareous lithotypes (as they usually outcrop at divides and because they undergo a slow pedogenesis), while the highest thickness values are situated in down-valley debris accumulations. The soil thickness map obtained by means of the GIST model has been validated before being used in the service. In order to validate the results, soil thickness was measured in 91 sample points during the field survey. The comparison between the expected (calculated by the GIST model) and observed (measured in the field) soil thickness measures reveals that the overall performance of the model is quite satisfactory: the mean absolute error is 28cm, with a 27,75cm standard deviation (Segoni, 2008). If we consider the accuracy needed in basin scale modellings and the fact that soil thickness in the Armea Creek catchment varies from 0 to 300cm, this degree of precision can be considered acceptable. Looking closer at the errors, the substantially correct estimations (error between -10cm and +10cm) are the 31%, and acceptable errors (abs errors from 11 to 30cm) are the 36%. The high errors are a small number and in their vicinities or in analogue positions correct estimations are achieved as well. This outcome suggests that the main errors could be due to an "ambient noise" which complicates the soil thickness spatial pattern and makes very difficult to model it in the Armea Creek basin. If we consider the four largest errors as anomalous data and we remove them from the sample point population, the mean absolute errors is reduced to 23cm with a 17,01cm standard deviation.

5.2 Island of Ischia

The island of Ischia is located in the southern part of the Tyrrhenian sea, between 40°44' North latitude and 13°56' East longitude, 33 km far from Naples. This island is 7 km wide from North to South and 10 km from East to West. The coastline is 39 km long and the total surface is 46 km^2.

The island of Ischia is a volcanic island even though the highest mountain, the Monte Epomeo (787 a.s.l.) is not a volcano but a horst of volcanic rocks uplifted by tectonic movements. The volcanic activity of Ischia has been characterized by small eruption quite distant in time between each other. The last one occurred in in 1301 D.C. (the Arso eruption, a flow which reached the coastline in the eastern part of the island) while the previous occurred during the roman age.

The island is divided in six municipalities: Ischia, Casamicciola, Lacco Ameno, Forio, Serrara Fontana e Barano. The total population is about 50.000 but in the summer season it can increase up to 300.000 people

5.2.1 Geological setting

The geologic history of Ischia begins when the tectonic stress regime in western margin of the central-southern apenninic chain became distensive. In this

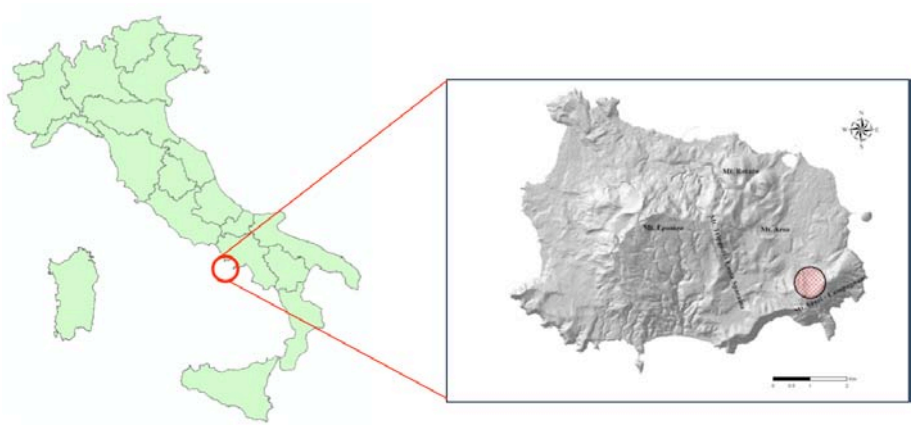

Figure 5.11: Geographic setting of the island of Ischia

context the tyrrhenian margin started to sink up to 3000m of depth b.s.l. The seafloor was characterized by a horst and graben structure and the main faults at the boundaries of the blocks were oriented East-Northeast/South-Southwest (known as anti-apenninic direction) and Northwest/Southeast (known as apenninic direction). One of these graben, extended in a Northwest/Southeast direction, is the Campanian plain which is interrupted by three structural high: the Campi Flegrei caldera and the Procida and Ischia volcanic islands. The faults that border this block have deeply influenced the past volcanic activity that was characterized by a trachitic, trachibasaltic, latitic and phonolitic magmatism.

During the Late Calabrian ingnimbritic eruptions overlaid a wide area of the actual tyrrhenian plain and when the stress regime became distensive and these rocks were thrown up to a deep marine environment, the igninbrites were altered and became green tuffs. Then a magmatic intrusion between the marine sediments and the green tuffs resulted in an uplifting of the entire area up to the emersion of a peninsula connected with the mainland by an isthmus (Figure 5.12). The uplifting due to the intrusion led to an additional fragmentation of the magmatic basin which assumed the horst and graben structure. About 28000 year ago another differential subsidence interested the area as a result of a huge explosive eruption. A new volcanic cycle began and different type of magmas erupted along the fractures according to the area of the volcanic basin from where the magmas were arisen. After the successive regional subsidence that interested the entire tyrrhenian sea, only the Ischia tectonic horst remained above the sea level Rittmann & Gottini (1980).

The Monte Epomeo, the highest mountain of Ischia, has been described in the first studies as a volcano (Fonseca, 1870; Fuchs, 1873; Mercalli, 1884). Just in the last decades the new theory proposed by Rittmann & Gottini (1980) has been accepted and the Monte Epomeo has been recognized as a structural horst instead of a volcano. Near the Monte Epomeo there are many eruptive centres, pyroclastic cones, lava domes end lava flows that have been active during and after the rising of the horst.

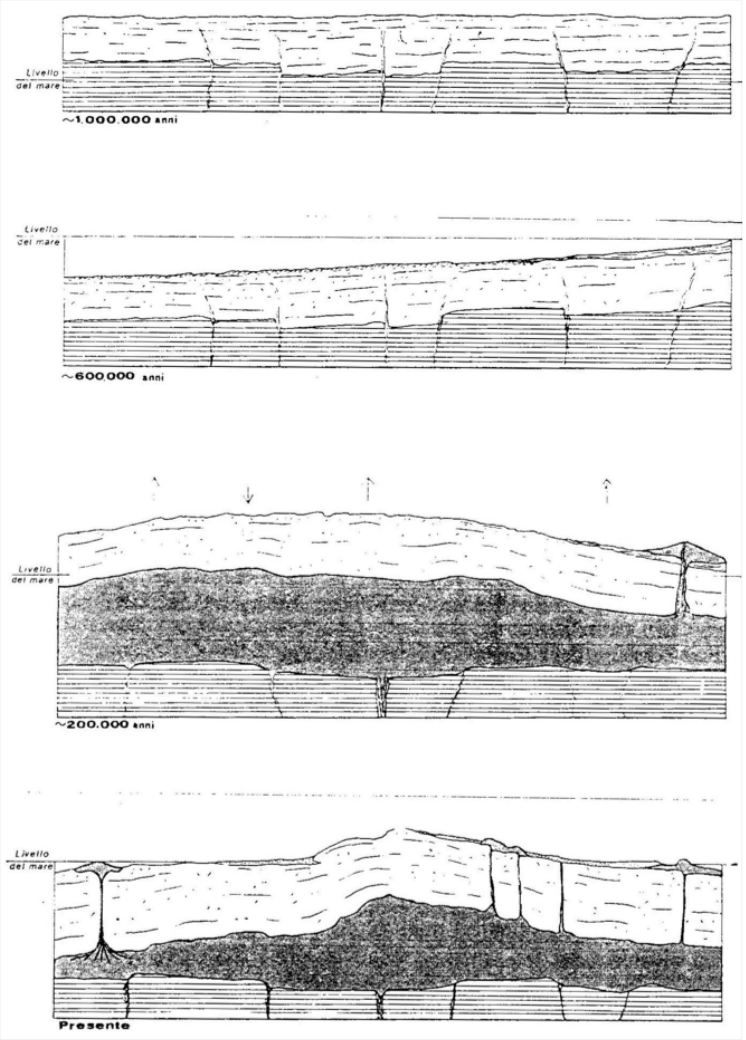

Figure 5.12: Geologic evolution of the island of Ischia (from Rittmann & Gottini, 1980). See text for explanation.

5.2.2 Volcanic activity and geologic formations

The volcanic activity can be divided in five phases:

1. Prior to 150.000 years ago
2. Between 150.000 and 75.000 years ago
3. Between 55.000 and 35.000 years ago
4. Between 28.500 and 18.000 years ago
5. Between 10.000 and 1302 years ago

The first two phases are grouped in a first main magmatic cycle while the last three compose a second cycle. The product of the first cycle can be found along the perimeter of the island (with the exception of the Lave del Rione Bocca formation) while the others related to the second cycle occupy indistinctly both the perimeter and the centre. Between these two cycles a break of the volcanic activity allowed the development of erosion surfaces and the deposition of alluvial sediments and slope detritus that can be found interposed between the product of the first and of the second magmatic cycle.

First phase:

During the first phase, thick pyroclastic flows (about 200m) intercalated by thin alkali-trachitic lava layers were deposited. The emission point of the products deposited during this phase cannot be found due to the lack of widespread outcrops. The few outcrops present in Ischia can be observed in the southern part of the island, along the "Scarrupata di Barano" cliff.

Second phase:

This phase is characterized by the formation of many alkali-trachitic lava domes. They probably developed for the uprising of magma along the boundaries of a calderic structure in the southern part of the island (Chiesa et al., 1985). The main domes are located in correspondence of Punta Imperatore, Monte Vezzi, Capo Negro, Sant'Angelo, Punta della Signora, Capo Grosso,Punta Chiarito, La Guardiola and Castello d'Ischia.

The following formations are included in this phase:

Lave del Rione Bocca: a trachitic lava flow along the western side of the Monte Epomeo. In the upper part this flow is made of scoriaceous layer while in the top, due to the alteration, the lava has a vacuolar aspect. The main body, highly fractured, is characterized by a dark grey color, aphanitic aspect with many sanidine crystals. According with Gillot et al. (1982) this formation has an age of 133.000 years. This is the only formation of the first cycle that can be found inland instead of on the perimeter of the island.

Formazione Superiore della Scarrupata di Burano: this formation can be divided in two part. The first one is made of pyroclastites, fall pumices with scoria and ossidiana layers. The second part is instead a lava flow with pyroclastic deposits which crops out along the north-western side of Monte Vezzi. The total thickness of the formation is about 85m while the thickness of the lava flow is 50m.

Volcanic center of Monte Vezzi: this formation is made by a trachytic volcanic dome. The core is a bright grey body highly fractured while on outer parts

the rocks became micro vacuolar. The promontories of Punta San Pancrazio e Punta della Cannuccia are entirely occupied by this formation.

Third phase:

The main formation that can be referred to this phase are:

Formazione del Pignatello: this formation, with a maximum thickness of 65m, is composed by layers, up to more than 1m, of fall dawn pumices and lapilli alternated with few black scoria layers.

Tufo verde del Monte Epomeo: this formation occupy the western part of the island and the area of the Monte Epomeo. The rocks have been dated by Gillot et al. (1982) at 55.000 years. The formation can be divided in three main facies: the soldered facies, which compose the tectonic horst of Monte Epomeo, is characterized by tuffs with biotite and alkali feldspar and layers of pumices. This facies is a subaerial deposit which filled the preexisting caldera and then was subjected to a marine transgression (Chiesa et al., 1985). This marine phase is very important because the circulation of water within the tuffs led to the alteration of the glauconite that give to the rocks the characteristic green color. The marine environment caused even the deposition of the Tufite del Monte Epomeo and the Colle Jetto formation.

The second facies is not soldered and enriched with a cineritic matrix. The main lithologies are those typical of a pyroclastic flow: ashes and pumices with abundant granular matrix and volcanic bombs. The main outcrops of this facies can be found in correspondence of Monte Vico, Punta Imperatore and along the Scarrupata di Barano.

The last facies is made of surge and pyroclastic flow deposits. This facies doesn't shows the characteristic green colour so it can be inferred that it was not subjected to the marine transgression like the others. It was deposited near the emission centre that was probably located between Sant'Angelo and Maronti. The main outcrops can be found at Sant'Angelo and to the north-east respect to the Lido dei Maronti.

Formazione di Citara: this formation is probably due to a single volcanic explosion occurred about 28.000 years ago (Rittmann & Gottini, 1980) with an emission centre that was probably located near Forio. After this eruption the laccolitic basin developed between the mesozoic limestones and the upper Formazione del Tufo Verde was emptied and this probably led to a new tectonic regime characterized by a differential subsidence. Recently many new eruptive centres have been recognized like those of Sant'Angelo, Pietre Rosse e San Montano (Chiesa et al., 1985). These centres should have been active between 44.000 and 35.000 years ago.

Fourth phase:

The volcanic products of this phase can be found mainly in the area of Panza and near Monte Vezzi, in the eastern part of the island. This phase has been mainly effusive resulting in many lava flows and lava dome like those that can be found in the area of Panza where they are overlaid by a pomiceous formation (Scarruppo di Panza) and by the alkali-trachitic lava flows of Schiappa and Pomicione. In the eastern part of the island this phase is represented by the Lave di Sant'Anna, a lava flow produced by an effusive event about 22.000 year ago. Can be included in this phase even the lapilli cones of Ciglio and Cava Petrella. In some areas, like near Monte Vezzi and Monte Cotto, the pumiceus deposit of this phase has been depisited directly on the top of the Tufo Verde del Monte Epomeo formation.

Fifth phase:

The fifth phase is characterized by many volcanic eruptions mainly occurred in the eastern part of the island. Many of the emission centres were disposed along the main faults oriented North/South which bound the eastern part of the Monte Epomeo horst. Along those faults there are the lava domes of Costa Sparaina, Monte Trippodi, Selva del Napolitano, Piedimonte and Cannavale for a total of 188 domes. Other domes aligned in correspondence of the fault oriented North-East/South-West, on the northern side of the horst, are those of Vateliero, Molara and Cava Nocelle. Where two fault systems intersect each other near Montagnone, many eruptive centres developed between the VIII century a.C. and the I century a.C. leading to the formation of many lava domes and pyroclastic cones. Along the same faults complex, in correspondence of a small graben, developed the volcanic centre of Porto d'Ischia whose eruption has been described by Plinio in "Naturalis Historia". Another volcanic system developed at the intersection of the faults systems oriented North/South and North-South/South-East is that of Monte Rotaro. This mountain is a strato-volcano characterized by an alternation between pumices and lavas. Punta la Scrofa along the coast is a lava flow originated from the Monte Rotaro volcano between 1.400 and 800 years ago (Gillot et al., 1982). Between 6.000 and 2.200 years ago (Gillot et al., 1982) a new eruptive center grew near Zaro, in the northern-western part of the island. The volcanic products of this eruptive center are the Zaro lava flow the pumiceous pyroclastic deposid in the Baia di San Montano. The last volcanic occurred in the Ischia island is the Arso lava flow that began in January 1302 and went on for two months (Chiesa et al., 1986). This flow originated along a fault oriented North/South near Fiaiano.

Other than all these volcanic units there are other two formations mainly composed of marine deposit and that overlay the Tufo Verde formation of the Monte Epomeo:

Tufite del Monte Epomeo: derived from the alteration, erosion and redeposition of the Tufo Verde formation it is composed of tuff with a green silty matrix and sanidino clasts, pumices and lavas. The thickness varies between 30 and 50 metres.

Colle di Jetto formation: this formation is composed of an alternation between white siltites, ashes and yellow sands with a maximum thickness of 100m. These deposits are the product of the erosion of the volcanoes of the area with the exception of the ashes that was originated during volcanic events in the area of the Campi Flegrei (Chiesa et al., 1985). The age of both this formation can be fixed between 55.000 (the age of the Tufo Verde formation) and 35.000 years ago (the age of the Citara formation) (Chiesa et al., 1985).

5.2.3 Geomorphological setting

The geomorphological evolution of the island of Ischia is strictly related with his tectonic and volcanic activity and in particular with the development of the Monte Epomeo structural horst. The uplifting of this horst started about 30.000 years ago with an asymmetric movement that led to the development of different morphology in different areas of island.

The southern slope of the Monte Epomeo horst, corresponding with the Fontana basin, is characterized by shallow detrital deposits derived from the superimposition of many debris flows, paleosoils and pyroclastic deposits (Bor-

toluzzi et al., 1983). In the southern part of the Fontana basin can be recognized more than one order of marine terraces (Del Prete & Mele, 1999). A peculiarity of this basin is the dendritic drainage pattern with deep v-shaped valley and widespread gully erosion.

The major vertical movements due to the asymmetric uplifting of the horst have taken place in the northern part of the island leading to the partition of the area in many isolated blocks bounded by slope faults. This area is characterized by a dendritic drainage pattern and a torrential regime.

The western sector of the island is similar to to northern one with sub-vertical slopes due to the fault movements and many fractured isolated blocks. Huge detritic deposit form an almost flat area characterized by slope angles lower than 10°. The drainage pattern is poorly developed in this sector with the only exception of the Corsare-Monterone torrent with many branches so as it can be classified as a second order stream.

The eastern part of the island is characterized by the presence of a near flat area, the Ischia graben, and it is limited towards South-East by the structural high represented by the Monte Vezzi, Monte Barano and Il Torone, towards West by the lava domes of Monte Trippodi and Costa Spariana, towards North-West by the craters of Fondo Ferraro and Porto D'Ischia and the domes of Montagnone and Maschiata. All the geomprphological features present in this sector are related with the volcanic activity and with the uprising of magmas through the main faults. The drainage pattern is poorly developed and often the streams don't reach the sea but flow into an endorheic basin.

Almost the entire island of Ischia is characterized by steep cliffs, up to 200 m high, for a total of 36 km. Locally along the coastline is possible to find small sandy and pebbly beaches, usually deposits of old landslides occurred along the the sheer cliffs behind.

Many areas of the island are obviously characterized by geomorphological features that can be related with the volcanic activity like remains of old cones (e.g. Monte Vico and Monte Rotaro), craters (e.g. Campotese and Fondo Ferraro) and crater edges (e.g. Scarrupo cliff).

5.2.4 Landslides type and occurrence

For the Island of Ischia the situation is more complex respect to the Armea basin as fewer information are available. Prior to 2006 very little information regarding shallow landslides are available. These events certainly have occurred in the past as the both the geologic and geomorphologic settings of the territory are very similar to other areas in Campania, namely volcanic soils overlying steep massifs, where landslides have occurred frequently and with catastrophic effects. Moreover, many debris flows deposits have been found within the volcanic succession the same as geomorphologic evidences of deep landslide especially an the western side of the island and near Monte Vezzi (de Vita et al., 2006). However, as no precise documentation exists regarding earlier events it is not possible to create a comprehensive landslide inventory.

Accurate information exists only regarding the 26 April 2006 rainfall event that triggered four landslides and caused the death of four people. These landslides were inventoried and the resulting map has been used for validation. Radar rainfall data have been acquired from civil protection authorities.

Figure 5.13: Landslide triggered by a heavy rainstorm in the morning of 30th of April 2006

5.2.5 Event occurred on 30$^{\text{th}}$ April 2006

In the morning of 30^{th} of April 2006, between the 6:00 and the 8:30 am, four debris flows occurred along the northern flank of Monte Vezzi, in Piano Liguori locality, triggered by heavy rainfall. These landslides involved two buildings, a quarry and a garbage compactor and four persons were killed in their home (Figure 5.13).

These flows were triggered in the highest part of Monte Vezzi, between 310 and 360 m a.s.l., involving up to 1 m of soil above a layer of coesive pyroclastic deposits. The morphological evidences suggest that these landslides were triggered as soil slip and then evolved as debris flow during the downstream runoff along the preexisting drainage channels. According with Casagli et al. (2007) the soil collapsed and evolved in a flow after the liquefaction of the involved material due to the increased pore pressure along the slip surface.

The landslides have been triggered by an intense rainstorm occurred between 9:00 am of 29^{th} April and 9:00 am of 30^{th} April. This rainfall was highly localized so as the only rain gauge that was active at theat time, located on Monte Epomeo, cannot record the entire rain pattern. The rainfall maps recorded by the Grazzanise weather radar, located near Neaples, have shown that the higher intensities were reached in the area of Monte Vezzi. In this area the cumulative rain for the 24h has been estimated between 150 and 200 mm (Casagli et al., 2007; Mattiangeli, 2007; Seggiani, 2008). The rain gauge located on the Monte Epomeo recorded only acumulated value of 40 mm and a maximum intensity of 13 mm/h thus demonstrating the importance of using a distributed value of

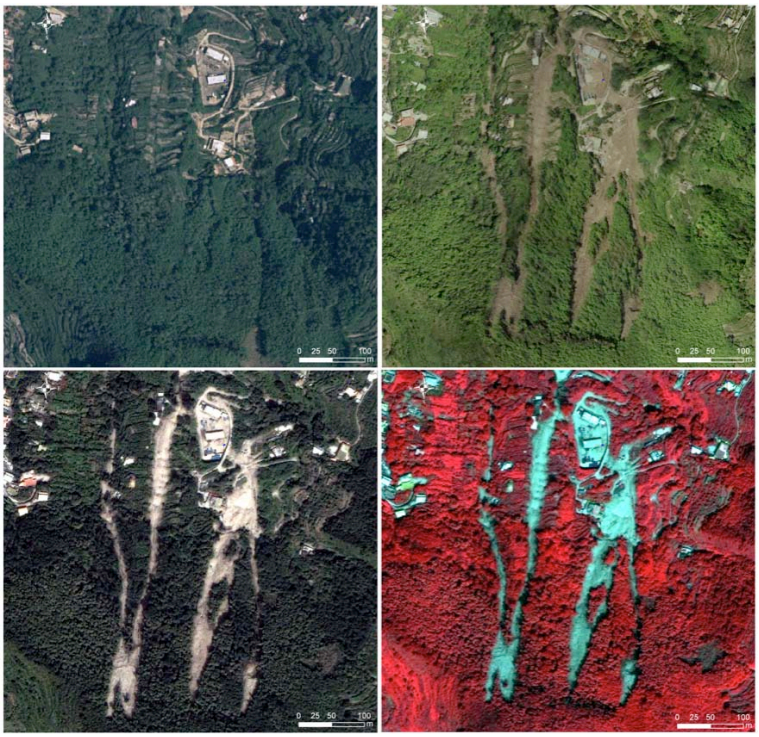

Figure 5.14: Satellite images showing the Monte Vezzi area before (upper left) and after (upper right) the occurrence of landslides.

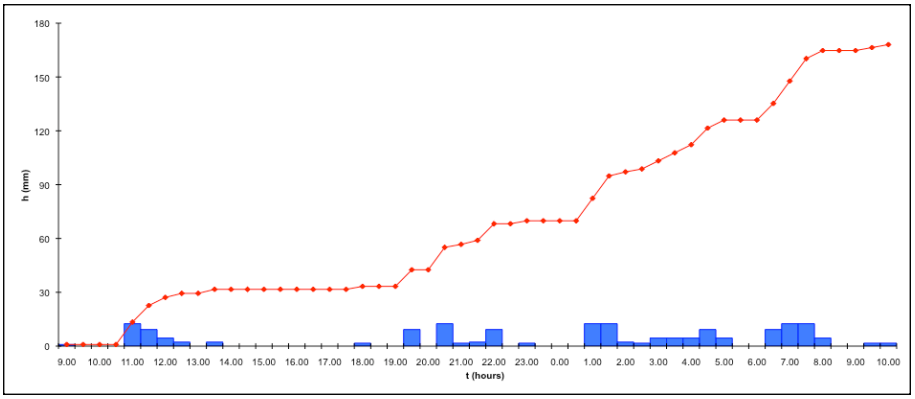

Figure 5.15: Intensities (mm/h) in blue and cumulative values (mm) in red registered by the Grazzanise wather radar for the Monte Vezzi area between 9:00am of 29/04/2006 and 10:00 am of 30/04/2006. Landslides occurred between 6:00 and 8:30 am of 30/04/2006.

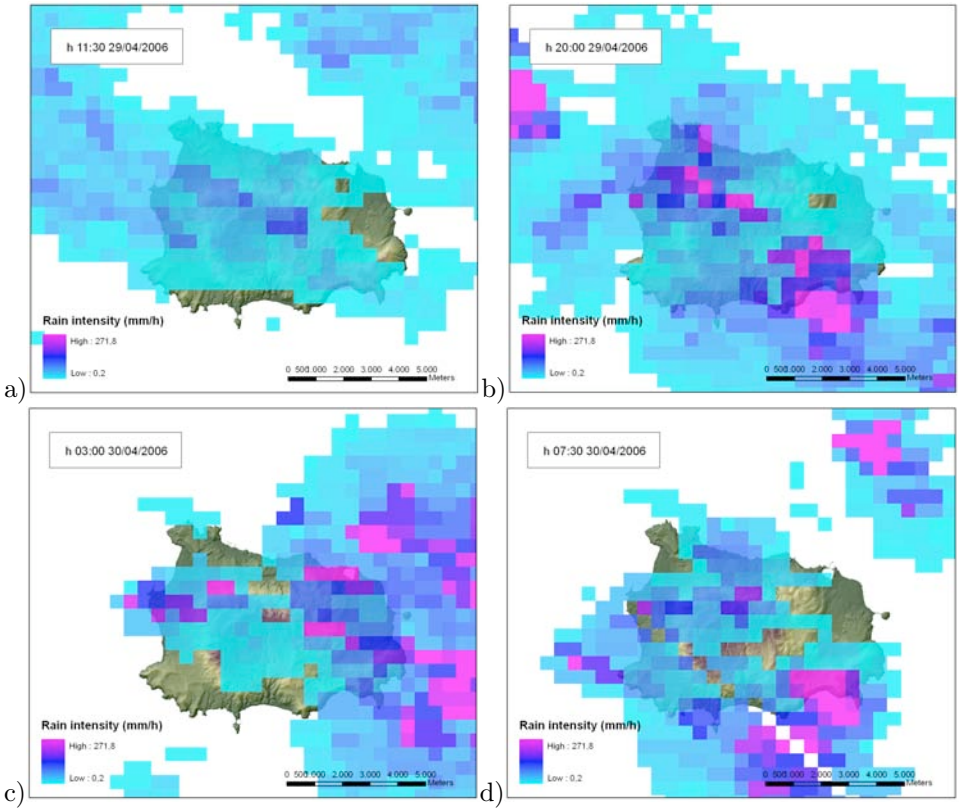

a) b) c) d)

Figure 5.16: Samples of rainfall intensity maps racorded by the weather radar of Grazzanise. a) Rainfall intensity racorded at 11:30 of 29/04/2006 b) Rainfall intensity racorded at 20:00 of 29/04/2006 c) Rainfall intensity racorded at 03:00 of 30/04/2006 d) Rainfall intensity racorded at 07:30 of 30/04/2006

rain patterns, like those recorded by means of wheather radars, for spatially distributed analisys of landslide hazzard. As Figures 5.15 and 5.16 show the entire rainfall event was discontinuous and composed of almost four high intensity and localized storm: the first between 11:00 and 13:00 am of 29/04, the second in the evening of 29/04 between 19:30 and 22:00, the third and more consistent between 1:00 and 5:00 am of 30/04 and the last one in the morning of 30/04 between 6:30 and 8:00 which finally led to slope failure. It is important to point out that this meteorological event didn't exceed the alert tresholds for the areas that were subjected to hydrogeological monitoring becouse of the extreme spatial variability of the rainfall intensities that cannot be recorded by rain gouges.

5.2.6 Fieldwork and base data collection

The aim of the fieldwork was to collect data regarding various aspects of the Ischia Island, with the main focus on soil parameters (e.g. thickness, hydraulic conductivity) on the entire island but with special attention in the areas where an exceptional storm triggered landslides in 30 April 2006. The data gathered

has been used for calibration and validation of the soil depth model and factor of safety models, as a part of the activities for the realization of the PREVIEW project.

The fieldwork has been organized in three main activities: soil depth measurements, sample collection and in situ tests. The whole work has been carried out on the entire island extension but with a particular attention for the area of the Monte Vezzi, where the 30th April 2006 event occurred. The collected samples come from the crown of the largest landslide (between a group of four failures) and will be used to determine geotechnical parameters in laboratory. Borehole Shear Tests were also carried out along with measurements of permeability with the Amoozemeter. More than one hundred kilos of disturbed samples was gathered from four different soil layers (wet pumice, dry pumice, wet ash, dry ash).

Soil depth data were collected by points in more than 130 sites and at each location the depth of the soil to the bedrock was measured with a tape measure. Where present the different soil layers were described, at least one photo was taken and the site coordinates and elevation were acquired by means of a GPS. This data was collected in the proximity of landslides and also in as many portions of the island as possible, including at low, intermediate and high elevations and in different geomorphic and geolithological settings. The aim was to acquire a spatially distributed data set representative of the different soil conditions present within the slopes.

5.2.7 Soil depth modeling

As for the Armea basin, the GIST model (Segoni, 2008) has been applied to evaluate the soil depth for the island of Ischia. The methodology used is the same described in section 5.1.11. The obtained soil thickness map (5m resolution) is shown in Figure 5.17 and, like for the Armea basin, even here a high dependence on bedrock lithology and on the relative position is clearly detectable. In fact a general tendency of the soil to thicken towards the valleys is noticeably and sharp discontinuities are met at the boundaries between very different volcanic lithology. Both trends match with field observations.

The highest soil thickness are met in the ashes and in the Ischia Graben characterized by gentle slopes in the northeastern part of the island. The shallowest are situated in the tuff lithotypes and in correspondence of the highest slope angles, like along the edges of the Monte Epomeo where the soil thckness is zero and it possible to observe widespread outcrops of the Tufite del Monte Epomeo.

The soil thickness map obtained by means of the GIST model has been validated before being used for the slope stability analysis. The comparison between the expected (calculated by the GIST model) and observed (measured in the field) soil thickness measures reveals that the overall performance of the model is quite satisfactory: the mean absolute error is 26cm, with a 33.62cm standard deviation (Segoni, 2008). Looking closer at the errors, the substantially correct estimations (error between -10cm and +10cm) are the 45%, and acceptable errors (abs errors from 11 to 30cm) are the 33%. The validation shows how the results of the GIST model for the island of Ischia are even better than those obtained for the Armea basin.

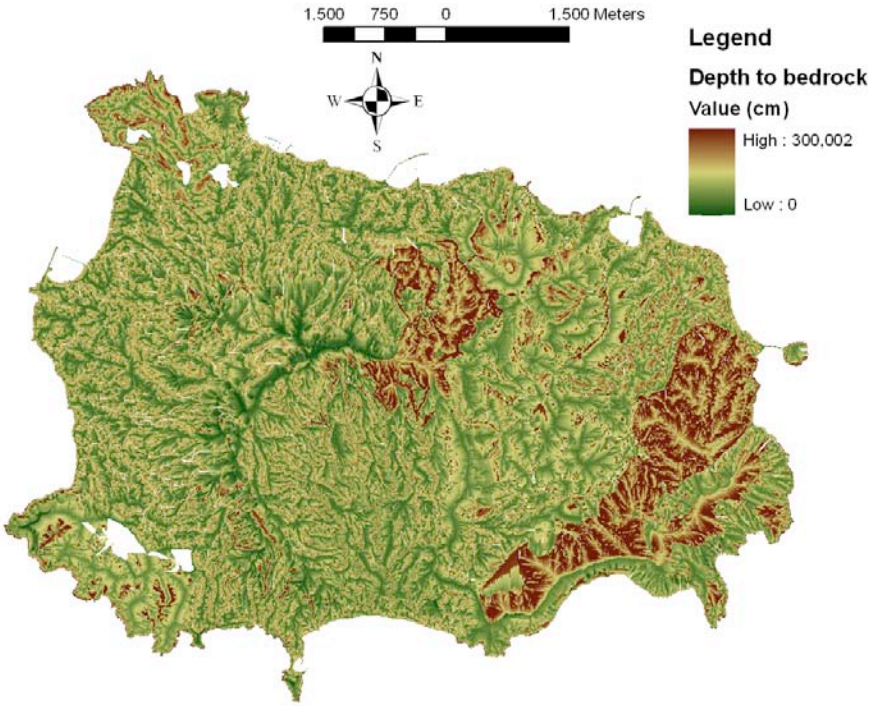

Figure 5.17: Depth to bedrock map of the island of Ischia obtained with the GIST model

Chapter 6

Proposed models for stability analysis

Many studies have shown that most shallow landslides are triggered by the infiltration of water into a slope (Campbell, 1975; Caine, 1980; Johnson & Sitar, 1990; Wieczorek, 1996; Iverson, 2000). However, this knowledge has not yet led to a reliable prediction of temporal occurrence, i.e. when the landslide will be triggered. For this reason many approaches focus more on predicting where a landslide will take place than on the timing. Susceptibility maps, for example, generally consider quasi-static parameters such as slope gradient and curvature, soil thickness, and permeability to provide an empirical indication of the predisposition of slopes to landsliding (Soeters & van Westen, 1996; Aleotti & Chowdhury, 1999; Guzzetti et al., 1999). This type of approach, however, is not very helpful in alerting civil authorities or other stakeholders to when a potential damaging event could occur. The use of rainfall triggering thresholds to determine when soil slips are likely to occur, on the other hand, is able to provide a temporal indication of landslide occurrence and a large body of literature exists on the topic (Innes, 1983; Caine, 1980; Wieczorek, 1987; Cannon & Ellen, 1985; Glade, 2000; Larsen & Simon, 1993; Gabet et al., 2004). When the rainfall threshold is exceeded during a storm an alert can be sent out by authorities to provide warning for potential landslides. The drawback of this method is that the spatial prediction is very coarse: usually these alerts are generically emitted for large regions without further indications of where landslides are more likely to occur. This method has the advantage of being relatively simple to implement. However, if both a spatial and a temporal prediction of shallow landslide occurrence are desirable the most effective approach is to use deterministic models that couple water infiltration schemes with a one-dimensional slope stability analysis (Montgomery & Dietrich, 1994; Wu & Sidle, 1995; Borga et al., 1998; Montgomery et al., 1998; Pack et al., 1998; Burton & Bathurst, 1998; Baum et al., 2002; Casadei et al., 2003; Crosta & Frattini, 2003; Simoni et al., 2008). If the rainfall characteristics of the triggering event are known these models become useful tools for modelling where and when shallow landslides are likely to occur at a basin scale. One of the next logical steps in the evolution of these models is the coupling with weather forecasts, which would make them valuable tools for forecasting possible shallow landslide generating events with a lead

time sufficient to provide alerts to authorities and the local population (Keefer et al., 1987; Aleotti, 2004; Schmidt et al., 2008).

6.1 Models

During this study two different approaches have been tested for the assessment of shallow landslides hazard. Both are physically-based distributed models that explicitly incorporate the dynamic variables like the degree of soil saturation and are based on a one dimension infinite slope stability analysis.

The first approach couples the C-DRIFT hydraulic model (section 4.4) with an algorithm that applies the Skempton solution to the infinite slope stability equation. The second and more complex approach is a modified version of the Iverson's model for landslides triggered by rain infiltration. It couples an hydrological model based on a reduced form of Richards equation with an infinite slope stability analysis. Due to the assumption needed to find the simplified solution for the Richards equation, the Iverson's model neglects the effect of soil suction to the overall effective cohesion. In this modified version the additional cohesion due to suction in unsaturated soils has been included within the slope stability model. Moreover the computer code implemented during this study allows to find a solution not just for a single rainfall event but even for complex storms characterized by different and alternating intensities both in space and time.

A distinctive feature of this new model is that it is projected to work in near real time. All the other existing software (like for example TRIGRS, based on the Iverson's model, or SEEP/W, based on an infinite element analysis) can work only as simulators after that the rainfall event is already occurred and eventually after that the landslides have already been triggered. The results of these softwares can be very useful for many scientific studies but cannot be used for the forecasting of shallow landslides or within a warning system for civil protection purposes. The main goal of the proposed model is the possibility to be used for near real time computation: as soon as new rainfall data are available, it computes the new pore pressure distribution within the soil and the new distributed map of factor of safety. If the input rainfall data are real time measured data, the software would achieve the present factor of safety. If instead the rainfall data are future projections of the present weather conditions (i.e. weather forecast), the resulting factor of safety map will represent future slope stability conditions and eventually would forecast the triggering of rainfall induced landslides.

Both these models neglect the effects of root cohesion and assume that the cohesive term within the slope is caused by soil particle cohesion only. This approach has two advantage: first, the estimate of stability is conservative because a slope considered as unstable may be actually stable if a significant amount of root cohesion is added to the shear strength. Second, the estimation of the cohesion is simpler and the model can be applied more easily in different areas characterized by different vegetation types but with the same soil properties. Moreover it has been noticed that the majority of shallow landslides and debris flows occurs at the interface between soil and bedrock that usually represent the slip surface. This means that the presence of root cohesion to have significant effect on slope stability, needs roots anchored in the bedrock. This is not the

case for vegetation type like those present in the two test sites (beeches, chestnuts and acacias) characterized by huge radial root growth but poor growth normal to the slope.

The first approach that uses the C-DRIFT hydraulic model has been tested only in the first test site, the Armea basin, because the data needed for the computation of the soil moisture, supplied by the CIMA center, were not available for the Ischia island. The second approach, the new modified Iverson's model , has been tested both in the Armea basin and on the island of Ischia.

6.1.1 Infinite slope model (ISM) and C-DRIFT hydraulic model

The first approach tested for shallow landslides hazard assessment in the Armea basin is composed of two different part: first the C-DRIFT hydraulic model is used to compute a distributed map of the soil moisture and then this map is used as an input for the slope stability model that supplies as outcome a distributed map of the factor of safety.

C-DRIFT (Continuous Discharge River Forecast) is a semi-distributed hydrological model able to simulate the discharge process, the evapotranspiration process and the hypodermic flow propagation within a basin, allowing a description of the soil moisture state in each pixel in which the basin is discretized (Gabellani, 2005). It solves the continuity equation and the energy balance using a modified Horton method to simulate the infiltration processes. The soil is considered as a porous medium and is schematized as a reservoir characterized by two parameters:

- Vmax, which represents the soil capacity expressed in millimeters (mm)
- f0, which represents the initial infiltration capacity for a dry soil expressed in millimeters per hour (mm/h)

Both these parameters are function of soil type and soil use. The data needed for the application of the model are a digital elevation model of the studied area, the soil properties maps, vegetation maps and meteorological data that should include rainfall amount, temperature and short wave radiation. Using the DEM the model can classify cells as slope-cells and drainage pattern-cells. Then in a second step the model computes for each cell the run-off time and assigns them a value of discharge velocity. The last step account for the relation between the incoming rainfall and the runoff time with the aid of a parameter (the curve number) useful to relate the total amount of rainfall with the resulting effective rainfall. This model has been originally developed not for the computation of the soil moisture but to simulate river discharge after the occurrence of a rainfall event; the results of this simulation can be very useful for floods forecasting and for the computation of floods hydrographs with a characteristic return period. Thus for this study the model has been adapted to explicitly find as main output just the soil moisture (that was anyway needed even for river discharge forecast) neglecting the computation of all the other outcomes. So the results of the application of the C-DRIFT model are hourly maps of soil moisture content which is expressed as degree of saturation defined as $V(t)/Vmax$ where V is the actual soil water content at time t and $Vmax$ is the soil retention capacity.

The slope stability model used here to compute the factor of safety is the infinite slope (Skempton & DeLory, 1957). In this analysis the soil is assumed to slide on a plane slip surface disposed sub-parallel to the ground. The slope is assumed to be infinite in extent and at an angle α to the horizontal. The groundwater conditions and the properties of the soil are assumed not to vary along the slip. Infinite slope model is a particular schematization of the limit equilibrium method which postulate that the slope may fail by a mass of soil sliding on a failure surface when the available shear strength of the soil is less than the shear stress due to gravity and to groundwater pore pressure.

The soil properties needed for the application of the infinite slope model are: effective cohesion (c), effective angle of internal friction (ϕ'), soil unit weight (γ) and water unit weight (γ_w). The other data needed are the slope angle (α), the slice depth (z) and the pore pressure at base (u). The classical form of the Skempton & DeLory (1957) solution to the limit equilibrium method for an infinite slope is:

$$FS = \frac{c' + \left[\gamma z \cos^2 \alpha - u\right] \tan \phi'}{\gamma z \sin \alpha \cos \alpha} \tag{6.1}$$

Since the majority of the shallow landslides occurs at the interface between soil and bedrock, the sliding slice depth z supplied to the model for the computation of the factor of safety is directly the depth to bedrock value obtained with the application of the GIST model (see sections 5.1.11 and 5.2.7). The pore pressure can even be written as follows:

$$u = \gamma_w h_w \tag{6.2}$$

This shows that pore pressure at base can be obtained multiplying the height of the water table (h_w) above the slip surface with the water unit weight (γ_w). Moreover the high of the water table (h_w) can be obtained combining the depth to bedrock with the degree of saturation in percentage ($s_{\%}$):

$$h_w = z s_{\%} \tag{6.3}$$

Since the value of $sat\%$ is the output of the C-DRIFT model, the main equation used here for the computation of the factor of safety is:

$$FS = \frac{c' + \left[\gamma z \cos^2 \alpha - \gamma_w z s_{\%}\right] \tan \phi'}{\gamma z \sin \alpha \cos \alpha} \tag{6.4}$$

6.1.2 Modified Iverson model (MIM)

The method proposed by Iverson (2000) is a combination of an infinite slope stability calculation with a transient, analytic solution for pore pressure response to steady state and transient rainfall infiltration. Some assumptions are needed to obtain the analytical solution for the Richards equation that governs the unsteady and variably saturated Darcinian flow of groundwater in response to rainfall. These assumptions include nearly saturated soil and relatively isotropic, homogeneous hydrologic properties. The first assumption allows to simplify the Richards equation by neglecting the effect of groundwater flow in unsaturated soils. Like suggested by Baum et al. (2002) and Baum et al. (2005), the saturated soil assumption is usually satisfied during the winter rainy season in many areas characterized by quite wet climatic conditions (i.e. the U.S. Pacific coast region)

but even after the occurrence of prolonged rainfall in areas usually characterized by dry conditions (Salciarini et al., 2006).

The model proposed here, uses the same solution suggested by Iverson to compute the pressure head distribution within a soil after a rainstorm. At the same time, some changes have been made to the form of the analytical solution due to the necessity of using this new model in near real time. All the past application of the Iverson's method to real case studies have been conducted as a simulation of the effect of rainfall on slope stability after the occurrence of the real event (Crosta & Frattini, 2003; Baum et al., 2005; Chien-Yuan et al., 2005; Salciarini et al., 2006). Even the available software that develop and extend the Iverson's method, like TRIGRS (Baum et al., 2002), are build to run after the occurrence of the event, when all the rainfall data are already available. These softwares need to have all the data, both static and dynamic (i.e. rainfall maps), before the starting of the simulation. The main goal of the model proposed here is that it is developed with the aim of being able to run in near real time. To achieve this result the model is projected to receive for every simulation not the entire time series of rainfall data but just a single rainfall intensity map and to remember during the next run the effect of the previous rainfall history. This approach allows to pass to the model every time a new map that could represent the present weather conditions or otherwise the forecasted ones. In this way it is even possible to use the model as a tool for the forecasting of shallow landslides.

Another peculiarity of the proposed model is that during the slope stability analysis it takes into account for the increase in strength and cohesion due to matric suction in unsaturated soil, that is where the pressure head is negative (Tsai et al., 2007). This features may seems apparently in conflict with the saturated soil assumption made for the hydrological model. But this is not the case because the two part are mathematically independent, even though included in the same computer code, and the results of the hydrologic model are used as an input for the slope stability analysis the same as the distributed value of effective cohesion that include the increase in strength due to soil suction.

The model can be divided in two independent part: the hydrological tool that calculate the pressure head distribution as a function of time and depth $\psi(Z,t)$ and the stability analysis that supply as outcome the distributed value of the factor of safety.

- **Hydrologic model**: the assumption of wet initial condition allows to neglect the gravity flux and the original Richards equation (equation 3.16) became

$$\frac{\partial \psi}{\partial t} = D_0 \cos^2 \alpha \frac{\partial^2 \psi}{\partial Z^2} \tag{6.5}$$

where D_0 is the maximum diffusivity and Z is the depth normal to the slope. The solution to this equation can be find fixing the following boundary conditions

$$\psi(Z,0) = (Z - d_Z)\,\beta \tag{6.6}$$

$$\frac{\partial \psi}{\partial Z}(\infty,t) = \beta \tag{6.7}$$

$$\frac{\partial \psi}{\partial Z}(0,t) = \begin{cases} -\frac{I_Z}{K_Z} + \beta & t \leq T \\ \beta & t > T \end{cases} \tag{6.8}$$

As already said in section 3.3.1T is the rainfall duration, d_Z is the water table depth in the vertical direction Z and β is the initial steady state pressure head distribution defined as

$$\beta = \cos^2 \alpha - \left(\frac{I_Z}{K_Z} \right)_{steady} \tag{6.9}$$

These boundary condition assumes a steady state pressure head distribution that at great depths below the water table the vertical groundwater became negligible but persist the steady state pressure head distribution and that Darcy's low governs the water entry at the ground surface. The pressure head distribution is defined by β when it is not raining ($t > T$) and by β plus a short time infiltration rate during rainfall ($t \leq T$). The solution thus became

$$\psi\left(Z, t \leq T\right) = \beta\left(Z - d\right) + Z\frac{I_Z}{K_Z}\left[R\left(t^*\right)\right] \tag{6.10}$$

$$\psi\left(Z, t > T\right) = \beta\left(Z - d\right) + Z\frac{I_Z}{K_Z}\left[R\left(t^*\right) - R\left(t^* - T^*\right)\right] \tag{6.11}$$

where $R\left(t^*\right)$ is the response function that depends only on normalized time defined as

$$R\left(t^*\right) = \sqrt{\frac{t^*}{\pi}} \exp\left(-\frac{1}{t^*}\right) - erfc\left(\frac{1}{\sqrt{t^*}}\right) \tag{6.12}$$

the normalized time are $t^* = \frac{t}{Z^2/\hat{D}}$ and $T^* = \frac{T}{Z^2/\hat{D}}$ where T is the rainfall duration and $\hat{D}$ is the effective hydraulic diffusivity defined as $\hat{D} = 4D_0 \cos^2 \alpha$. In equations 6.10 and 6.11 the first term $\beta\left(Z - d\right)$ is a constant and can be considered as a steady state component of the pressure head (ψ_0). Thinking in terms of time steps (t_{int}), if $t_1 = t_2 = \ldots = t_n = t_{int}$ thus the equation 6.10 can be written as

$$\psi\left(Z, t_1, I_{Zt1}\right) = \psi_0 + Z\frac{I_{Zt1}}{K_Z}\left[R\left(t_1\right)\right] \tag{6.13}$$

$$\psi\left(Z, t_2, I_{Zt2}\right) = \psi_{t1} + Z\frac{I_{Zt1}}{K_Z}\left[R\left(t_1\right)\right] + Z\frac{I_{Zt2}}{K_Z}\left[R\left(t_2\right)\right] \tag{6.14}$$

And so

$$\psi\left(Z, t, I\right)_n = \psi\left(Z, t, I\right)_{n-1} + Z\frac{I_{Ztn}}{K_Z}\left[R\left(t_n\right)\right] \tag{6.15}$$

where $\psi\left(Z, t, I\right)_n$ is the pressure head distribution at time t_n obtained after n time steps. Thus for each time steps the equations 6.10 and 6.11 became

$$\psi\left(Z, t^*\right)_n = \psi\left(Z, t^*\right)_{n-1} + Z\frac{I_Z}{K_Z}\left[R\left(t^*\right)\right] \quad \text{for } t^* < T^* \text{ (during a rainfall)} \tag{6.16}$$

$$\psi\left(Z, t^*\right)_n = \psi\left(Z, t^*\right)_{n-1} + Z\frac{I_Z}{K_Z}\left[R\left(t^*\right) - R\left(t^* - T^*\right)\right] \quad \text{for } t^* > T^* \text{ (after a rainfall)} \tag{6.17}$$

these last two equation are used within the model to evaluate the pressure head distribution at each time steps. The obtained value is than used as input for the slope stability analysis at time t_n.

- **Slope stability model**: the stability analysis is based on the limit equilibrium method for an infinite slope. The adopted solution for the infinite slope model is that proposed by Skempton & DeLory (1957) but in the form suggested by Iverson (2000). In this equation the factor of safety is described as a function of depth and time and it is divided in a time varying component FS' and a steady background component FS_0 :

$$FS\left(Z,t\right) = FS_0\left(Z\right) + FS'\left(Z,t\right) \tag{6.18}$$

$$FS_0\left(Z\right) = \frac{\tan\varphi}{\tan\alpha} + \frac{c}{\gamma_S Z \sin\alpha\cos\alpha} - \frac{\psi_0\left(Z\right)\gamma_W \tan\varphi}{\gamma_S Z \sin\alpha\cos\alpha} \tag{6.19}$$

$$FS'\left(Z,t^*\right) = -\frac{\left[\psi\left(Z,t^*\right)_n - \psi_0\left(Z\right)\right]\gamma_W \tan\varphi}{\gamma_S Z \sin\alpha\cos\alpha} \tag{6.20}$$

where α is the slope angle, φ is the soil friction angle, c is the cohesion, γ_S is soil unit weight and γ_W is the unit weight of groundwater. The results of the equations 6.16 and 6.17 are used in equation 6.20 to compute the factor of safety at depth Z. Equation 6.16 is used to compute the pressure head at depth Z during a rainfall and the 6.17 when the rain has stopped. As will be showed in the next section, this model calculate the factor of safety at different depth and the value Z that determines the depth of landsliding is the first that yields a value equal to one. Depending on the depth at which the model is working, the sign of pressure head shows if the soil is saturated or unsaturated (Tsai et al., 2007). If $\psi\left(Z,t^*\right)_n$ is positive the soil is saturated and the factor of safety can be calculated using directly equations 6.19 and 6.20. If instead the pressure head is negative, the soil is unsaturated and it is necessary to take into account for the increase in shear strength due to soil suction. For describing the state of the stress in unsaturated soils has been used the independent stress state variable approach of **?** which states that

$$\tau = c' + \left(\sigma - u_a\right)\tan\varphi + \left(u_a - u_w\right)\tan\varphi^b \tag{6.21}$$

and

$$c = c' + \left(u_a - u_w\right)\tan\varphi^b \tag{6.22}$$

φ^b is an additional friction angle needed to account for the contribution of the matric suction to shear strength. The effective cohesion c indicates an increase in strength as matric suction increases. This increase can be defined using the φ^b angle as shown in 6.22. While the value of the water pressure u_w can be easily find multiplying the pressure head obtained with 6.16 and 6.17 with the unit weight of groundwater γ_W, to find the value of φ^b it is necessary to know the degree of saturation of the soil (S) and to use the following equation (Vanapalli et al., 1996)

$$\tan\left(\varphi^b\right) = \tan\left(\varphi\right)\left(\frac{S - S_r}{100 - S_r}\right) \tag{6.23}$$

where S_r is the residual degree of saturation in percent. The degree of saturation of soils depends on their water content and porosity (p). For groundwater flow through an unsaturated soil, the coefficient of permeability is not a constant but a function of soil suction thus to infer the degree

of saturation of a soil it is necessary to use the soil-water characteristic curve (SWCC) that defines the relationship between the suction and the volumetric water content. Drawing the SWCC for a soil characterized by a certain porosity, from the regression line it is possible to estimate the volumetric water content because the soil suction is know and is equal to $\psi\left(Z,t^*\right)_n\gamma_W$:

$$V_w = m\psi\left(Z,t^*\right)_n\gamma_W + q \tag{6.24}$$

where m and q are coefficients characteristic of the curve of that particular soil. The degree of saturation in percent is obtained dividing for the porosity:

$$S = \frac{V_w}{p} \tag{6.25}$$

Using the obtained value in equation 6.23 it is possible to find the φ^b of that particular soil to be used in equation 6.19. Finally the slope stability equation are

$$FS\left(Z,t\right) = \frac{\tan\varphi}{\tan\alpha} + \frac{c}{\gamma_S Z\sin\alpha\cos\alpha} - \frac{\psi_0\left(Z\right)\gamma_W\tan\varphi}{\gamma_S Z\sin\alpha\cos\alpha} - \frac{\left[\psi\left(Z,t^*\right)_n - \psi_0\left(Z\right)\right]\gamma_W\tan\varphi}{\gamma_S Z\sin\alpha\cos\alpha} \tag{6.26}$$

for saturated soils and

$$FS\left(Z,t\right) = \frac{\tan\varphi}{\tan\alpha} + \frac{\left\{c' + \left[-\psi\left(Z,t^*\right)_n\gamma_W\right]\tan\varphi\left[\frac{\left[\frac{m\psi\left(Z,t^*\right)_n\gamma_W+q}{p}\right]-S_r}{100-S_r}\right]\right\}}{\gamma_S Z\sin\alpha\cos\alpha} -$$

$$- \frac{\psi_0\left(Z\right)\gamma_W\tan\varphi}{\gamma_S Z\sin\alpha\cos\alpha} - \frac{\left[\psi\left(Z,t^*\right)_n - \psi_0\left(Z\right)\right]\gamma_W\tan\varphi}{\gamma_S Z\sin\alpha\cos\alpha} \tag{6.27}$$

for unsaturated soils (i.e. when $\psi\left(Z,t^*\right)_n$ is negative).

The coefficient m and q are different for different types of soil so it would be necessary to build many SWCC for soil characterized by different porosities. Using values of porosity taken from the literature (Krahn, 2004; Kim et al., 1998) for different types of granulometry (from sand to clay) many SWCC have been used to find the m and q parameters. Then a sensitivity analysis has been conducted to find out how the final factor of safety is influenced by different m and q parameters. The results obtained maintaining fixed the other soil parameters and varying m and q have shown that the differences between these factor of safety values are very small, less than 0.01 in absolute value (see table 6.1). For this reason it has been decided to use fixed mean values of m and q, respectively 0.0011 and 0.4464.

Instead the comparison between the results of equation 6.26, that doesn't takes into account for the soil suction, and the equation 6.27, that accounts for the contribution of the matric suction to shear strength, show differences in the final values of FS up to 0.4 thus resulting very important in the total computation of the factor of safety (see Figure 6.1).

Granulometry	m	q	K	FS
Sand	0.0008	0.3113	10^{-5}	1.567
Silty sand	0.0013	0.5282	10^{-7}	1.560
Silt	0.0011	0.4581	10^{-6}	1.565
Silty clay	0.0013	0.5127	10^{-8}	1.569
Clay	0.0010	0.4220	10^{-9}	1.563
Mean values	0.0011	0.4464		1.564

Table 6.1: Comparison between FS values obtained for different granulometries using equation 6.27

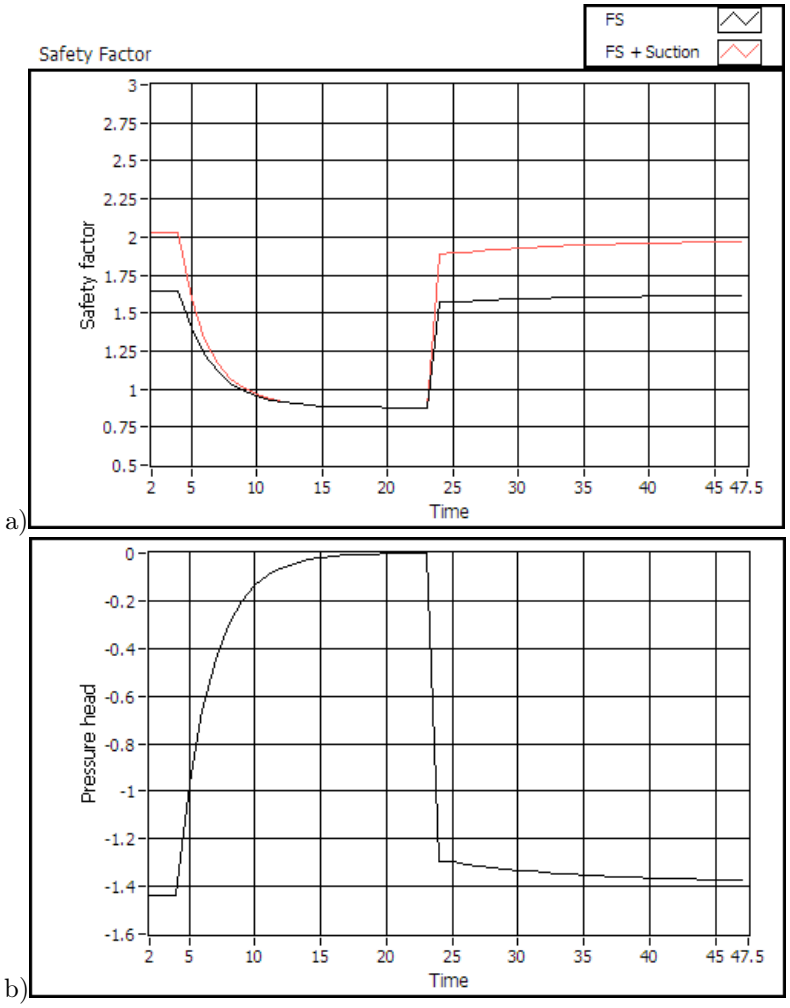

Figure 6.1: Results of a time varying computation of the factor of safety for a single cell: a) Comparison between FS values calculated with the equation 6.26 not considering the suction (black line) and values calculated with 6.27 that takes into account for the effect of suction (red line). The FS is computed at a depth of 0.8 m after the beginning of a rainfall characterized by varying intensity (ranging between 5 and 40 mm/h) with time step of 30 minutes. b) Time varying values of the pressure head distribution used for the computation of the factor of safety.

6.2 Algorithms and computer codes

The models described in section 6.1 have been used to develop two software for computing the distributed factor of safety. These softwares operate on gridded maps of a geographical area and accept input from a series of ASCII text files. All the input data are allowed to vary over the gridded area thus making it possible to analyse slope stability over geologically complex terrains and after complex rainstorms characterized by varying intensities in space and time.

The input and output data format used for the developed softwares is the ARC/INFO ASCII GRID (with .asc or .txt file extension). This file format is a space delimited text file that can be viewed and edited with a simple text editor. It has been chosen because it represents the better data format for the interexchange of geographical data between different geographic information systems (GIS) softwares (like ESRI ArcGIS, GRASS, Mapserver, GeoMedia ecc...) and works very well for every computer platform, from Microsoft Windows to Linux. Moreover almost every GIS software includes routines to import and to export this file format thus making very easy both to build and visualise the input and output of the software in a GIS environment. The first six lines of this kind of file is the header that indicate the reference of the grid: the numbers of rows and columns, the western (left) x-coordinate and southern (bottom) y-coordinates, the length of one side of each square cell and the value that is regarded as missing or as "no data" value (Figure 6.2). The header is followed by the values listed in the order they would naturally appear (left-right, top-down).

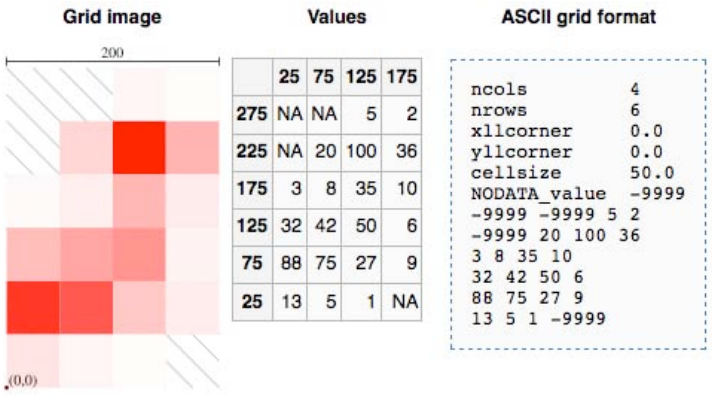

Figure 6.2: Example of how a grid image (left) can be represented in the ASCII GRID format (right)

6.2.1 Programming language and development platform

These software have been developed using the C++ programming language on a mixed Linux and MacOSX computer platform. The main advantage of using this language is that the main code can be compiled with one of the several available compilers and then would work for almost every operative systems. For this work the code has been developed with the Apple Xcode developer tools package and compiled with the GNU g++ compiler. Moreover the obtained

binary-executable file is usually quite fast with computation times definitely lower than any other gis tools or script.

Both the developed softwares run in a simple input/output command windows like any command line UNIX tool and with almost none user interaction. The advantage of a command line software is that it can be integrated in systems scripts to solve particular problems like repetitive or automatic tasks.

6.2.2 Main features of the developed software: infinite slope model and C-DRIFT

The first developed software uses equation 6.4 to calculate the distributed factor of safety for the studied area using the soil moisture map provided by the C-DRIFT hydrologic model. The factor of safety is calculated only at the interface between the soil an the bedrock, at a depth corresponding to the soil thickness provided by the GIST model. This software contains only the module for the slope stability analysis while the hydrologic modelling with C-DRIFT is performed at the CIMA. All the input data are in ascii grid format. The command line needed to run the program in a terminal window is:

```
./SKEMPTON_FS cohesion_map.asc friction_angle_map.asc
   soil_moisture_map.asc slope_map.asc soil_unit_weigh
   .asc depth_to_bedrock_map.asc factor_safety_map.asc
```

As shown by the string command above, the arguments needed by the software (here compiled with the name of "*skempton*") are seven, six input arguments and one output arguments, and must be ordered as follows:

1. The distributed map of the *cohesion* in Pascal for the different lithologies or soils.
2. The distributed map of the *friction angle* values in degree for the different lithologies or soil.
3. The distributed map of the *soil moisture* in percentage. This map should be that obtained using the C-DRIFT hydrologic model.
4. The distributed map of the *slope angle* in degree obtained by a geomorphological analysis of an high resolution digital elevation model of the studied area.
5. The distributed map of the *soil unit weight* in kN/m^3
6. The distributed map of the *soil thickness* or depth to bedrock. This can be a fixed value or the results of a model (like the GIST model used for this study) in meters.
7. The last argument is the name of the output file that will be recorded at the end of the run containing the distributed values of the *factor of safety.*

All the input data must be in the same folder of the executable file and are all used to solve the equation 6.4. During the execution of the code, before the computation of the FS, an internal routine checks all the input data and if one

of them is missing or incomplete, stops the run and provides as output an error message.

See Appendix A for the complete source code.

6.2.3 Main features of the developed software: modified Iverson model

The source code for the slope stability analysis that takes into account for the transient rainfall infiltration is more complex than the previous one because it includes the hydrological model for the computation of the pressure head distribution (section 6.1.2). For this reason the code is not only longer and more complex but it needs even many more different input files every times it is lunched.

This software is projected to be used in near-real time or every fixed time steps (*t_int*). As a consequence many of the file names to be supplied with the string command for the execution of the program, even though representing the same physical properties, are twofold and characterized by two different suffix:

- *file_new*: the suffix new is used for the files that will be written as new output files and that will be then used as input files for the next run of the program (e.g. *pressure_head_new.asc*).
- *file_old*: the suffix old is used for the files that represent the input data needed for the execution of the program during the present run of the model. These files were those written as output during the previous run of the program (e.g. *pressure_head_old.asc*).

The command line needed to run the program in a terminal window is:

```
./IVERSON_SF cohesion_map.asc friction_angle_map.asc
   rainfall_intensity.asc slope_map.asc
   soil_unit_weigh.asc depth_to_bedrock_map.asc
   conductivity_map.asc T_rain_old.asc T_rain_new.asc
   factor_safety_map.asc pressure_head_old.asc
   pressure_head_new.asc mean_intensity_old.asc
   mean_intensity_new.asc rain_count_old.asc
   rain_count_new.asc
```

The arguments needed by the software (here compiled with the name of "*IVERSON_SF*") are sixteen, eleven input arguments and five output arguments, and must be ordered exactly as in the command line above. Here follows the description of each input arguments and their role in the computation of the factor of safety:

1. The first is the distributed map of the *cohesion* in Pascal for the different lithologies or soils.
2. Then the distributed map of the *friction angle* values in degree for the different lithologies or soil.
3. The third file is the *rainfall intensity* in mm/h that will be used as the main input for the hydrological model and to compute the transient groundwater pressure head.

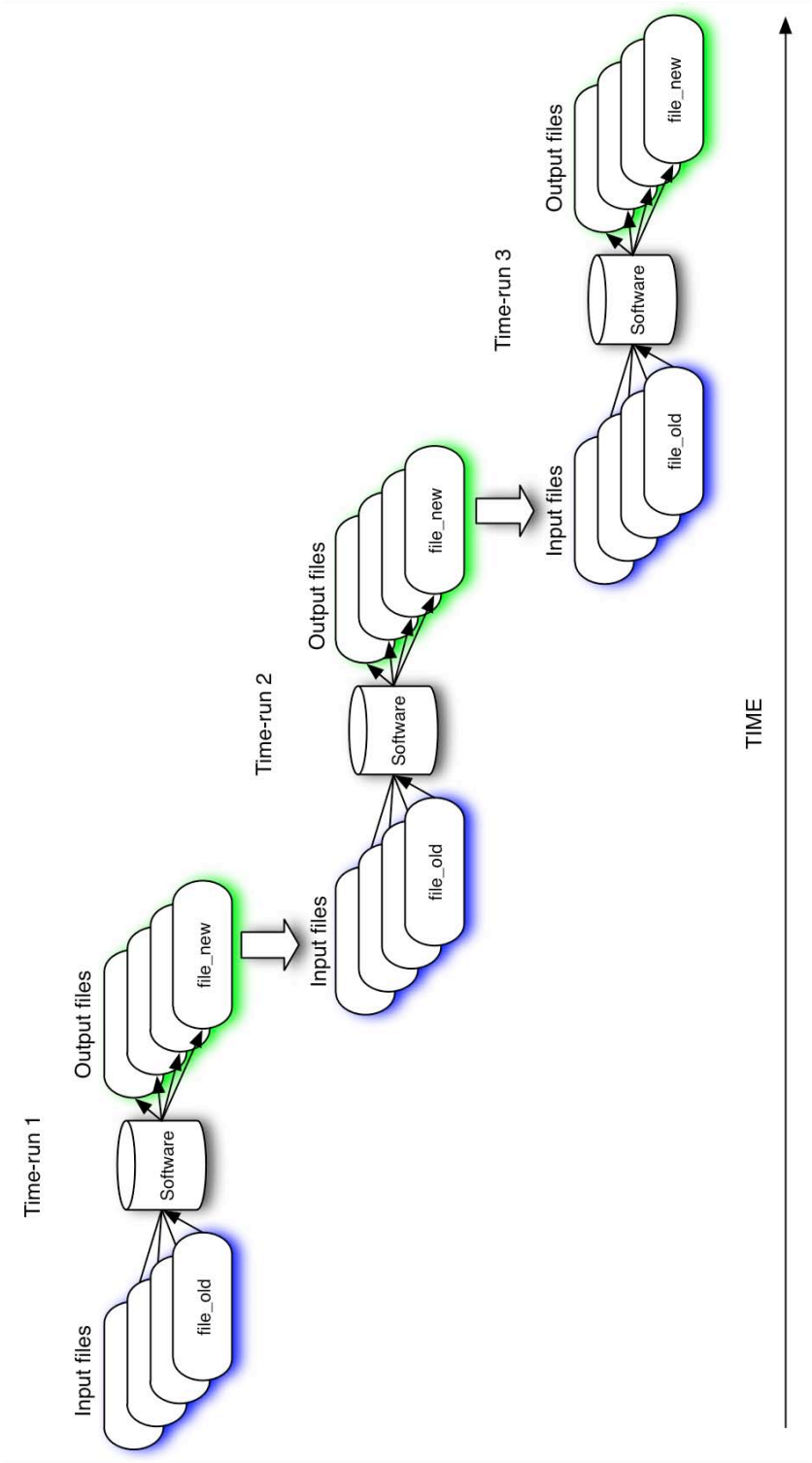

Figure 6.3: Real time capabilities of the modified Iverson model: during each run of the software (time-run 1, time-run 2, time-run 3) the input files with the "_old" suffix come from the previous computation. The output files with "_new" suffix are than used as input files in the next computation.

4. The same as for the previous software, the fourth file is the distributed map of the *slope angle* in degree obtained by a geomorphological analysis of an high resolution digital elevation model of the studied area.

5. Then there is distributed map of the *soil unit weight* in kN/m^3

6. The distributed map of the *soil thickness* or depth to bedrock. This can be a fixed value or the results of a model (like the GIST model used for this study) in meters.

7. The seventh file is a distributed map of the *hydraulic conductivity* expressed in m/s.

8. The file *T_rain_old* contains, as a distributed value, the time passed (in second) since the last rainfall occurrence. This value is needed to calculate the pressure head distribution that is strictly related to the time passed since the last rainfall.

9. The file *T_rain_new* is the value of the T_rain_old updated with the new information obtained from the rainfall intensity file. If it is not raining (i.e. rainfall intensity is null) the T_rain_old value is updated adding the amount of second equal to the time passed between the last and the present run (equals to t_int). If it is raining (i.e. rainfall intensity > 0) the T_rain_new value is set as equal to t_int. This is one of the output file recorded during every run of the software.

10. The tenth argument is the name of the output file that will be recorded at the end of the run containing the distributed values of the *factor of safety*. The FS value is here computed at many depth, from few centimeters up to the maximum thickness of the soil but this file records just the lowest value find within the entire thickness.

11. The *pressure_head_old* file is the old value of the distributed pressure head and is used in the present computation as a starting condition to evaluate the new pressure head distribution with the new rainfall intensity or after a new t_int of no rain condition. These values are expressed in meters.

12. The *pressure_head_new* is the output file that contains the values of the new pressure head distribution. This file will be used in the next computation as a starting condition to evaluate the next pressure distribution.

13. The file named *mean_intensity_old* contains the mean intensity of the last rainfall occurred in each pixel. This value is used in the computation of the pressure head in the case of no rain, when the last intensity value is needed the same as the time passed since the last rainfall (T_rain_old).

14. The *mean_intensity_new* file is an output file that contains the mean_intensity_old file updated with the present rainfall condition. If it doesn't rain, the value remains the same as in the previous file, if it rains the new mean intensity is substituted to the old value.

15. The *rain_count_old* file contains the number of time steps of the last consecutive rain. It is needed to calculate the mean intensity value to be used in the computation of the pressure head in case of no rain.

16. The *rain_count_new* file is an output file containing the rain_count_old file updated with the new rainfall condition. If it doesn't rain, the value remains the same as in the previous file, if it rains and in the previous time step it was already raining the new value is increased by one, if it rains and in the previous time step it was not raining the assigned value is 1.

As for the other software all the input data must be in the same folder of the executable file. During the execution of the code, before the computation of the FS, an internal routine checks all the input data and if one of them is missing or incomplete, stops the run and provides as output an error message.

One of the main features of this software is the possibility to perform the slope stability analysis at different depth. In the beginning of the code a variable sets the number of layers n at which the FS will be computed. The soil thickness is then divided by the n layers to define the depths to be used during the computation. So for each pixel, n values of FS are obtained, each corresponding to the different depths. At the end of the software run, not all FS values are registered in the output file but just the lowest one, that is the value indicating the highest probability of slope failure. The depth at which this value has been calculated is neglected and not registered simply because the only aim of this software was to infer the slope stability, not to estimate the amount of soil involved in the slide.

Here follows a step by step description of the code and of the algorithm (graphically shown in the flow chart of Figure 6.4):

- Every input file are opened and read. A routine checks if any of the input data is missing or incomplete. All these values are stored in internal arrays that will be then used by every equation included in the code.

- The first cycle calculate for every cell the T_rain_new value: if the intensity value is equal to zero (i.e. no rain condition) the t_int value is added to the T_rain_old value. Otherwise the new value is t_int and this means that it is has been raining for the last t_int second.

- Another cycle updates the value of the mean intensity according with last recorded rainfall intensity in the mean_intensity_new file.

- The effective hydraulic diffusivity is computed using the maximum characteristic diffusivity that governs the transmission of pressure head.

- The initial depth of the water table is computed using the last pressure head distribution

- Then it is needed the steady background pressure head distribution to use as a minimum lower limit and this is obtained from the equation 3.20

- Now all the data needed for the computation of the new pressure head distribution are available and can be obtained using equations 6.16 and 6.17. The maximum pressure head value is reached in fully saturated conditions,

that is when the pressure head equals the soil thickness. The value of the pressure head is computed at many depth, from a few centimeters up to the maximum soil thickness and than recorded in the pressure_head_new file.

- The factor of safety at different depth is computed with equations 6.26 and 6.27. Using the values of the pressure head the system can distinguish is the depth at which the FS is calculated is in saturated (new pressure head > 0) or unsaturated conditions (new pressure head < 0).
- For each pixel, between all the FS values calculated at different depths, only the lower one (i.e. the one with higher risk of failure) is chosen and recorded in the output file (factor_safety_map).
- The last routine in the code updates rain_count_new that contains the number of time steps of the last consecutive rain: if it doesn't rain, the value remains the same as in the previous file, if it rains and in the previous time step it was already raining the new value is increased by one, if it rains and in the previous time step it was not raining the assigned value is 1.

All this operation, during a complete run of the model, are intended to be applied one time for every cell or pixel covering the studied area. During the computation of the groundwater pressure distribution, it is here assumed that surface runoff occurs only when the precipitation on each cell exceed its infiltrability. In that case the ratio $\frac{I_Z}{K_Z}$ is assigned equal to unity in equations 6.16 and 6.17 since the saturated hydraulic conductivity equals the infiltrability due to the assumption of saturated and tension saturated soil (Hillel, 1982; Iverson, 2000).

See Appendix B for the complete source code.

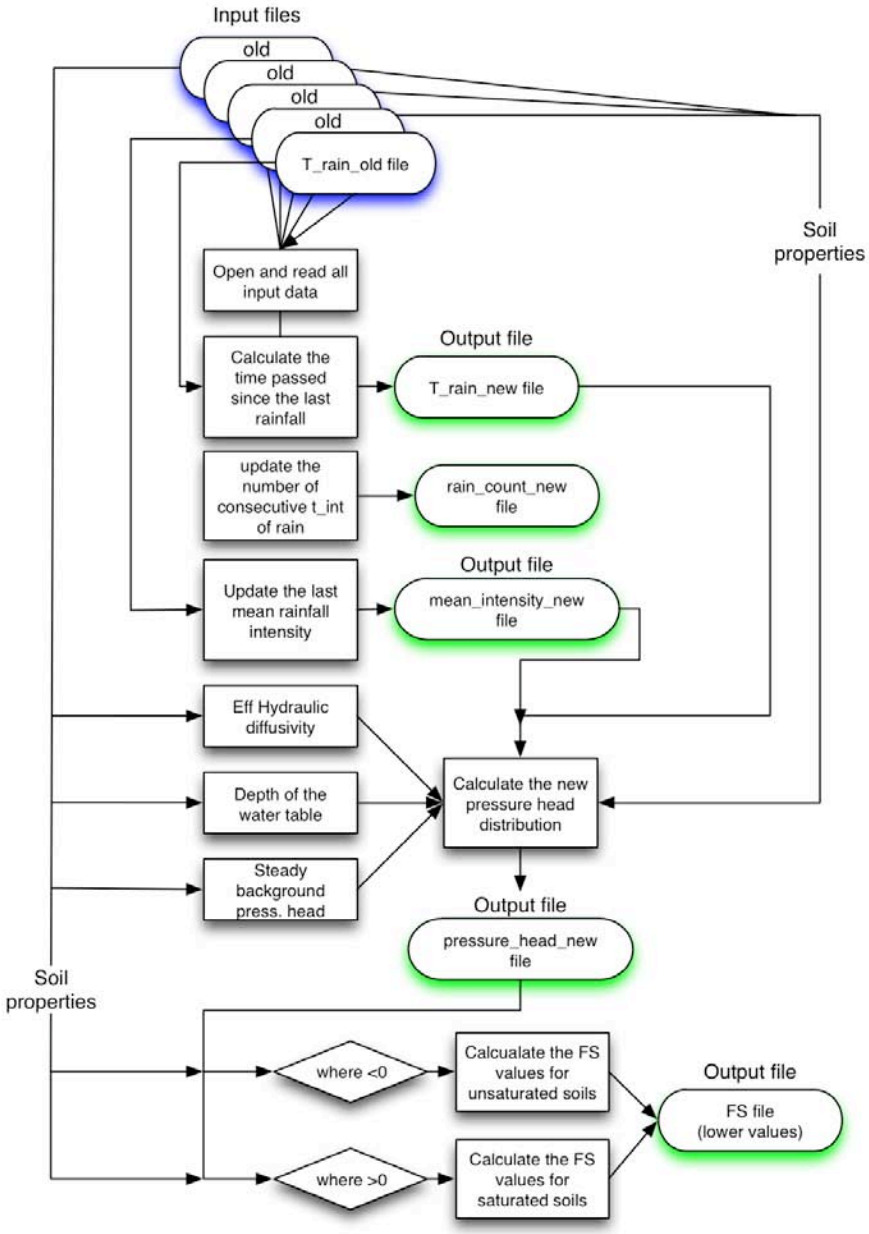

Figure 6.4: Flow chart of the software for the computation of the factor of safety in near-real time using the modified Iverson model. See section 6.2.3 for a detailed description.

Chapter 7

Test areas: slope stability computation

A minimum set of thematic data is needed in order to build a physically based model for hydrogeological simulations able to reproduce soil moisture conditions of a hillslope and to asses a slope stability analysis. These data regards land use, soil, topography and spatial data on geology (lithology/ rock type and structure), and geomorphology. Therefore, the characterization of the study areas in terms of soil properties, soil cover and soil use is a crucial step.

The factors that control the hydrological processes and the stability at the slope scale can be divided into two main groups (Wu & Sidle, 1995): the almost-static data and the dynamic data. In the first group can be included all the soil properties (like the mechanical characteristics, the soil thickness, the permeability) and the topographical features (like the digital elevation model and the slope map). Usually the stationary data are used for susceptibility analysis and to infer the spatial probability of landslides occurrence (Crosta & Frattini, 2003). The dynamic data include instead variables like the degree of saturation of a soil or the rainfall intensity that are useful for the characterization of the temporal pattern of landslides. Since the objective of this study was to develop a system for shallow landslides hazard assessment being able to predict the occurrence of failure in time and in space, both the almost-static data and the dynamic data were needed for the two test sites.

7.1 Stationary input data

The almost static or stationary input data are those that can be considered invariable for short time period ranging from years to centuries. In detail, the stationary data needed for the computation of the factor of safety with the two developed softwares are: soil effective cohesion, friction angle, slope, soil unit weigh, soil thickness and permeability.

The data needed to characterize the mechanical behaviour of the soils can be obtained directly from in situ analysis, from laboratory analysis of samples or from literature where the data are available for lithotype similar to those present in the studied areas. The main problem is to obtain a distributed values of these data because of the variability that usually affects soil properties like cohesion

and permeability due to many reasons (i.e. type of bedrock, the presence of roots, soil use). To obtain the distributed maps of these data, using the available geological maps, the studied areas have been divided into zones characterized by the same lithology. For every pixel covering the same lithology, a singular value of the soil properties has been assigned. At the end of this processes, many distributed maps of the soil properties were obtained, each reflecting the lithological zonation of the test area. With this approach we have obtained maps that take into account only the variability due to different lithotype. The different type of bedrock has been considered as the most important factor affecting the spatial variability of soil strength parameters. Nevertheless it is important to remember that neglecting all the other factors that could influence the spatial uncertainty of the soil properties, may lead to some errors in the final results of the model.

Saturated hydraulic conductivity was measured with an Amoozemeter in several sites and at different depths. These results have been integrated with values measured in similar texture features derived from an online data set (USDA, 2006; Simoni et al., 2008). Laboratory tests like shear test and sieving have been performed on the samples to determine grain size distribution, plasticity indexes, angle of internal friction, etc. The results of borehole shear test (BST) has been used to determine the effective cohesion and the internal friction angle. The results of these analysis have been integrated with those obtained by Mattiangeli (2007) for the island of Ischia. Estimates of soil thickness were based on the results of the GIST model that has been applied in both the test sites (Section 5.1.11 and 5.2.7).

7.1.1 Armea basin

For the Armea basin the stationary data were obtained from in situ test, from laboratory analysis of samples and from data set already available at the Earth Science Department of Florence. These data are:

- Cohesion
- Internal friction angle
- Soil unit weight
- Coefficient of permeability

In table 7.1 are shown the values of these properties for each different lithology of the Armea basin.

Formation or lithotype	C (KPa)	φ (deg)	γ (N/m^3)	K (m/s)
Recent alluvial deposit	1	35	22	$1*10^{-3}$
Recent alluvial terraces	2	26	20	$2*10^{-3}$
Ancient alluvial deposit	3	27	20	$1*10^{-3}$
Detrital deposits	4	28	20	$1*10^{-3}$
Pliocenic sands	6	26	21	$1*10^{-3}$
Argille di Ortovero	10	20	20	$3*10^{-6}$
Breccie di Taggia	7	34	21	$4*10^{-3}$
Conglomerati di Monte Villa	6	30	20	$2*10^{-3}$
Complesso di progressione (sandstones)	5	27	24	$2*10^{-4}$
Complesso di progressione (marnous-clays flysh)	12	18	23	$3*10^{-6}$
Flysh di Sanremo - Marne di Sanremo	11	21	24	$3*10^{-5}$
Flysh di Sanremo - Calcari di Monte Saccarello	10	22	24	$2*10^{-5}$
Arenarie di Bordighera (distal facies)	6	27	24	$5*10^{-4}$
Arenarie di Bordighera (channel facies)	7	29	24	$8*10^{-4}$
Formazione di San Bartolomeo	6	27	23	$4*10^{-5}$

Table 7.1: Summary of the soil properties values used as an input for the two developed models in the Armea basin

7.1.2 Island of Ischia

For the Island of Ischia the stationary data were obtained from the in situ tests, from laboratory analysis of samples and from literature (Mattiangeli, 2007; Cattoni et al., 2007; Crosta & Dal Negro, 2003; Casagli et al., 2007; Apuani et al., 2005; Calcaterra et al., 2003; Frattini et al., 2004). These data are:

- Cohesion
- Internal friction angle
- Soil unit weight

- Coefficient of permeability

In table 7.2 are shown the values of these properties for each different lithology. While in the Armea basin different formations were characterised by different lithotype and different soil properties, in the island of Ischia different volcanic formations are characterized by the same lithotype and texture features. Therefore in Table are shown just the values assigned to each lithotype (see figure 7.1) instead of the list of all the volcanic formation (totally more than 80).

Lithotype	C (KPa)	φ (deg)	γ (N/m^3)	K (m/s)
Pyroclastites	2	19	10	$3*10^{-4}$
Lavas	9	37	18	$2*10^{-6}$
Detrital deposits	4	28	11	$2*10^{-4}$
Tuffs	5	26	15	$6*10^{-4}$
Ashes	1	36	9	$1*10^{-6}$
Breccias	3	25	13	$2*10^{-4}$

Table 7.2: Summary of the soil properties values used as an input for the two developed models in the Island of Ischia

7.2 Dynamic input data

The non stationary data needed by the developed softwares to compute the factor of safety are of two types:

- Soil moisture maps (needed for the infinite slope model and supplied by the C-DRIFT hydraulic model)
- Rainfall intensity maps (needed for the modified Iverson model and obtained by the reflectivity maps of ground based weather radars corrected with rain gauges measurements where available)

Since the soil moisture maps where available only for the Armea basin, supplied by the CIMA using the C-DRIFT hydraulic model, the infinite slope model has been applied just in that test area. The radar rainfall maps where instead available for both the sites so it has been possible to test the developed software both on the Armea basin and in the Island of Ischia.

7.2.1 Armea basin

The dynamic data needed for the Armea basin where all supplied by the CIMA. As will explained in the next chapter, the data supplied by the CIMA are used in near real time within a network that includes many research centre and ends with the publication of the factor of safety maps on a Web-GIS platform. For this real time computation are used the soil moisture maps that the C-DRIFT model computes every every 6 hours. At the same time and with the same frequency the CIMA provides the rainfall intensity maps, to be used as an input for the modified Iverson model.

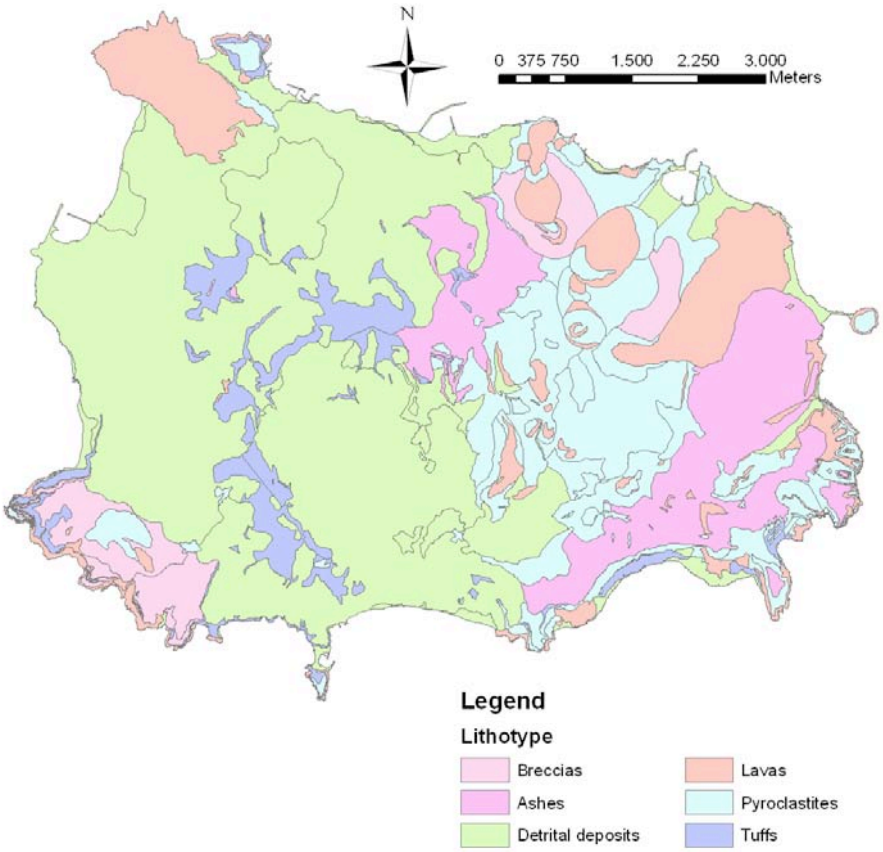

Figure 7.1: Schematic lithologic map of the Island of Ischia

Since one of the objective of this study was to test the slope stability models with real cases actually occurred, many rainfall and soil moisture maps where collected regarding the event occurred on 8^{th} December 2006 (section). In order to remove the errors due to the weather forecast uncertainty, the data regarding the December 2006 event were not forecast but actually measured values. This dataset is composed of 24 map of rainfall intensity measured by the Monte Settepani radar, located near Savona. Each map contains the distributed values of rainfall intensity with cells of 1000 m. The values contained in these maps have been corrected with the rain gauges measurements. The dataset provided by the CIMA includes also 24 soil moisture maps calculated using the rainfall maps as an input for the C-DRIFT hydraulic model. All the meteorological data regarding the Armea basin are characterized by a temporal resolution of one hour.

	Real Time	Historical Data
Type	Soil moisture maps and rainfall intensity maps	Soil moisture maps and rainfall intensity maps
N° of maps	1 soil moisture map every 6h, 1 rainfall map every hour	24 soil moisture maps and 24 rainfall maps (6 Dic 2006)
Spatial resolution	Downscaled to 5m for moisture maps and 1 km for rainfall maps	Downscaled to 5m for moisture maps and 1 km for rainfall maps
Temporal resolution	6h for the soil moisture maps, 1h for rainfall maps	1h for both the soil moisture maps and for the rainfall maps

Table 7.3: Summary of the meteorological data available for the Armea basin and used for the validation of the two developed softwares and for the building of the near-real time shallow landslides forecasting system.

7.2.2 Island of Ischia

For the Island of Ischia it were available just the data regarding the rainfall event occurred on 30 April 2006. Unfortunately the CIMA was not able to control the weather radar located near Ischia so it has not been possible to build there a real time service for the forecasting of shallow landslides. For the same reason the soil moisture maps were not available so the infinite slope model coupled with the C-DRIFT model has not been tested on this site. However the Italian Air Force supplied the weather data recorded by the Grazzanise radar, located near Naples. These data cover the two days before the triggering of the landslides, 29th and 30th April 2006, and include rainfall intensity maps with a temporal resolution of 30 minutes and a spatial resolution of 500 m. This dataset has been used to test the modified Iverson model in this second test site.

	Real Time	Historical Data
Type	None	Rainfall intensity maps
N° of maps		96 (total) covering 29-30 April 2006
Spatial resolution		500 meters
Temporal resolution		30 minutes

Table 7.4: Summary of the meteorological data available for the Island of Ischia and used for the validation of the modified Iverson model

Chapter 8

Warning system in near-real time and Web-GIS

One of the main objectives of this thesis was to build a warning system that should be able to obtain in near-real time the rainfall data, compute the factor of safety and publish the results on a Web-GIS platform. Even though to test and validate the two developed model it is possible to simulate a real time computation using radar data regarding past events (as will be shown in chapter 9), to build a real warning system it is necessary to have a continuous data supply covering the entire studied area. Unfortunately this has been possible just for the Armea basin where the real time radar data are supplied by the CIMA which directly control the Monte Settepani weather radar. For the Island of Ischia instead, the only meteorological data obtained were those regarding the landslides event occurred in April 2006. These data were recorded by the Grazzanise weather radar and supplied by the Italian Air Force that unfortunately cannot provide at the moment real time data. For this reason the warning system in near-real time has been developed and is already active just for the Armea basin.

Since this study was part of the PREVIEW European project, a third partner, the Telespazio S.p.A. located in Rome, was chosen to host the Web-GIS software (Mapserver) needed for the publication of the results of the warning system on the web (Ciccodemarco et al., 2007).

8.1 Data transmission and synchronization in real time

The data needed by the two developed software can be divided in two groups: stationary data (i.e. soil properties) and dynamic data (rainfall intensity and soil moisture maps). The stationary data needed were already present in the server of the Earth Science Department of Florence (DST-UNIFI), in the same place where the slope stability softwares is installed. On the other side, the dynamic data are instead collected and stored in a server of the CIMA. Finally the results of the model should be moved to Rome, in the Telespazio server in order to by published on the Web-GIS. For these reasons it has been necessary

to build a network via the web to exchange the data between the servers as soon as they were available.

The network realized for the development of the warning system is thus composed of three Linux servers: one is located in Savona at the CIMA, one in Florence at the Earth Science Department and one in Rome at Telespazio. With the use of synchronization tools like wget and rsync, data are moved from one server to another as soon as they are created in near real time. The data flow starts in Savona where they receive data from the Monte Settepani radar and compute these data to produce weather forecast and soil saturation maps of the Armea basin. Using a synchronization tool the meteorological data are transferred on the server of the Earth Science Department. That server contains already data about geomorphological and geotechnical properties. A shell script check every five minutes if new data are available and as soon as it finds a new rainfall or saturation map, the stability analysis software is lunched. The software, using as input data the maps of the geomorphological and geotechnical properties and the new rainfall intensity (or saturation map), produce as output an updated map of the factor of safety of the Armea basin. Then this new map is transferred on the Telespazio server where it's published on a WebGIS platform and sheared with the end users and local authorities via web (Figure 8.1). One of the most important thing of this data flow is that the hole procedure is completely automatic and it's even quite efficient because it needs just between ten and fifteen minutes from the computation of a new saturation map to the publication of the new factor of safety map on the WebGIS.

8.2 System scripts and automation of the model

As already said, the network build for the landslides warning system is composed of 3 Linux server. The central server, that controls the others is that located at the Earth Science Department in Florence. On our server many system script, written in bash scripting language are used to make the hole processes automatic and with no need of external operation. Within these script the system is forced to download the new meteorological data from the CIMA server, to compute the new factor of safety using the softwares installed and to upload the results to the Telespazio server in a special folder where they can be directly read by the Web-GIS software.

The core of the synchronization between servers is an open source software named *rsync*, a software application for Unix systems which synchronizes files and directories from one location to another while minimizing data transfer using delta encoding when appropriate. This software works in command line mode and in scripting mode so it can be used to perform repetitive jobs and scheduled tasks. Moreover rsync works using the secure transfer protocol *ssh* (secure shell). It uses public-key cryptography to authenticate the remote computer and allow the remote computer to authenticate the user, when necessary. Rsync is here used in conjunction with another open source software named *Cron*, a program that enables Unix users to execute commands or groups of commands automatically at a specified time/date. These tasks are often termed as Cron jobs. Crontab (CRON TABle) is the file which contains the schedule of Cron entries to be run at a specified times. Another Unix tool used within the scripts is *Date*, normally used to displays the time and date in a terminal window, but

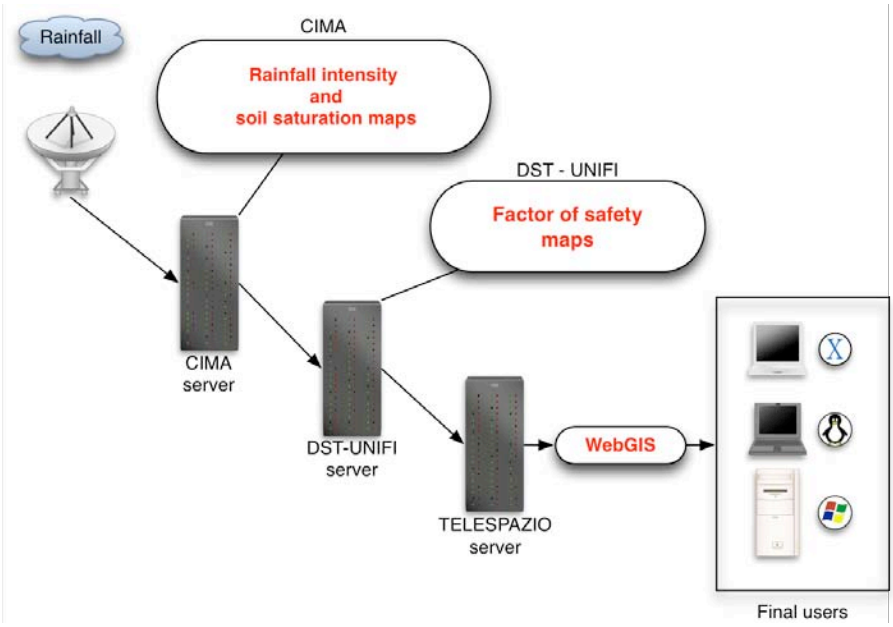

Figure 8.1: Scheme showing the network realized for the development of the shallow landslides warning systems. From left to right, the radar catch the rain reflectivity, the CIMA compute the rainfall intensity map and the soil moisture maps that are then uploaded to the DST-UNIFI server where the factor of safety map is calculated using the two developed software. Finally the results are uploaded to the Telespazio server where they are published on the Web-GIS. The final users can see and download the data using a simple web browser and independently of the operative system they are using (Linux, Mac OSX, Windows).

needed here to include the time and date in the names of the old and new maps used during the execution of the script.

Here follows an example of the scripts used for the automation of the system:

```
#!/bin/bash # Script for to be scheduled at 12.00 am

cd /home/georete/automatic_fs/fs_maps/

# Checks if the FS map of 12.00 is already present in
   the server
if [ -r "FS_$(date +%Y%m%d)_1200_01.asc" ];
then
   echo "The file FS_$(date +%Y%m%d)_1200_01.asc is
      already present in the server!";
exit
else cd /home/georete/lisa.cima.unige.it/
   mappe_saturazione;
fi
```

```
# If it's not present tries to calculate...
# First it checks if there is a new soil saturation
    maps
if [ -r "mappa_saturazione_08$(date +%j)1200-wstep.txt
    " ];
then
# If a new soil saturation map is founded, launches
    the software for the stability analysis:
    echo "Found the saturation maps 08$(date +%j)
       12:00... Compute the factor of safety:";

cp mappa_saturazione_07$(date +%j)1200-wstep.txt /home
    /georete/automatic_fs/;
cd /home/georete/automatic_fs/;

./skempton coes.asc ang_attr.asc mappa_saturazione_08$
    (date +%j)1200-wstep.txt slope.asc gamma.asc dtb.
    asc FS_$(date +%Y%m%d)_1200_01.asc;

rm mappa_saturazione_08$(date +%j)1200-wstep.txt;
cp FS_$(date +%Y%m%d)_1200_01.asc /home/georete/
    automatic_fs/fs_maps_telespazio/;
mv FS_$(date +%Y%m%d)_1200_01.asc /home/georete/
    automatic_fs/fs_maps/;

rsync -avz -e "ssh" /home/georete/automatic_fs/
    fs_maps_telespazio unifi@spatial.telespazio.it:/usr
    /data/projects/preview/ll/liguria/safety_factor/NRT
    ;

cd /home/georete/automatic_fs/fs_maps_telespazio/;
rm FS_$(date +%Y%m%d)_1200_01.asc;

else
#If the new soil saturation map is not founded exit
    from the script...

  echo "CIMA has not yet provided the new soil
     saturation map 08$(date +%j)...Try again later!";

exit
fi
```

There should exist one of this script file for every expected rainfall intensity map or soil saturation map (one every hour and one every six hours int this case).

Step by step, the automation of the warning systems works as follows:

- In the central server (DST-UNIFI) a Cron scheduled tasks checks every

five minutes if in the CIMA server are available new data and when it finds something new, download the data using the rsync synchronization tool.

- With the stationary data already present in the server and with the new dynamic data obtained by the CIMA, the slope stability software compute the factor of safety map recording the results in a new ascii file.
- The new factor of safety is uploaded to the Telespazio server using the rsync synchronization tool in a particular folder where the Mapserver Web-GIS software can immediately read the maps.
- Every time a user connects via web to the link corresponding to the Web-GIS, the new updated factor of safety map can be viewed, queried and eventually downloaded if further analysis are needed.

The near-real time warning system has been active since January 2007 and is still active in present days (November 2008).

8.3 Publication of the results on the web using Web-GIS service

A Web-GIS is a software used to display and manage geographical data on the web in a way similar to what can be do with a normal GIS software on a desktop pc. In a Web-GIS is usually possible to visualize many geographical layers, to perform panning and zooming and to query the data the same as in desktop environment. The major difference is that the geographical layers, the geographical database and the GIS software itself are stored on a remote server instead on the pc from where you are working. As shown in Figure 8.2, a Web-GIS can be described as composed of almost three major part:

- A geographical database (like PostGIS or PostgreSQL) where the geographical layers are stored and organized
- A Web-GIS software (like Mapserver) that has the ability to read and manage the data and to transform the content of the database in images of various format (i.e. jpg or bmp) that can be easily viewed on the web.
- An HTTP server (like Apache) that should work as an interface between the server computer itself and the users that are trying to connect via the web using the standard web protocol http (Hyper Text Transfer Protocol).

The major advantage of using a Web-GIS, or like in the case of the PREVIEW project, of share the result of the model using a Web-GIS, is that in every moment whoever has an internet connection can see in near-real time the updated data using a normal web browser. Moreover at the present time many mobile phones have the capability to surf the web using browsers expressly developed for those devices. These are usually totally compatibles with the http standard and so can result very useful to monitor the Web-GIS even in emergency condition when it's not always possible to have a laptop and an internet connection.

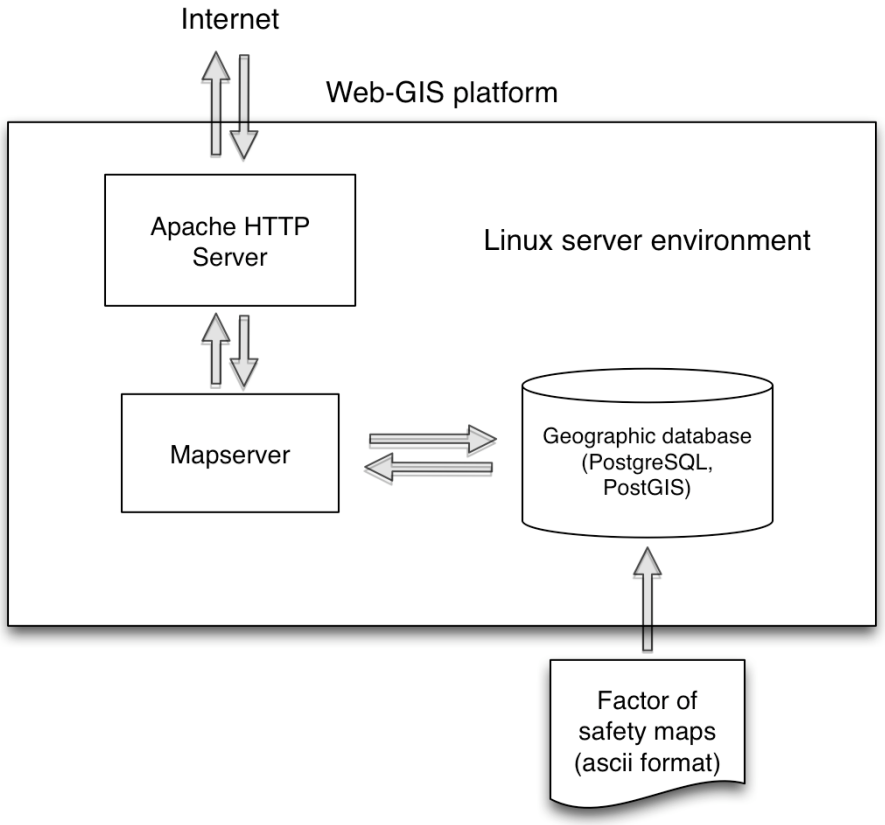

Figure 8.2: Scheme showing the main components of a Web-GIS platform

As already said the Web-GIS platform, where the results of the slope stability model for the Armea basin are uploaded, is hosted in the Telespazio server, located in Rome. On that server are constantly and automatically uploaded using rsync all the new meteorological data provided by the CIMA and the new factor of safety maps computed with the slope stability software for the Armea basin. Once these data are in the Web-GIS database, as soon as an external user will try to add a new geographical layer during a Web-GIS session, he will find even the new updated data. In this way the user has the opportunity to see the stability condition for the Area basin in near-real time. The time occurred to complete the entire chain, from the rainfall intensity measurement to the publication of the factor of safety map on the Web-GIS, ranges from 15 to 20 minutes.

The Web-GIS interface (Figure 8.3) is organized in a way similar to those of the more common gis software: on the left side there is a list of all the available layers, in the centre there is the screen were the active layers are shown and in the upper part a toolbar permits to choose between various tools to operate on the layers (zoom in, zoom out, pan, query, previous extent, next extent). The user who needs to perform further analysis can download the original data in grid-ascii format and use them on a normal gis software.

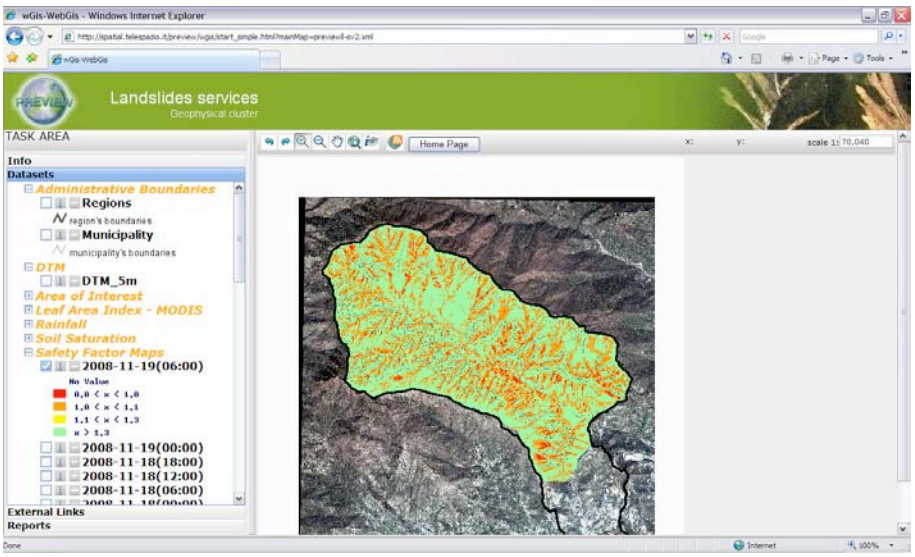

Figure 8.3: The Web-GIS interface for the Armea basin viewed using Microsoft Explorer web browser

The geographical layers constantly hosted and updated on the Web-GIS are (for the Armea basin):

- Administrative boundaries
- Soil depth map
- Digital elevation model
- Leaf area index (LAI, the ratio of total upper leaf surface of vegetation divided by the surface area of the land on which the vegetation grows)
- Satellite image acquired on 13th of March 2007
- Rainfall intensity maps
- Soil moisture map
- Factor of safety maps

Even tough the near-real time radar data are still not available for the Island of Ischia and thus the warning system is not active for this area, the Web-GIS structure has already been developed (Figure 8.4). It contains for the moment just the data regarding the landslides event occurred in April 2006 and the results of the near-real time simulation. The geographical layers hosted on the Web-GIS for the Island of Ischia are:

- Administrative boundaries
- Soil depth map
- Digital elevation model

- Leaf area index
- Satellite image
- Rainfall intensity maps (29-30 April 2006)
- Factor of safety maps (29-30 April 2006)s

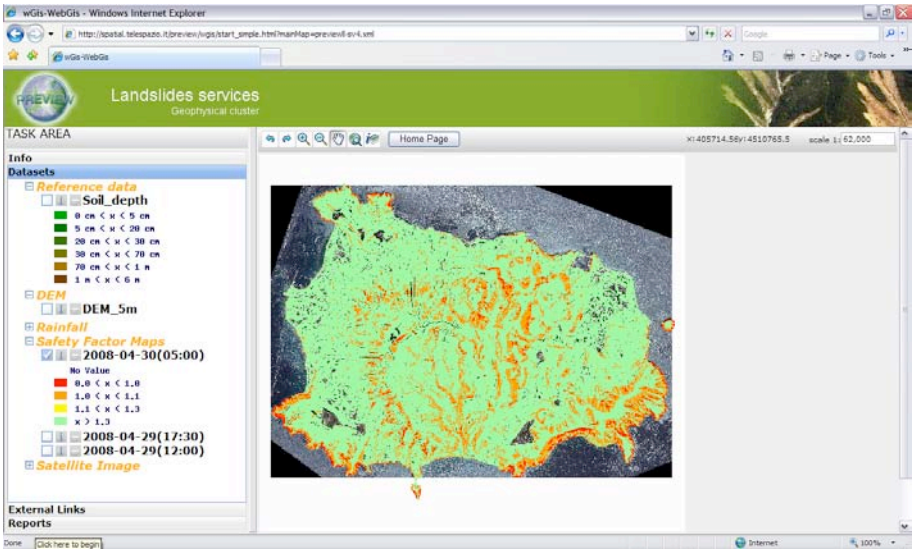

Figure 8.4: The Web-GIS interface for the Island of Ischia viewed using Microsoft Explorer web browser

Chapter 9

Results and validation

In this chapter will be shown the results of the near-real time simulation performed using historical weather data in order to evaluate the capabilities to forecast the occurrence of shallow landslides of the two developed models. Since no important landslides have occurred in the Armea basin when the warning system was active, there's not the possibility to evaluate the functionality of the warning system with real time data.

It is here important to remark that testing the two softwares with historical data has no influence on the final results of the models. One of the advantages of this approach is that it is possible to remove the error due to the uncertainty in the weather forecast because we are using the real rainfall intensity actually measured by the radar instead of a projection made with a numerical model. In this way any final error of the the slope stability models can be only due to the models themselves or to the uncertainty in the soil properties distributions but not to low quality weather forecasts. Another major advantage is that thanks to the data collected during the fieldwork and to the landslide database build with the satellite image (see section 5.1.8.2) it has been possible to compare the results of the model with the landslides actually occurred.

9.1 Results

The results presented here have been obtained running the two softwares with the input stationary data shown in Section 7.1 and with the meteorological data provided by the CIMA and by the Italian Air Force. For the Armea basin both the rainfall intensity maps and the soil moisture maps computed using the C-DRIFT hydraulic model were available. Thus in that test site it has been possible to test both the infinite slope model, that needs as input the soil moisture maps, and the modified Iverson model that uses the rainfall maps to evaluate the transient groundwater pressure. On the contrary in the Island of Ischia just the rainfall intensity maps were available so as just the modified Iverson model has been tested in that test site.

All the factor of safety maps are here presented with the same legend, classified in four classes, characterized by not fixed steps, that has been chosen just to make more clear the variations in the stability conditions. The only values that should be considered unstable according with the effective stress principle

are those equal or lower than unity (red class in the legend).

9.1.1 Armea basin: December 2006 event

Here are presented the results obtained with the two developed model for the Armea basin.

Results obtained with the **infinite slope model coupled with the C-DRIFT hydraulic model:**

The infinite slope model used to compute the factor of safety maps needs as input the soil moisture maps provided by the CIMA instead of the rainfall intensity maps. The soil moisture is calculated using the hydraulic model C-DRIFT, that even thought projected to forecast floods, can be used to infer the amount of water that remains in the soil as groundwater after a rainfall. The initial slope stability conditions obtained for very low soil moisture and no rain condition (using the soil moisture map of 8th December 2006 at 00:00) are shown in Figure 9.1a. On that map the majority of the analyzed cells are obviously stable with some exceptions for a few areas in red that results unstable probably due to wrong values in the initial stationary data. These areas are usually the result of a compounding between high slope angles and high soil depth. That could be due to an overestimated soil thickness calculated with the GIST model or to a wrong slope angle as a consequence of the dem approximation. Figure 9.1b shows instead the final factor of safety resulting after a day of intense rainfall and computed using the soil moisture map of 22:00. It appears immediately that the unstable cells in red are a quite huge percentage of the total area, surely many more of the landslides actually occurred on 8th December 2006.

To describe the results and the behaviour of the model in response to rainfall it is important to show not only the beginning and the final output of the computation like in Figure 9.1, but even to show how the slope stability changes with time according with the results of the model during different time of the day. Unfortunately the exact time of the occurrence of the landslides it is not known. It has been possible just to infer that all the landslide were triggered in the afternoon between 12:00 and 23:00 pm. In Figure 9.2 a portion of the basin has been chosen to show the variation with time of the factor of safety. The chosen area can be considered as representative of the entire basin and has been selected since there some landslides occurred on that day and thus is possible to directly compare the forecast of the model with the reality.

In Figure 9.2 are shown 6 representative moments chosen between the results obtained with the infinite slope model. In the first three pictures (9.2a, 9.2b, 9.2c) no significant changes in the factor of safety maps can be observed, even though at 05:00 it was already raining. The response of this model to rainfall seems quite slow and the first visible changes in slope stability can be found in the Figure 9.2d (16:00) with a slight decrease in the factor of safety. The values continue to decrease in the last two Figures 9.2e and 9.2f. A definite decreasing trend of the factor of safety values is thus evident starting from 16:00. According with these results the studied area should have become unstable starting from 19:00 when wide zones assume values lower than one. The red cells are at 22:00 far more than the total areas of the actually occurred landslides thus showing an

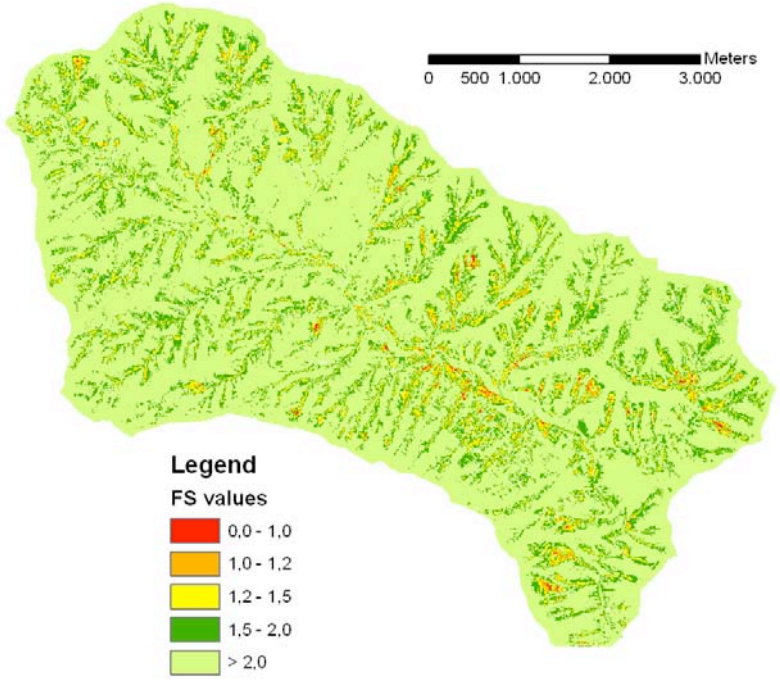

a)

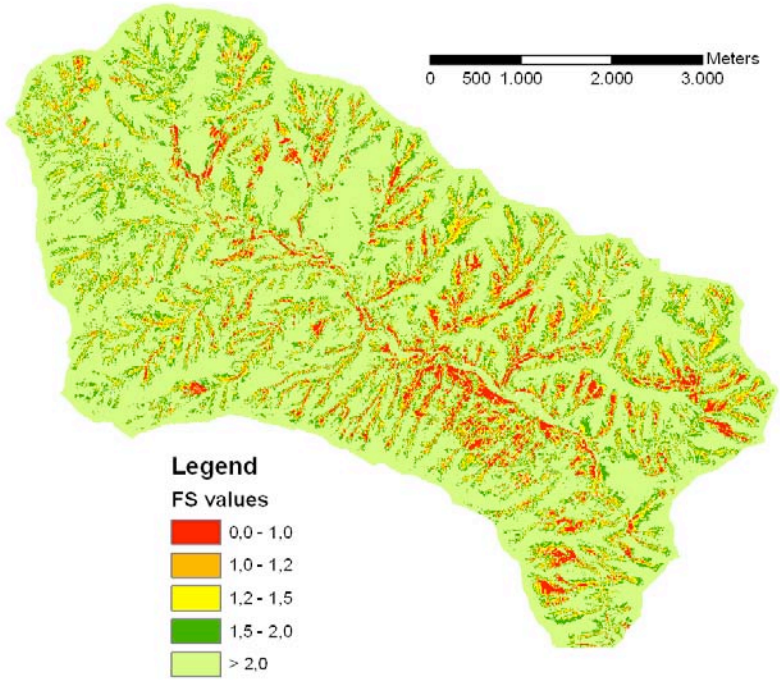

b)

Figure 9.1: a) Initial conditions (8th December 2006 h 00:00) and b) final conditions (8th December 2006 h 22:00) computed with the infinite slope model coupled with the C-DRIFT hydraulic model for the Armea basin.

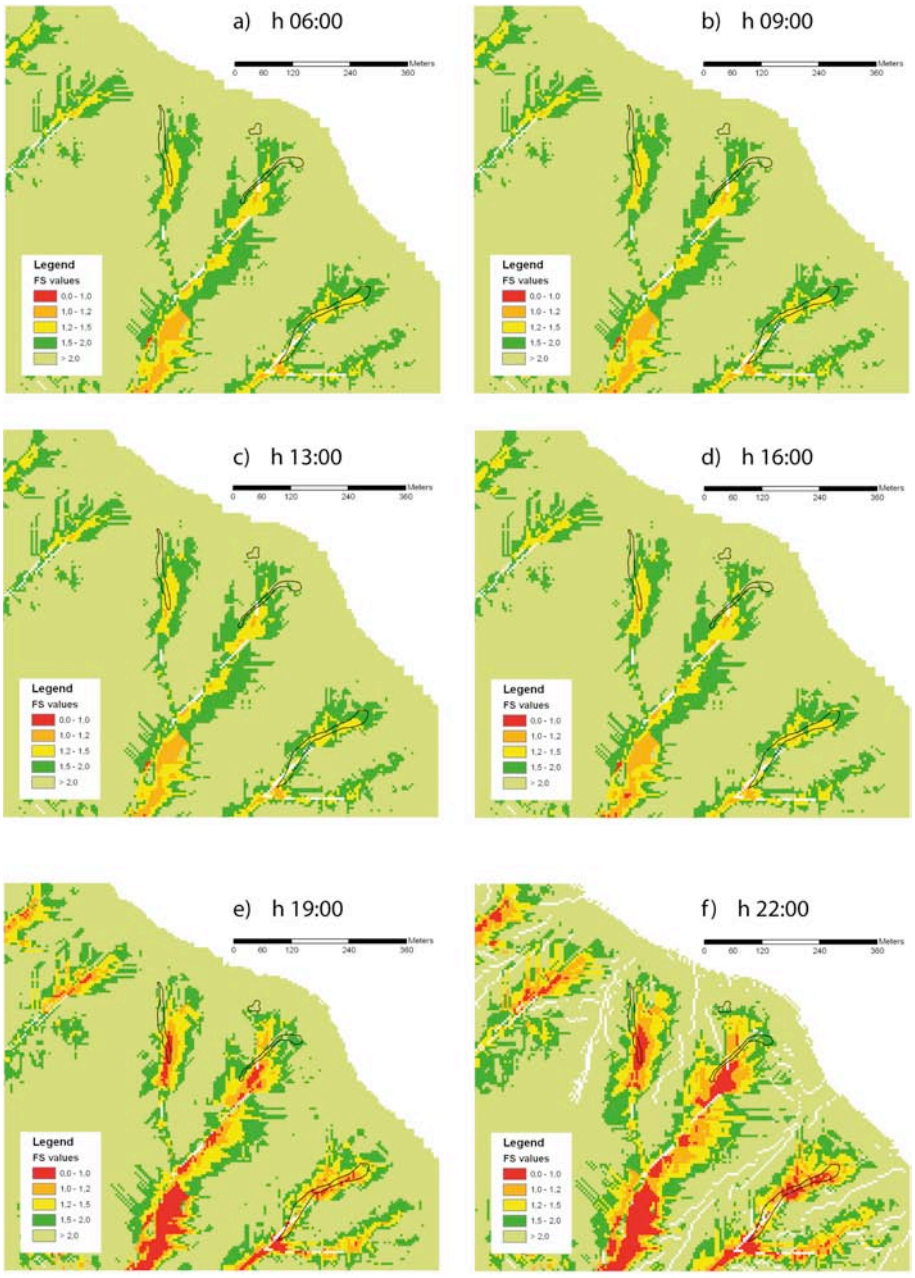

Figure 9.2: Results of the infinite slope model coupled with the C-DRIFT hydraulic model for the Armea basin. The area shown here is located in the central-northern part of the basin. The black lines overlaid on the factor of safety maps represents the contours of actually occurred landslides. See text for further explanation about the slope stability conditions at different times.

overestimation of the slope instability. Furthermore in the left-upper corner of Figure 9.2f two unstable areas are present where instead no landslides occurred. These two areas can be considered as two cases of false positive, that is when the model forecasts a landslide in an area that instead remains stable.

In the case that the warning system was active and was using this model to calculate the factor of safety, the instability would have been recognized quite late in the afternoon, not earlier than 19:00, thus with some delay with presumed time of occurrence of the landslides (mid afternoon).

Results obtained with the **modified Iverson model:**

The factor of safety maps presented here have been computed with the modified Iverson model that uses as input the rainfall intensity maps provided by the CIMA and includes in its core an hydrologic model based on a linear solution of the Richards equation needed to calculate the transient groundwater pressure head distribution.

In Figure 9.3a are shown initial stability conditions when the soil is almost dry and unsaturated (8th December 2006 at 00:00). As expected the majority of the cells are stable (pale green) with few exception probably due to errors in stationary input data (usually high slope angle in areas with high soil thickness). The altered areas in dry condition, with factor of safety values ranging between 1.0 and 1.5 (yellow and orange pixels) could represent zones more prone to slope instability. These zones would became unstable as soon as the soil will be saturated by rain. Figure 9.3b shows the factor of safety map resulting from the computation at 19:00 when, after a day of heavy rainfall, the soil was quite wet and many areas are accounted as unstable. Comparing the worst stability condition obtained using the two different stability models (Figure 9.1b and 9.3b) it is immediately clear that the unstable areas obtained with the modified Iverson model are far less than those obtained with the other. This should be considered as a good result since the false positive cases decrease in comparison with real landslides.

In Figure 9.4 are shown 6 factor of safety maps for successive times centered in the same area as in Figure 9.2 but obtained with the modified Iverson model. Here the definite decreasing trend of the factor of safety values like in 9.2 is no more present. The response of the model to heavy rainfall is faster and at h 13:00 some cells became already unstable (Figure 9.4c). The same instability is pointed out at 16:00 and at 19:00 (Figure 9.4d and 9.4e) while a decrease can be observed at 22:00 (Figure 9.4f). The results of this model appear to be more strictly linked with the occurrence of rainfall thus resulting in a decrease of the factor of safety as soon as the infiltrating rain starts to increase the groundwater pressure and the water table starts to rise. Moreover it is important to remember that the modified Iverson model is projected to evaluate the factor of safety at different depths and to record the lowest value in the final output file. This could result in more realistic behaviour especially in presence of high soil thickness, where unstable conditions could be reached within the soil instead that at the interface between soil and bedrock. At the same time the groundwater pressure in response to infiltrating rain could grow downward starting from the soil surface and achieving the critical value before reaching the bedrock.

The amount of unstable cells shows a good agreement with the total area of the real landslides (bounded by black lines in Figure 9.4) even though they don't

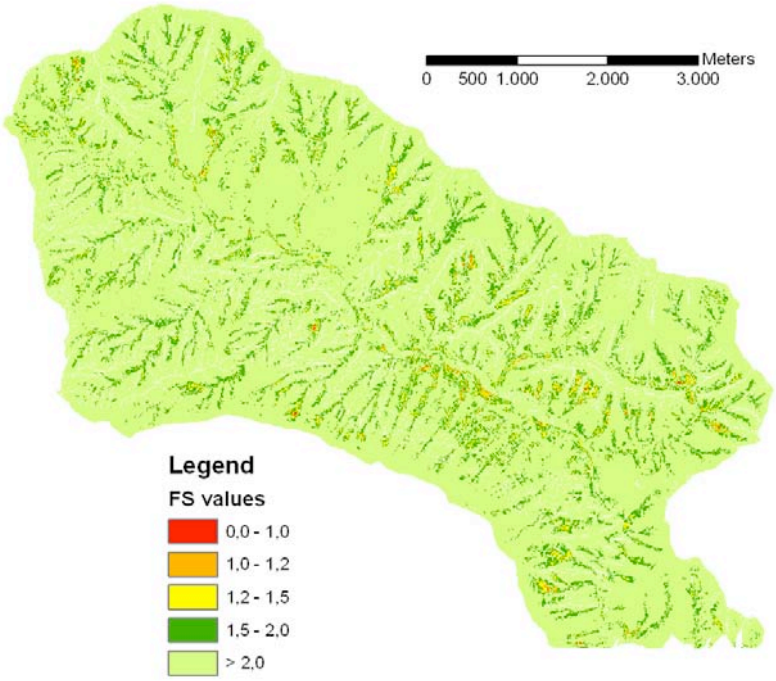

a)

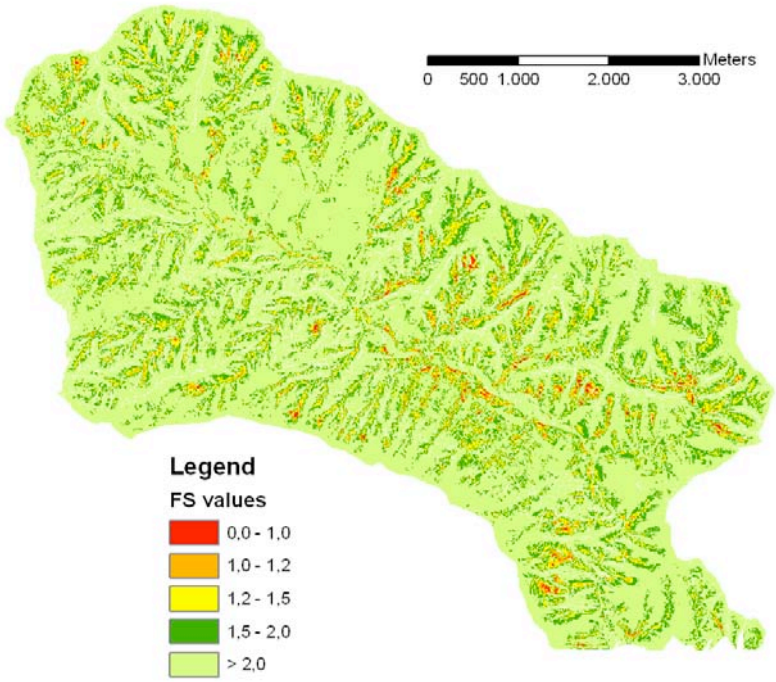

b)

Figure 9.3: a) Initial conditions (8th December 2006 h 00:00) and b) final conditions (8th December 2006 h 19:00) computed with the modified Iverson model for the Armea basin.

mach in term of spatial distribution. In other words the forecasted landslides, that seems to mach in terms of number of unstable cells with the real landslides, are wrongly located respect to the landslide scars. It must be stressed that in terms of warning system capabilities, this spatial error would have not affected the final results because the system would have alerted anyway for the occurrence of landslides, independently from their location. The majority of the cell included in the real landslides perimeters are classified as at risk, with values of the factor of safety ranging between 1.0 and 1.5.

In the case that the warning system was active and was using this model to calculate the factor of safety, the instability would have been recognized starting from 13:00, thus a few hours earlier than the presumed time of occurrence of the landslides.

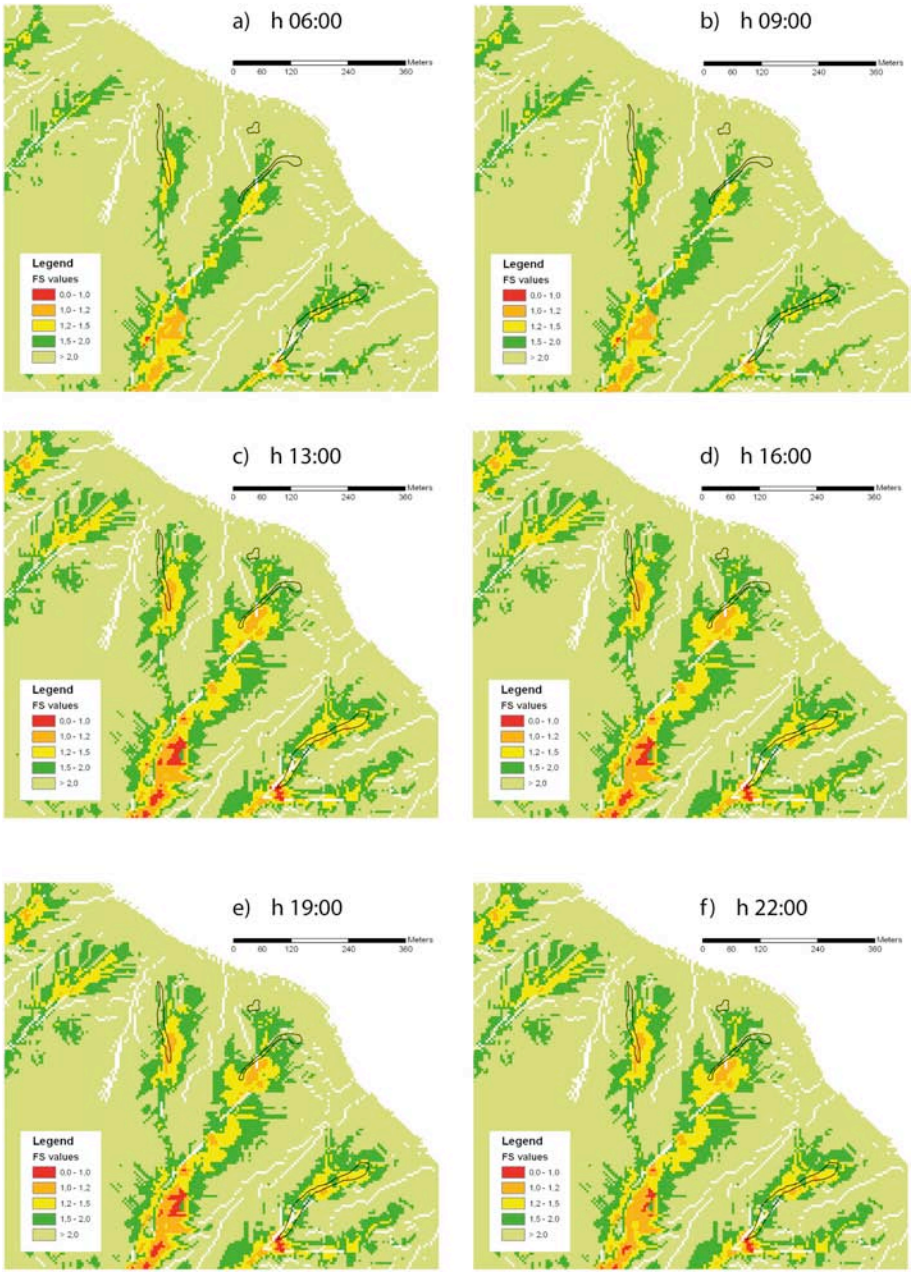

Figure 9.4: Results of the modified Iverson model for the Armea basin. The area shown here is located in the central-northern part of the basin and is the same shown in Figure 9.2 in order to permit a direct comparison between the results of the two models. The black lines overlaid on the factor of safety maps represents the contours of actually occurred landslides. See text for further explanation about the slope stability conditions at different times.

Summary of the results:

The results of the two models appear quite different, not only for the final results but even for the behaviour during and after the occurrence of rainstorms. The first model, coupled with the C-DRIFT hydraulic model, has a quite slow response to the infiltrating rain thus leading to a delay in the forecast of landslide occurrence. Moreover it seems to overestimate the instability in many areas and this could results in many false alarm or false positive cases. The modified Iverson model achieves better results both in terms of time accuracy of the forecasted landslides and in the total amount of unstable cells when compared with landsliding areas. Not so many false alarms are found in the total results of the model even though the spatial accuracy can be somewhere quite poor. In fact many of the forecasted unstable cells don't overlap with the landslides actually occurred and are instead located slightly downstream.

Both the models seems to be deeply affected by the original digital elevation model (DEM) from where the slope map was derived. For example where the slope is unnaturally high due to wrong approximation introduced during the creation of the DEM, the cell are classified as unstable even for dry conditions. Moreover, since this DEM is derived from a topographic map surely older than 2000 (see section 5.1.8.2), the morphology used to test the two models doesn't take into account for the landslides occurred during the 2000 event (section 5.1.7) that in some cases have deeply changed the slope profile. As a consequence a few landslide forecasted by both the models, that could be classified as false positive if compared just with the 2006 event, perfectly mach with landslides occurred in November 2000 (Figure 9.5 and 9.6).

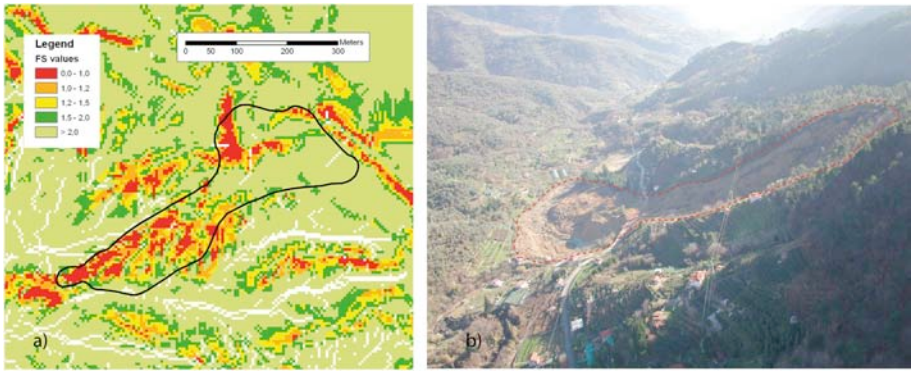

Figure 9.5: The big landslides occurred in November 2000 in the Armea basin which killed 2 people in their house. a) Factor of safety map (8th December 2006, h 22:00) obtained with the infinite slope model for this area; in black the perimeter of the landslide. b) View from the North of the landslide; in red the perimeter of the landslide.

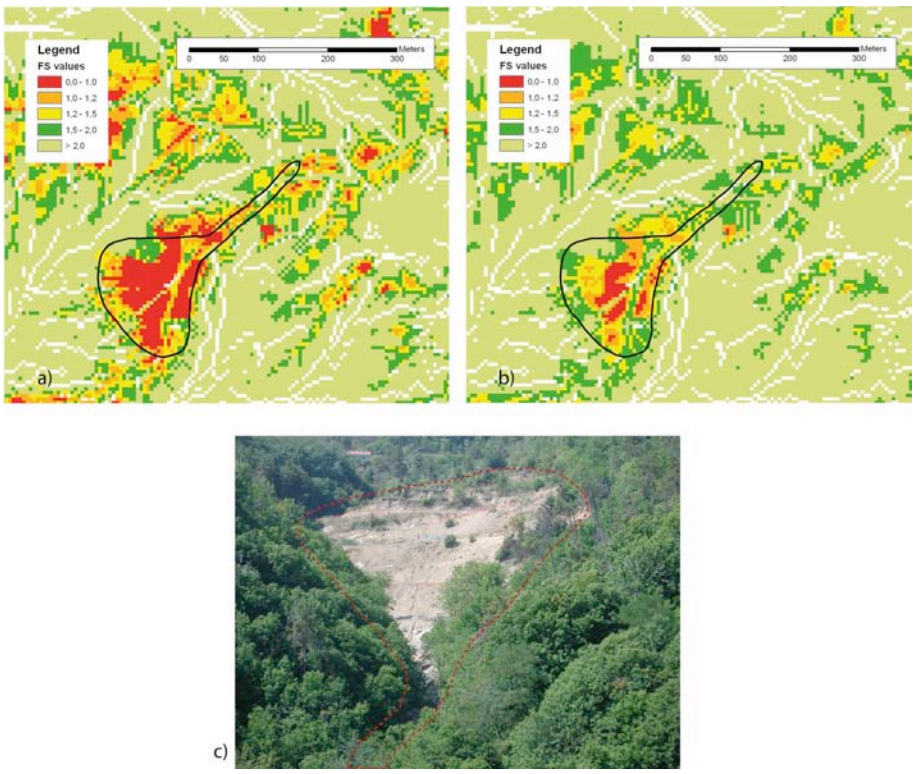

Figure 9.6: A big landslides occurred in November 2000 in the Armea basin. a) Factor of safety map (8th December 2006, h 22:00) obtained with the infinite slope model for this area; in black the perimeter of the landslide. b) Factor of safety map (8th December 2006, h 16:00) obtained with the modified Iverson model for this area; in black the perimeter of the landslide. c) View of the landslide from North-East; in red the perimeter .

9.1.2 Island of Ischia: April 2006 event

Here are presented the results obtained only with the modified Iverson model since no soil moisture maps were available in order to apply even the other developed software in the Island of Ischia.

Results obtained with the **modified Iverson model:**

The input data used to test the modified Iverson model on the Island of Ischia are rainfall intensity maps recorded by the Grazzanise weather radar, located near Naples, and provided by the Italian Air Force. These data have a temporal resolution of 30 minutes, from 00:00 of 29th April 2006 to 23:30 of 30th April 2006 for a total of 96 maps. The major landslides occurred on that date were all located along the Northern side of Monte Vezzi, in the South-Eastern part of the island, and were triggered between 06:00 and 08:00 of 30th April 9.7.

In Figure 9.8a are shown the initial stability condition, at 08:30 of the 29

Figure 9.7: Localization of the Northern side of Monte Vezzi, where four debris flow occurred between 06:00 and 8:00 of 30th April 2006.

April, before the beginning of the rain. As in the case of the Armea basin, even here the initial conditions show many cells at risk with values of the factor of safety between 1.0 and 1.5 and a few unstable cells even in dry condition. These cells, mainly located along the steep cliffs of the island, are deeply affected by the high slope angle which plays an important role in defining the balance between the resisting force and the driving force (see equation 3.15). In these cases, i.e. when the slope exceed 60°, even thin soil deposits can be classified as unstable. The final conditions shown in Figure 9.8b are referred to the morning of 30th April h 08:00 when the landslides were just occurred. In that case many area are classified as at risk or unstable due to the saturated condition of the soil that were reached during the night after many subsequent rainstorm.

The peculiarity of the rainfall event occurred between 09:00 of 29th April and 09:00 of 30th April is that the storms have been very intense and highly localized. The factor of safety maps presented here obviously take into account for this spatial variability. To show the results of the model and how the factor of safety values were changing with time, many factor of safety maps are presented, centered on the area were the landslides occurred. It is here necessary to show many more maps than those needed for the Armea basin because many subsequent rainstorms, all characterized by complex spatial patterns, have occurred in the previous 24h before the landslides triggering thus leading to complex and not linear variations of the factor of safety values. Since the soil was almost dry, after the first rainfalls no significant changes in the factor of safety can be observed. The first variations can be observed starting from 18:30 (Figure 9.9) when the soil should have been almost saturated. At 19:00 the cells along the Northern side of Monte Vezzi are classified as unstable for the first time. In the following time steps, in conjunction with no rain conditions, the factor of safety increases as soon as the soil water flows downward and at 20:30 the area is again stable. Between 21:00 of 29th April and the 00:00 of 30th the FS values shows minor fluctuations and this time gap can be considered as substantially stable, even though still ready to abrupt decreases as a consequence of the high soil moisture content. The occurrence of new rainfalls force the system to a decrease

in the FS values and the entire area is classified as unstable for the entire time period ranging between 00:30 and 03:00 am. The slope is again stable after that time but definitely saturated and now even small amounts of infiltrating rain can lead to instability. The factor of safety values are again in the red class for a time period of 2 hours, between 04:00 and 06:00. The factor of safety map of 06:00 probably matches with the occurrence of the first two landslides. The last instability is achieved in the gap between 07:30 and 08:00 and these could correspond with the occurrence of the last two debris flows. Starting from 08:30 of 30th April the slope is again stable and the high factor of safety values persist for all the successive hours.

In summary, the behaviour of the model in response of successive heavy rainfall changes with time as soon as the soil wetness increase. First, when the soil is almost dry, the factor of safety varies gradually and more slowly when rain stars to infiltrate. Both the decrease (after a rainfall) and the increase (during the successive no rainfall period) of the factor of safety values is more gentle and gradual (see Figure 9.9). When instead, after this first cycle, a new rainstorm occurs, the FS values drops slowly to unstable values probably due to the amount of groundwater still present in the soil. This fast variations persist even during the following cycles of alternating rainfall and no rainfall condition.

In the case that the warning system was active and was using this model to calculate the factor of safety, the instability would have been recognized starting from 19:00 of 29th April. In the successive hours, the the system would have alert for slope instability other 3 times: at 00:30, at 04:00 and finally at 07:30. At least the first three alert signal would have been send surely prior to the occurrence of the landslides.

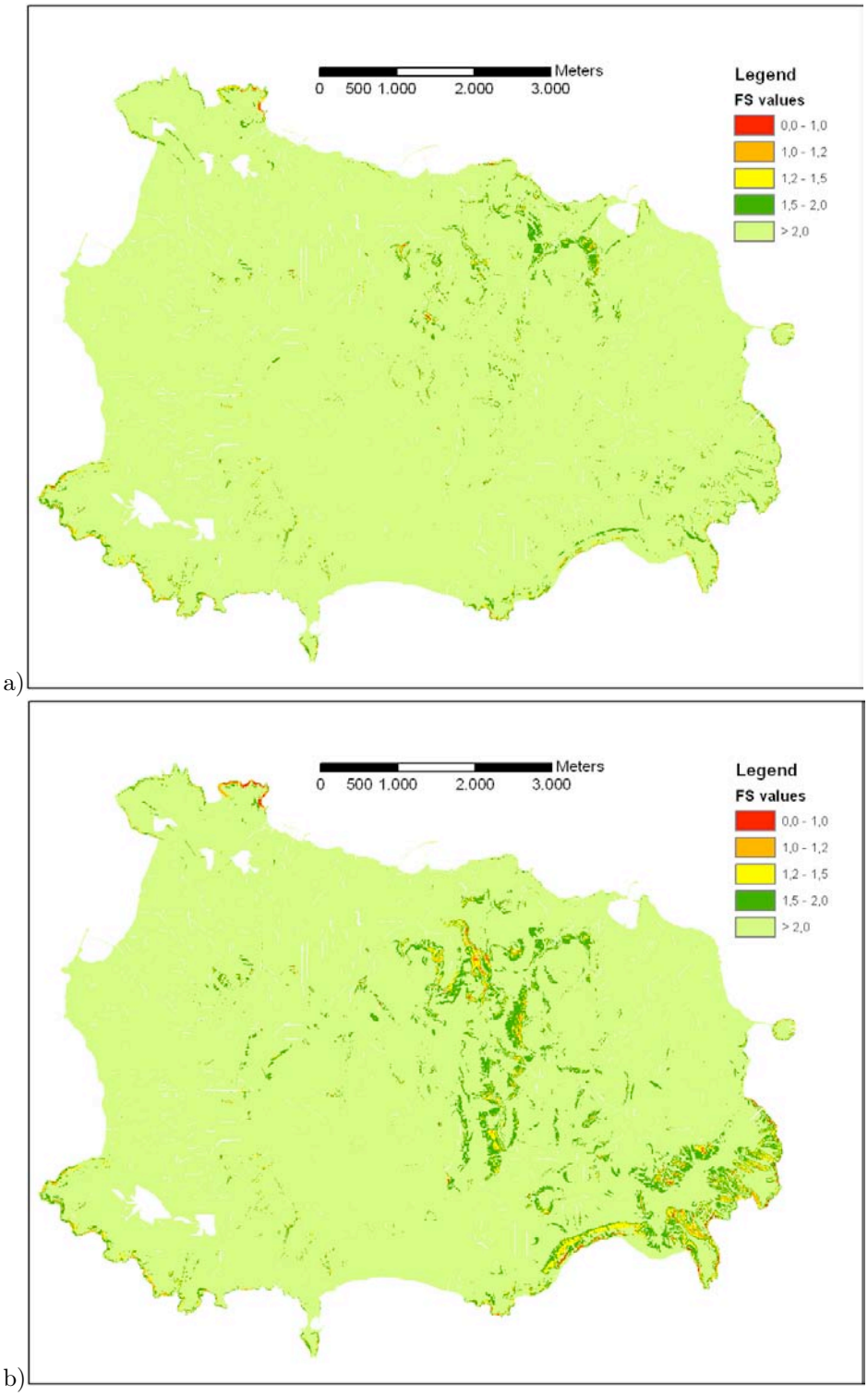

Figure 9.8: a) Initial conditions (29th April 2006 h 08:30) and b) final conditions (30th April 2006 h 08:00) computed with the modified Iverson model for the Island of Ischia.

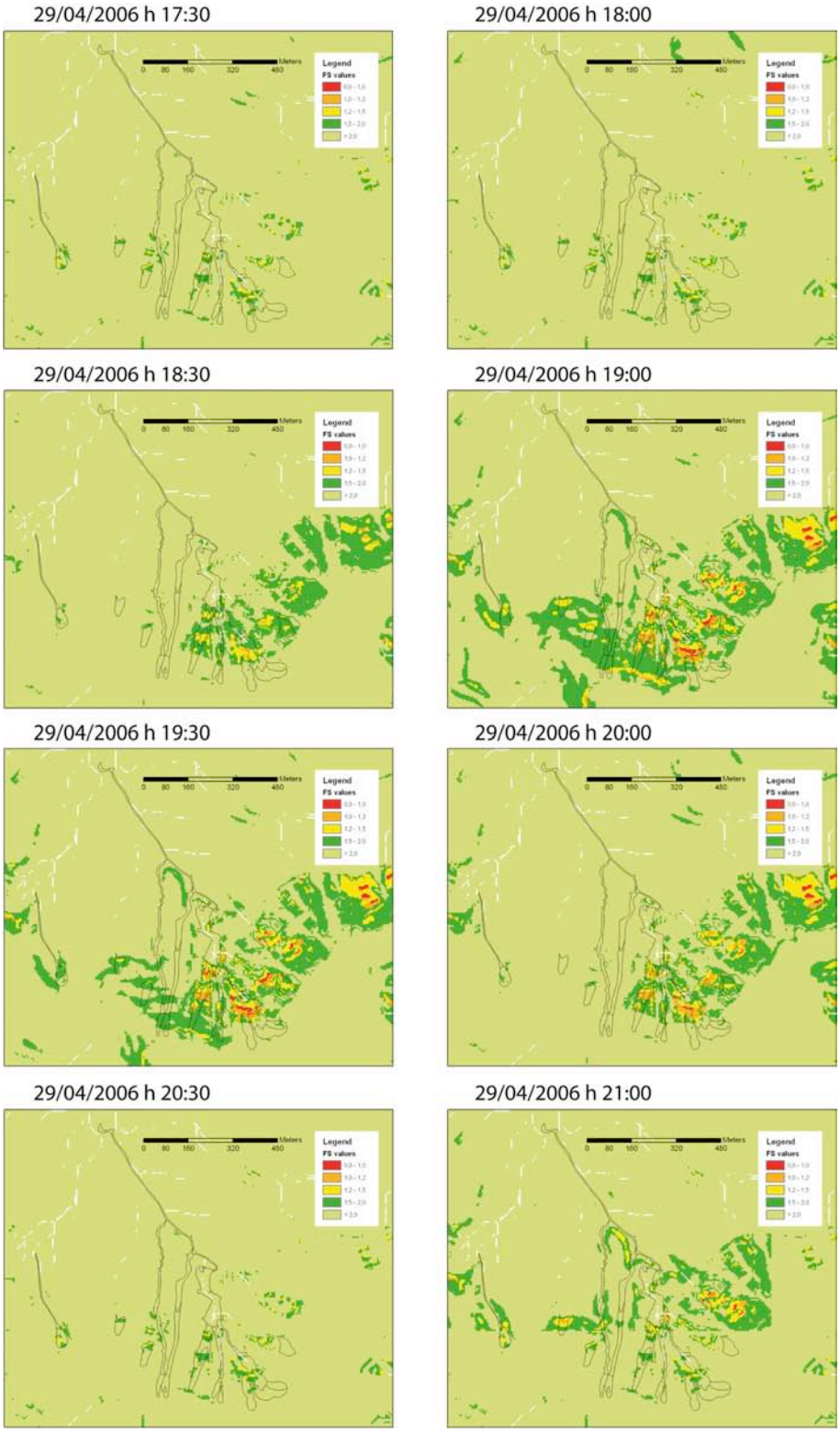

Figure 9.9: Factor of safety maps camputed by the modified Iverson model between 17:30 and 21:00 of 29th April 2006.

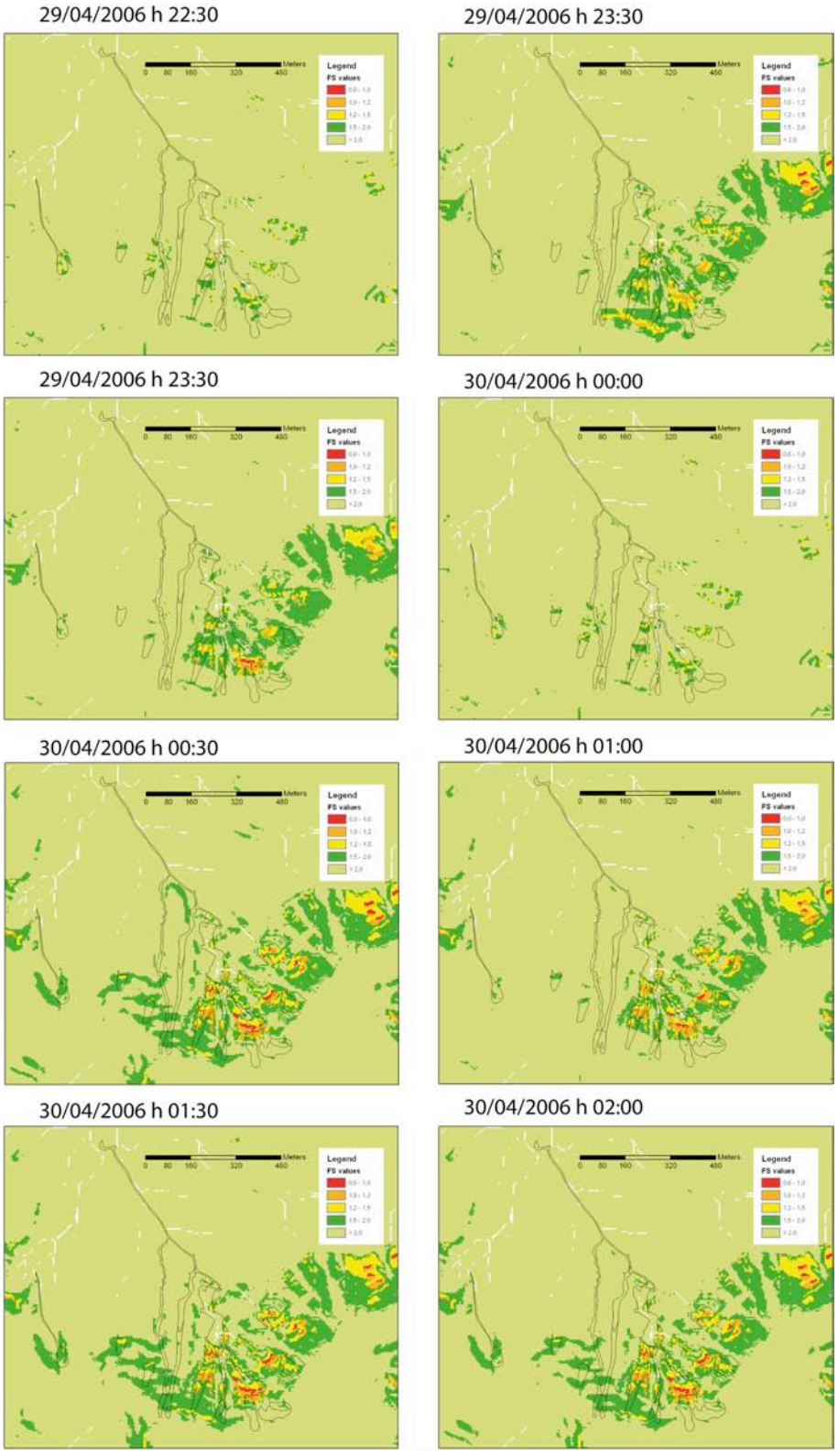

Figure 9.10: Factor of safety maps camputed by the modified Iverson model between 22:30 of 29th April and 02:00 of 30th April 2006.

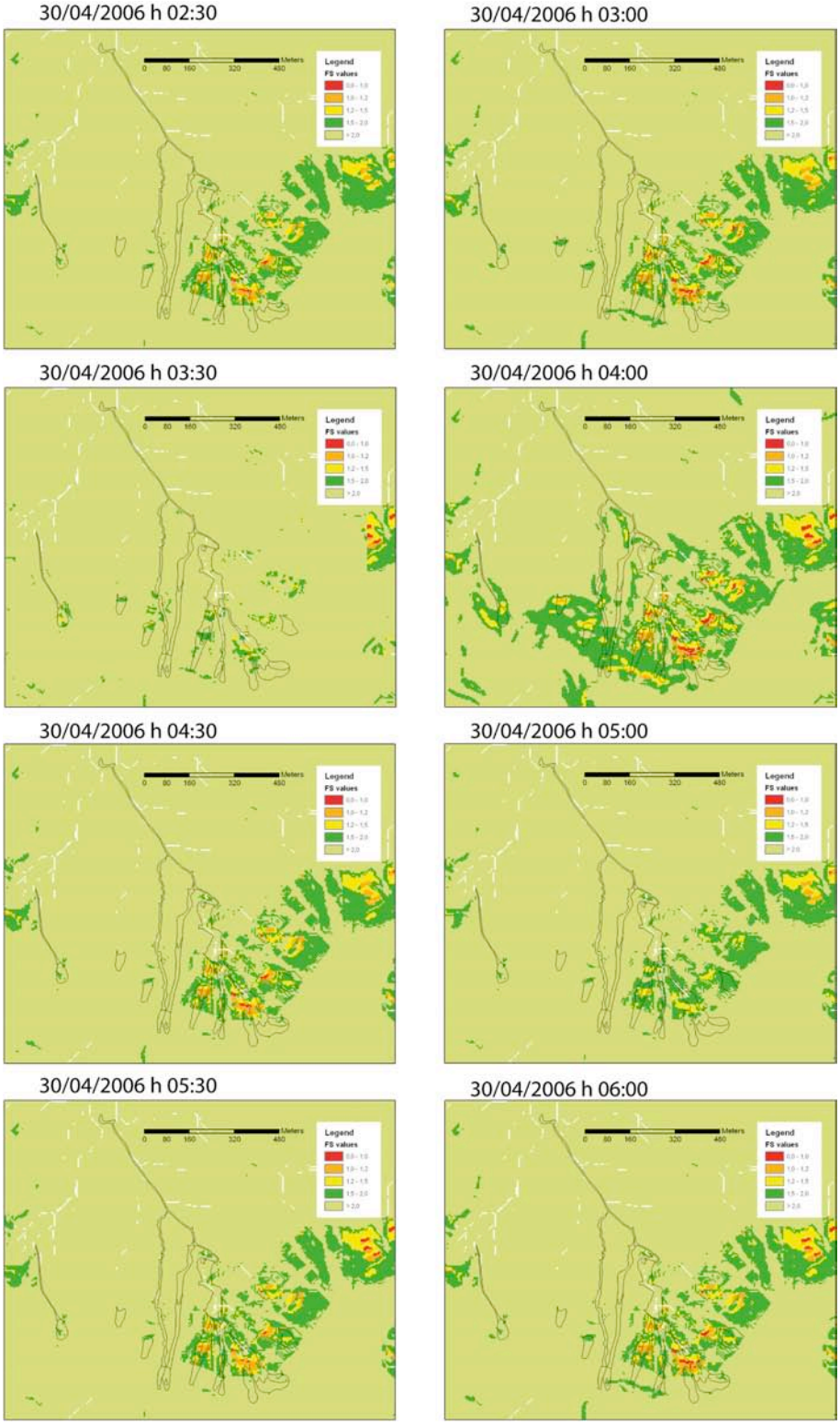

Figure 9.11: Factor of safety maps camputed by the modified Iverson model between 02:30 and 06:00 of 30th April 2006.

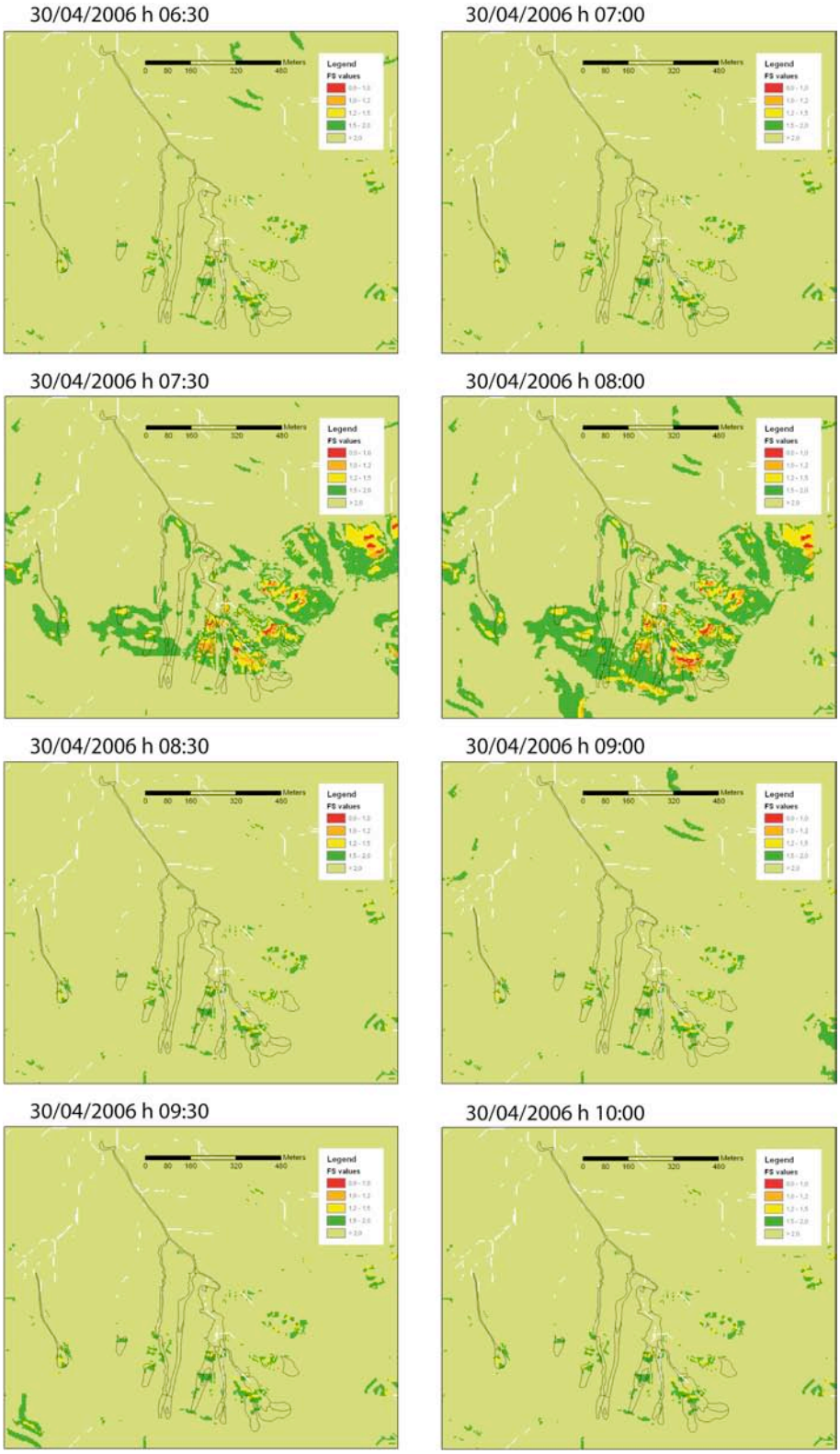

Figure 9.12: Factor of safety maps camputed by the modified Iverson model between 06:30 and 10:00 of 30th April 2006.

9.2 Model validation: Armea

Usually the validation of a distributed slope stability model consist in the comparison between a landslide inventory map and the final distributed factor of safety as provided by the model based on a simple polygon overlay (Salciarini et al., 2006; Crosta & Frattini, 2003; Schmidt et al., 2008). Since a new landslides database has been build using the satellite image acquired after the December 2006 rainfall event (see section 5.1.8.2) it has been possible to compare the results of the two models with the new inventory to find out their performance.

The landslide database built using the satellite image contains geographical informations about the location and the shape of the perimeter of each landslide. A cell of the factor of safety map should be considered unstable when its value is equal or lower than 1.0. But uncertainty derives from how to consider a prediction as accurate. How many pixels within the landslide area should have a value near or below unity? Is one unstable pixel enough to destabilize a larger area? Where should the unstable pixels be located within the landslide scar? The simple comparison between the landslide perimeter and the entire amount of pixels included in that area could lead to a wrong interpretation of the results. So it has been chosen a minimum percentage of unstable pixels (10%) that should be included within the landslide perimeter in order to establish if a prediction is accurate. For each single landslide the cells included in the perimeter have been extracted (Figure 9.13) and the relative percentage of pixels with values lower than 1.1 has been calculated in a GIS environment.

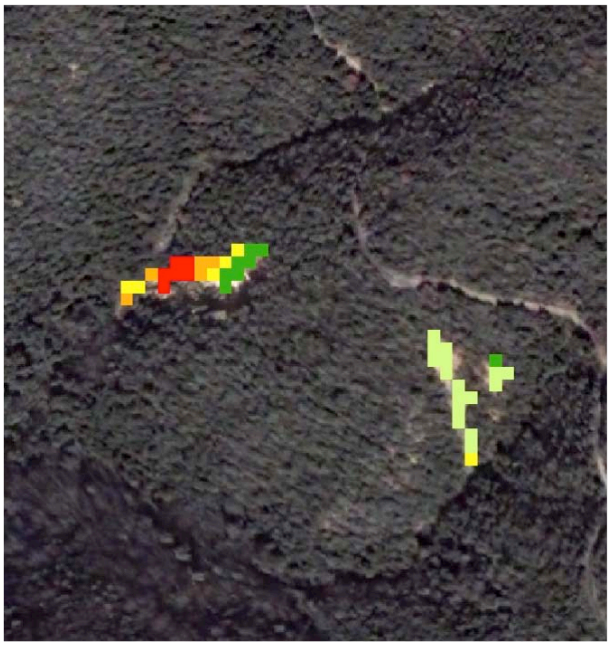

Figure 9.13: Extraction of the pixels covering landslide areas

Figure 9.14a shows the frequency classes of unstable pixels versus the number of landslides relative to the factor of safety maps computed with the infinite

slope model coupled with the C-DRIFT hydraulic model. The first frequency class 0-10 includes 49 landslides that can be classified as landslides that have not been forecasted by the model. The sum of all the other frequency class (29) is the number of landslides with more than 10% of unstable pixels and can be classified as landslides well forecasted by the model (Figure 9.15a). The data used for this comparison are limited to the new landslides (or reactivation of old ones) occurred during the December 2006 rainfall event.

As said in section 9.1.1, the morphology used to test the two models doesn't take into account for the landslides occurred during the 2000 event that in some cases have deeply changed the slope profile. To test how this could affect the results, the factor of safety maps have been compared with another inventory map that includes both the new 2006 landslides and those occurred in November 2000. Using the same approach as above, the results are in this case definitely better (see Figures 9.14b and 9.15b): the amount of landslides not forecasted by the model is 169 while the accurate predictions are 217.

The same frequency analysis has been conducted for the maps obtained with the modified Iverson model. First using the 2006 database only and then both the 2006 and 2000 landslides inventory maps. The results are shown in Figures 9.16 and 9.17. The first frequency class includes 41 landslides that can be classified as landslides that have not been forecasted by the model while the sum of all the other frequency classes, that is is the number of landslides with more than 10% of unstable pixels, are totally 37. Using the inventory map that includes the landslides occurred in 2000 and 2006, the results are even better with a total of 251 accurate predictions and 134 missed predictions.

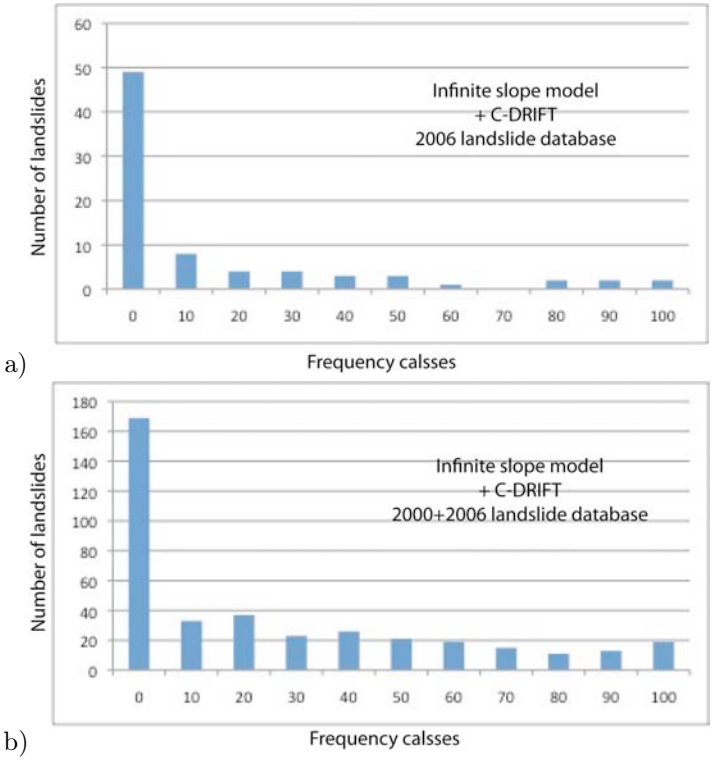

Figure 9.14: Chart showing the number of landslides for each frequency class. Each frequency class is defined by the percentage of unstable pixels respect to the landslide polygon. These data have been extracted from the factor of safety map provided by the infinite slope model compared with: a) the 2006 landslides inventory map. b) both the 2000 and 2006 inventory maps.

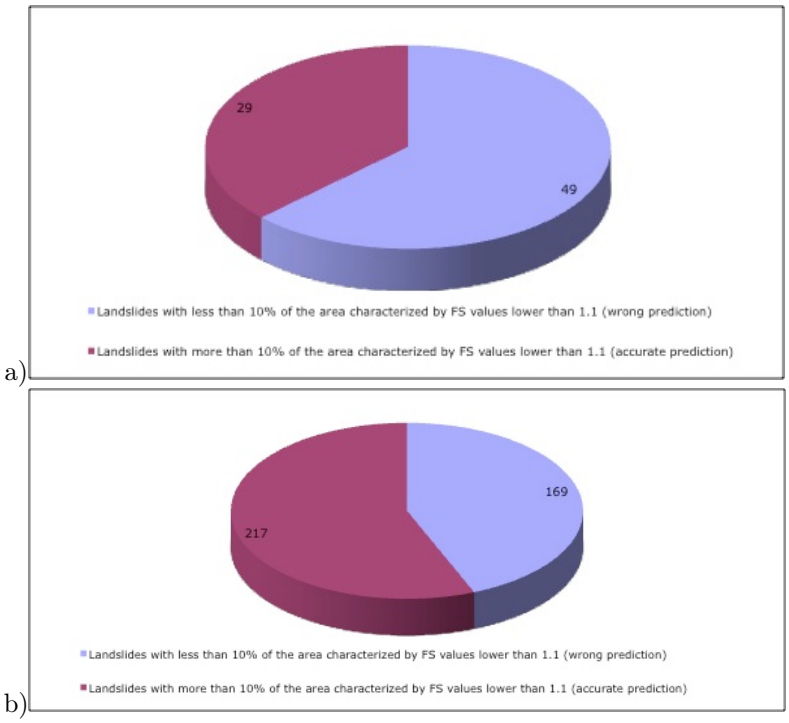

Figure 9.15: Pie charts of the results obtained using the infinite slope model. a) Summary of the results obtained using just the 2006 inventory map. b) Summary of the results obtained using the 2000 and 2006 inventory maps.

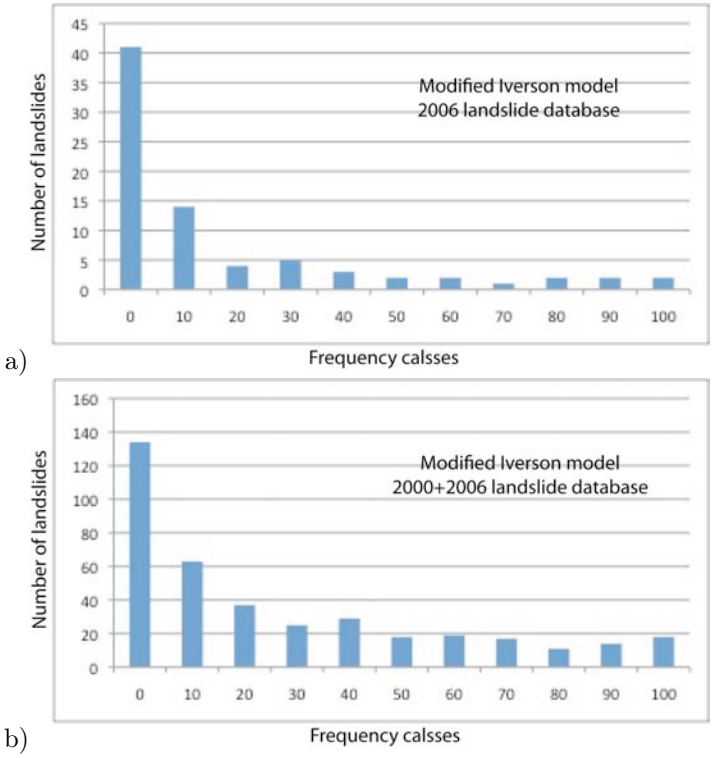

Figure 9.16: Chart showing the number of landslides for each frequency class. Each frequency class is defined by the percentage of unstable pixels respect to the landslide polygon. These data have been extracted from the factor of safety map provided by the modified Iverson model compared with: a) the 2006 landslides inventory map. b) both the 2000 and 2006 inventory maps.

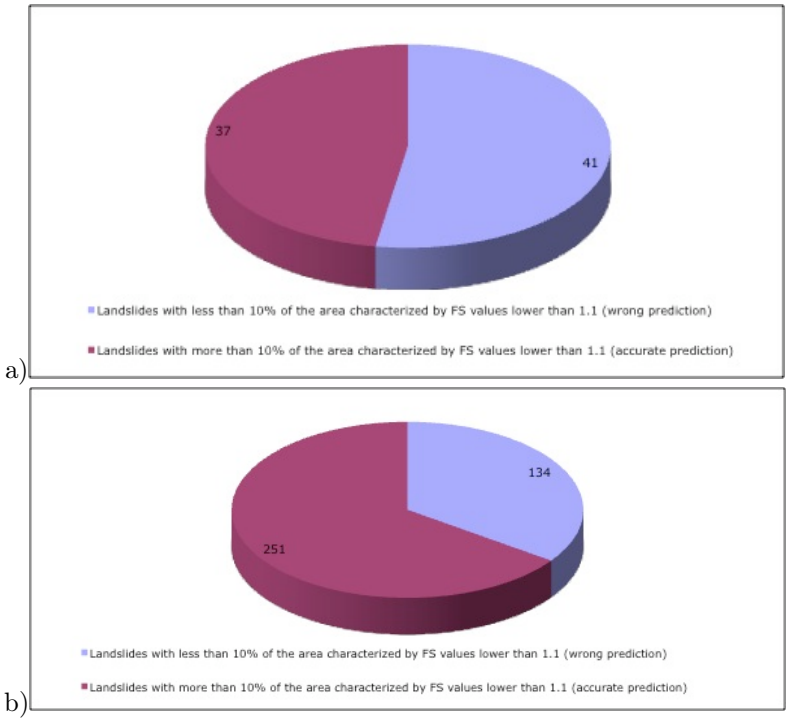

Figure 9.17: Pie charts of the results obtained using the modified Iverson model. a) Summary of the results obtained using just the 2006 inventory map. b) Summary of the results obtained using the 2000 and 2006 inventory maps.

9.3 Model validation: Ischia

Unfortunately, due to the lack of a good widespread landslide inventory map, it has not been possible to perform a spatial validation of the results obtained with the modified Iverson model when applied in the Island of Ischia. The only detailed information regarding the April 2006 event are limited to those landslides occurred in the Monte Vezzi area. For those debris flows it is clear the good spatial accordance between the unstable pixels of the factor of safety maps and the triggering zones of the landslides (Figure 9.12). This is particularly true for the first two eastern landslides (the ones that involved buildings and killed four persons) which reach unstable conditions with values lower than unity at least 4 times in the 24h before the triggering. The other two landslides and a smaller one located more to the West are characterized by higher factor of safety values, even though ranging between 1.0 and 1.2 and thus to be classified as at risk.

9.4 Basin scale balance and discussion of the results

The validation based on a simple polygon overlay doesn't offer a convincing evaluation of the effectiveness of the two developed models, mainly because of the high spatial variability of the model parameters in space and time. To offer a measure of the models performance that are directly linked to intensity and risk prediction another approach can be proposed, with the aim of evaluating the effectiveness of the two model at the basin scale. These model are in fact intended not to be a valuable tool for single landslides forecast but to be used within a warning system to issue an alarm for shallow landslides in wide areas.

For this reason it has been performed a total balance between predictions and observations at the basin scale, independently of where the unstable cells were located respect to the landslides scar. Obviously for cases like those shown in Figure 9.4 the results are definitely better with almost a 90% of accordance between the the landslides polygon area and the unstable cells as predicted by the model even though not perfectly overlapping. The summary of this balance is shown in Table 9.1. As expected, the simple infinite slope model doesn't achieve very good results due to the widespread tendency to underestimate the factor of safety values. As a consequence many areas are classified as unstable and the gap between predictions and observations is quite high if compared with the 2006 event (6,44%) or with the 2000 event (5,22%). For the same reason the percentage of false positive respect to the total area is high, 6,01% for the 2006 event and 6,21% for the 2000 event, while the false negative are 0,14% for the 2006 event and 1,08% for the 2000 event (Table 9.1). The false positive are here defined as the area classified as unstable minus the total area interested by landsliding in percentage respect to the total area of the basin. The false negative are instead defined as the percentage, respect to the total area, of cells classified as stable but where instead a landslide has occurred. The total errors, resulting from the addition of the false positives with the false negatives, is for the infinite slope model 6,15% (2006 event) and 7,28% (2000 event).

The modified Iverson model achieves, with this new approach, quite good results: observed areas with slope instability are 0,16% of the entire basin for

the 2006 event and 1,41% for the 2000 event while the model forecasts a total of 0,66% of unstable cells. In this case the gap between predictions and observations is quite low: just 0,50% higher than the total unstable cells observed during the 2006 event and 0,75% lower than the value resulting from the 2000 event. The false positives are quite low (0,61% for the 2006 and 0,56% for the 2000) the same as the false negatives (0,16% for the 2006 and 1,35% for the 2000). The total errors resulting from the analysis of the factor of safety maps computed with the modified Iverson model are 0,77% (2006 event) and 1,91% (2000 event). These values are definitely better than those obtained with the infinite slope model (Table 9.1). The drastic reduction of false positives of the modified Iverson model respect to the other can be probably ascribed to the effect of matric suction that in the infinite slope model is not taken into account. When the soil is not completely saturated, the matric suction produces a macroscopic increase in shear strength so as the final factor of safety value can be increased up to 0,4.

	Infinite slope model	Modified Iverson model
Observed 2006	0,16%	0,16%
Observed 2000	1,41%	1,41%
Predicted (total)	6,63%	0,66%
False positives (2006)	6,01%	0,61%
False negatives (2006)	0,14%	0,16%
Total error (2006)	6,15%	0,77%
False positives (2000)	6,21%	0,56%
False negatives (2000)	1,08%	1,35%
Total error (2000)	7,28%	1,91%

Table 9.1: Results of the balance between predictions of the models and observation at the basin scale.

Generally speaking the false positive error is a minor one because the absence of a landslides doesn't necessary mean that a certain slope can became unstable if subjected to slightly different conditions in the range of the uncertainty of the model (Crosta & Frattini, 2003). Moreover, when managing natural hazards, it is safer to be conservative, but many false alarms, especially when the stability model is used as the core of a warning system with civil protection purpose, can result in many troubles for local authorities and stakeholders. On these basis, the modified Iverson model, accounting both low false positive percentage and small gap between the actual unstable areas and the total extension of cells with FS values lower than 1.0, seems to perform definitely better respect to the

other. The infinite slope model in fact, even though characterized by low false negative percentage, similar to the value accounted by the other software, is characterized by a quite high amount of false positive cells. Using this model within a warning system, this huge amount of false positive could dramatically penalize the effectiveness of the warning system forcing to issue an alert even with small amount of infiltrating rain. The applicability of the modified Iverson model is moreover not affected by the existing spatial error within the results. To issue an alert for wide areas (even for a few square km) is instead of great importance not the exact location of the unstable cell but the total amount of the landsliding areas. When the amount of forecasted unstable cells exceeds a certain threshold is then necessary to issue an alarm, and it doesn't mind if the landslides then occur slightly far from the predicted cells. From this point of view, in order to be used within a warning system at the scale of the basin, the modified Iverson model performs definitely better so as it could be feasible to be chosen as the definitive core of the automatic warning system.

Chapter 10

Conclusions

During this PhD thesis an integrated procedure for the forecasting and warning of shallow landslides has been developed for civil protection purposes. First of all two pilot areas have been chosen in order to test the warning system and the slope stability models developed during this study. The two test sites, the Armea basin and the Island of Ischia, were chosen because, even though both quite prone to the occurrence of shallow landslides, they are characterized by a different lithology (sedimentary and volcanic). This has made it possible to test the models in different geologic contexts and to prove their effectiveness under different initial conditions. During the field work on those sites many data regarding the soil properties have been collected by means of in situ tests and laboratory analysis of the collected samples. The available geologic maps have been checked and in some cases corrected. In the Armea basin heavy rainfalls triggered many shallow landslides on 8th December 2006. In the days after this event a specific fieldwork has been carried out with the aims of collecting information on the new landslides and updating the landslides inventory map. Since during the fieldwork it was not possible to reach every zone of the basin, a new Quickbird high definition satellite image was acquired on 13th March 2007. The image was orthorectified and then, by means of photointerpretation performed in a GIS environment, a new landslide database was created. These information have been used to validate the warning system in the Armea basin.

Two different slope stability models have been developed and then tested in the proposed test areas. The first model is composed of two parts: a hydraulic model and a slope stability model. The hydraulic model, C-DRIFT, is hosted and controlled by the CIMA; it provides the soil moisture maps that are then used as input for the infinite slope stability model hosted in the UNIFI server (Section 6.1.1).

The second model, a modified version of the Iverson model, entirely run in the UNIFI server and calculates the transient pressure head distribution and the factor of safety taking into account the effect of soil suction when the soil is not completely saturated (Section 6.1.2). Moreover this model is projected to assess the factor of safety at different depths and to record the lowest value in the final output file. The meteorological data used as input are rainfall intensity map measured by ground based weather radar. The data collected during the field work are used as stationary input data to be provided to both the models (Chapter 7).

To apply these distributed models in wide areas two different softwares have been developed (Section 6.2). These codes are projected to be automatically executed by a Unix-based operative system (Linux, Mac OSX, Solaris...) with the support of system scripts and scheduled tasks (Section 8.2).

In parallell with the development of the two models, a warning sistem has been built on. This system is composed of three Linux servers connected to one another via web: the first one, located at the CIMA, is where the meteorological data are stored at first; then these data are moved to the UNIFI server where the factor of safety maps are computed using the two developed softwares. Finally the results of the stability analysis are uploaded to the Telespazio server in order to make them available within the geographic database and to allow the users to view and download the data through a Web-GIS platform (Section 8.3). The whole chain is entirely controlled and activated by the central server (UNIFI server) by means of syncronization tools to move the data and system sripts to make all the processes completely automatic. At the moment the warning system is active only in the Armea basin because for the second test site, the Island of Ischia, the near-real time wheather data are not yet available.

To test the effectiveness of the two models, near-real time simulations have been performed in the two test sites using actual real time data but measured during the past rainfall events: December 2006 for the Armea basin and April 2006 for the Island of Ischia (Chapter 9). The landslides triggered by rainfall during these two events were known thanks to the data collected during the fieldwork and to the photointerpretation performed on satellite images. Through the analysis of the factor of safety maps obtained during these simulations, it has been possible to evaluate the behaviour of the models in response to different and complex rainfall patterns. Moreover, comparing the results of the softwares with the new landslide inventory maps, has been provided a spatial validation of the two models for the Armea basin.

These results show that the predicted spatial landslide distribution is qualitatively comparable with the spatial distribution of the inventory map obtained through the photointerpretation of the satellite image. However predicting the exact location of landslides, especially for wide areas, is extremely challenging and the results of the two models show in many cases a not perfect overlap between the predicted unstable cells and the areas of the observed landslides.

To be used within a warning system, the model should be able to catch the exact amount of unstable cells along a slope or for the entire basin rather than the exact location of each lanslide. For this reason an analysis has been conducted on the results to find out the level of accuracy of both models at the basin scale (Section 9.4). The infinite slope model, even tough characterized by low false negatives (i.e. missed landslides), provides too many false positives so as, if used in a warning systems, would result in too many false alarms. Otherwise the modified Iverson model achieves quite good results, with both low false negatives and low false positives. For these reasons this model can be considered as the best one to be applied as the definitive core of the automatic warning system.

10.1 Further developments

The two developed models achieve quite good result in both test sites, but the modified Iverson model provides by far the better results and it has been chosen as the definitive stability model to be emploied within the warning system. Moreover it has the advantage of using the rainfall intensity maps as input instead of soil moisture maps. This allows its applicability to be extended to any areas covered by a ground-based weather radar since the rainfall intensity map is a standard product of these measuring devices.

Further developments of the warning systems should include the activation of the service in the Island of Ischia as soon as the near-real time data will be available. As previously said the entire chain, from the automatic factor of safety computation to the publication of these maps on the Web-Gis, is already setted and only rainfall input data are missing.

The final performances of the modified Iverson model could be improved considering the uncertainties in the parameters of the soil as suggested by Schmidt et al. (2008) and Simoni et al. (2008). The cohesion and the friction angle could be considered as random variables within a given distribution. Describing the uncertainty of those variables with probability density functions would improve the results even if on the other side the whole procedure would become more time consuming. A solution to the increased computation time could be to develop a new software which should include special libraries and algorithm such as MPI (Message Passing Interface). With this new application program interfaces inside the code, the software would be able to be executed in parallel by many calculator at the same time, thus drastically reducing the time needed for every run.

Bibliography

Alberoni P, Nanni S, 1992 "Application of an adjustment procedure for quantitative rainfall evaluation" in "Advances in hydrological applications of weather RADAR, Proc. of the 2 ndInternational Symposium on Hydrological Applications of weather RADAR",

Aleotti P, 2004 "A warning system for rainfall-induced shallow failures" *Engineering Geology* **73** 247–265

Aleotti P, Chowdhury R, 1999 "Landslide hazard assessment: summary review and new perspectives" *Bulletin of Engineering Geology and the Environment* **58** 21–44

Alonso E, Gens A, Josa A, 1990 "A constitutive model for partially saturated soils" *Géotechnique* 40–3

Anbalagan R, Singh B, 1996 "Landslide hazard and risk assessment mapping of mountainous terrains—a case study from kumaun himalaya, india" *Engineering Geology* **43** 237–246

Apuani T, Corazzato C, Cancelli A, Tibaldi A, 2005 "Physical and mechanical properties of rock masses at stromboli: a dataset for volcano instability evaluation" *Bulletin of Engineering Geology and the Environment* **64** 419–431

Baeza C, Corominas J, 2001 "Assessment of shallow landslide susceptibility by means of multivariate statistical techniques" *Earth Surface Processes and Landforms* **26** 1251–1263

Bagnold R, 1954 "Experiments on a gravity-free dispersion of large solid spheres in a newtonian fluid under shear" *Proceedings of the Royal Society of London. Series A, Mathematical and Physical Sciences (1934-1990)* **225** 49–63

Baum R, Coe J, Godt J, Harp E, Reid M, Savage W, Schulz W, Brien D, Chleborad A, McKenna J, et al., 2005 "Regional landslide-hazard assessment for seattle, washington, usa" *Landslides* **2** 266–279

Baum R, Savage W, Godt J, 2002 "Trigrs: A fortran program for transient rainfall infiltration and grid-based regional slope-stability analysis" *Open-file Report. U. S. Geological Survey*

Beven K, Lamb R, Quinn P, Romanowicz R, Freer J, 1995 "Topmodel" *Computer Models of Watershed Hydrology* **18** 627–668

Birkeland P, 1984 "Soils and geomorphology" *New York*

Bishop A, 1955 "The use of the slip circle in the stability analysis of slopes" *Geotechnique* **5** 7–17

Bishop A, 1959 *The Principles of Effective Stress* (Norges Geotekniske Institutt)

Bolt G, 1956 "Physico-chemical analysis of the compressibility of pure clays" *Geotechnique* **6** 86–93

Bonham-Carter G, Agterberg F, Wright D, 1989 "Weights of evidence modelling: a new approach to mapping mineral potential" *Statistical Applications in the Earth Sciences: Geol. Survey Canada Paper* 89–9

Borga M, Dalla Fontana G, Da Ros D, Marchi L, 1998 "Shallow landslide hazard assessment using a physically based model and digital elevation data" *Environmental Geology* **35** 81–88

Bortoluzzi G, Grimaldi R, Italiano A, 1983 "Osservazioni geomorfologiche sul versante meridionale dell'isola d'ischia" *Centro studi sull'isola d'Ischia: Ricerche, contributi e memorie* **II** 257–265

Brabb E, 1984 "Innovative approaches to landslide hazard and risk mapping" *Proceedings, IV International symposium on Landslides. Toronto, Ontario, Canada* 307–323

Braun J, Heimsath A, Chappell J, 2001 "Sediment transport mechanisms on soil-mantled hillslopes" *Geology* **29** 683–686

Brundsen D, Doornkamp P, Fookes D, Kelly J, 1975 "Large scale geomorphology mapping and highway engineering design" *Quartely Journal of Engineering Geology* **8** 227–253

Buchanan P, Savigny K, 1990 "Factors controlling debris avalanche initiation" *Canadian Geotechnical Journal* **27** 659–675

Burton A, Bathurst J, 1998 "Physically based modelling of shallow landslide sediment yield at a catchment scale" *Environmental geology(Berlin)* **35** 89–99

Caine N, 1980 "The rainfall intensity-duration control of shallow landslides and debris flows" *Geografiska Annaler* **62** 23–27

Calcaterra D, Coppin D, Palma B, Parise M, Orsi G, de Vita S, di Vito M, 2003 "Slope processes in weathered volcaniclastic rocks of the camaldoli hill (naples, italy): Geomorphologic and engineering-geological aspects" in "EGS-AGU-EUG Joint Assembly, Abstracts from the meeting held in Nice, France, 6-11 April 2003, abstract# 10281",

Campbell R, 1975 "Soil slips, debris flows and rainstorms in the santa monica mountains and vicinity, southern california" *U.S. Geological Survey Professional Paper* **851** 51pp.

Cannon S, Ellen S, 1985 "Rainfall conditions for abundant debris avalanches, san francisco bay region, california" *California Geology* **38** 267–272

Canuti P, Casagli N, 1996 "Considerazioni sulla valutazione del rischio da frana" *In:"Fenomeni franosi e centri abitati" Atti del Convegno, 27 maggio 1994, Bolgna, CNR-GNDCI* **846** 58 pp.

Carson M, Kirkby M, 1972 *Hillslope form and process* (Cambridge University Press)

Casadei M, Dietrich W, Miller N, 2003 "Testing a model for predicting the timing and location of shallow landslide initiation in soil-mantled landscapes" *Earth Surface Processes and Landforms* **28** 925–950

Casagli N, Guerri L, Righini G, Ferretti A, Colombo D, Prati C, 2005 "Integrated use of ps and very high resolution optical images for supporting landslide risk management" in "Symposium on Microwave Remote Sensing of the Earth, Oceans, Ice and Athmosphere",

Casagli N, Nocentini M, Farina P, Falorni G, Lombardi L, Righini G, Tofani V, Vannocci P, 2007 "Analisi dei fenomeni franosi avvenuti nel versante settentrionale del monte vezzi (isola di ischia) il 30 aprile 2006" *Rapporto n° 2.1 - Dipartimento di Protezione Civile*

Casagrande A, 1979 *Liquefaction and Cyclic Deformation of Sands: A Critical Review* (Harvard University)

Cattoni E, Cecconi M, Pane V, 2007 "Geotechnical properties of an unsaturated pyroclastic soil from roma" *Bulletin of Engineering Geology and the Environment* **66** 403–414

Chien-Yuan C, Tien-Chien C, Fan-Chieh Y, Sheng-Chi L, 2005 "Analysis of time-varying rainfall infiltration induced landslide" *Environmental Geology* **48** 466–479

Chiesa S, Cornette Y, Forcella F, Gillot P, Pasquar G, Vezzoli L, 1985 "Carta geologica dell'isola di ischia" *CNR, Progetto Finalizzato Geodinamica, Roma*

Chiesa S, Poli S, Vezzoli L, 1986 "Studio dell'ultima eruzione storica dell'isola di ischia" *Bollettino GNV* **1** 153–166

Cho S, Lee S, 2001 "Instability of unsaturated soil slopes due to infiltration" *Computers and Geotechnics* **28** 185–208

Ciccodemarco S, Ciminelli M, Corsi M, Pellegrino D, Rutigliano S, Falorni G, Leoni L, Righini G, Manuta P, 2007 "La piattaforma webgis per il monitoraggio del rischio frane nel progetto preview" *MondoGIS* **63** 23–27

Cinti L, 2007 "Valutazione di parametri topografici e dello spessore di coperture superficiali nel bacino del torrente armea, finalizzata allo studio di fenomeni franosi" *Università delgli Studi di Firenze, Tesi di Laurea*

Conacher A, Dalrymple J, 1977 *The Nine Unit Landsurface Model: An Approach to Pedogeomorphic Research* (Elsevier Scientific Pub. Co.)

Costa J, 1984 "Physical geomorphology of debris flows" *Developments and applications of geomorphology* 268–317

Crosta G, Dal Negro P, 2003 "Observations and modelling of soil slip-debris flow initiation processes in pyroclastic deposits: the sarno 1998 event" *Natural Hazards and Earth System Sciences* **3** 53–69

Crosta G, Frattini P, 2002 "Rainfall thresholds for triggering soil slips and debris flow" *Proc. 2nd Plinius Int. Conf. on Mediterranean Storms, Siena, Italy, in press*

Crosta G, Frattini P, 2003 "Distributed modelling of shallow landslides triggered by intense rainfall" *Natural Hazards and Earth System Sciences* **3** 81–93

Crozier M, Glade T, 1999 "Frequency and magnitude of landsliding:fundamental research issues" *Zeitschrift fur Geomorphologie* **115** 141–155

Cruden D, 1991 "A simple definition of a landslide" *IAEG Bull.* 27–29

Cruden D, Varnes D, 1996 "Landslides type and processes" *Landslides: Investigation and Mitigation* 39–75

de Vita S, Sansivero F, Orsi G, Marotta E, 2006 "Cyclical slope instability and volcanism related to volcano-tectonism in resurgent calderas: The ischia island (italy) case study" *Engineering Geology* **86** 148–165

Del Prete O, Mele R, 1999 "L'influenza dei fenomeni d'instabilità di versante nel quadro morfoevolutivo della costa dell'isola di'ischia" *Bollettino della Società geologica italiana* **118** 339–360

Denlinger R, Iverson R, 1990 "Limiting equilibrium and liquefaction potential in infinite submarine slopes" *Mar. Geotechnol* **9** 299–312

Dhakal A, Sidle R, 2004 "Distributed simulations of landslides for different rainfall conditions" *Hydrological Processes* **18** 757–776

Dietrich W, Bellugi D, de Asua R, 2001 "Validation of the shallow landslide model, shalstab, for forest management" *Water Science and Application* **2** 195–227

Dietrich W, Montgomery D, 1998 "Shalstab: a digital terrain model for mapping shallow landslide potential" *NCASI (National Council of the Paper Industry for Air and Stream Improvement) Technical Report, February*

Dietrich W, Reiss R, Hsu M, Montgomery D, 1995 "A process-based model for colluvial soil depth and shallow landsliding using digital elevation data" *HYDROLOGICAL PROCESSES* **9** 383–383

Ellen S, 1988 "Description and mechanics of soil slip/debris flow in the storm of january 3-5, 1982, in the the san francisco bay region, california" *U.S. Geological Survey Professional Paper* **1434** 64–111

Ermini L, Catani F, Casagli N, 2005 "Artificial neural networks applied to landslide susceptibility assessment" *Geomorphology* **66** 327–343

Ferraris L, Gabellani S, Rebora N, Provenzale A, 2003 "A comparison of stochastic models for spatial rainfall downscaling." *Water Resources Research* **39** 1368

Ferraris L, Rudari R, Siccardi F, 2002 "The uncertainty in the prediction of flash floods in the northern mediterranean environment" *Journal of Hydrometeorology* **3** 714–727

Fonseca F, 1870 *Geologia dell'Isola d'Ischia*

Frattini P, Crosta G, 2005 "Deliverable 3 - report on spatially distributed deterministic models and rainfall thresholds" *LESSLOSS Risk Mitigation for Earthquakes and Landslides Integrated Project*

Frattini P, Crosta G, Fusi N, Dal Negro P, 2004 "Shallow landslides in pyroclastic soils: a distributed modelling approach for hazard assessment" *Engineering Geology* **73** 277–295

Fredlund D, 1987 "Slope stability analysis incorporating the effect of soil suction" *Slope Stability: Geotechnical Engineering and Geomorphology. John Wiley and Sons New York. 1987. p 113-144, 31 fig, 10 tab, 25 ref.*

Fredlund G, Rahardjo H, 1993 *Soil mechanics for unsaturated soils* (John Wiley and Sons)

Fuchs C, 1873 "Monografia geologica dell'isola d'ischia con carta geologica 1:25.000" *Mem. per serv. alla descrizione della carta geologica d'Italia*

Gabellani S, 2005 *The propagation of uncertainty in the rainfall-runoff models for operational flood forecasting* Ph.D. thesis PhD Thesis

Gabellani S, Giannoni F, Parodi A, Rudari R, Taramasso A, Roth G, 2005 "Applicability of a forecasting chain in a different morphological environment in italy" *Advances in Geosciences* **2** 131–134

Gabet E, Burbank D, Putkonen J, Pratt-Sitaula B, Ojha T, 2004 "Rainfall thresholds for landsliding in the himalayas of nepal" *Geomorphology* **63** 131–143

Gallipoli D, Gens A, Sharma R, Vaunat J, 2003 "An elasto-plastic model for unsaturated soil incorporating the effects of suction and degree of saturation on mechanical behaviour" *Geotechnique* **53** 123–136

Gee M, 1992 "Classification of landslide hazard zonation methods and a test of predictive capability, vol. 2" *Proc. 6th International Symposium on Landslides, Christchurch, New Zealand* 947–952

Giannoni F, Roth G, Rudari R, 2000 "A semi-distributed rainfall-runoff model based on a geomorphologic approach" *Physics and Chemistry of the Earth, Part B* **25** 665–671

Giannoni F, Roth G, Rudari R, 2005 "A procedure for drainage network identification from geomorphology and its application to the prediction of the hydrologic response" *Advances in Water Resources* **28** 567–581

Gillot P, Chiesa S, Vezzoli L, 1982 "33000 yr k-ar dating of the volcano-tectonic horst of the isle of ischia, gulf of neaples" *Nature* **229** 242–244

Glade T, 2000 "Applying probability determination to refine landslide-triggering rainfall thresholds using an empirical "antecedent daily rainfall model"" *Pure and Applied Geophysics* **157** 1059–1079

Green W, Ampt G, 1911 "Studies on soil physics, 1. the flow of air and water through soils" *J. Agric. Sci* **4** 1–24

Guillot G, Lebel T, 1999 "Approximation of sahelian rainfall fields with meta-gaussian random functions" *Stochastic Environmental Research and Risk Assessment* **13** 113–130

Guimarães R, Montgomery D, Greenberg H, Fernandes N, Trancoso Gomes R, de Carvalho O, 2003 "Parameterization of soil properties for a model of topographic controls on shallow landsliding: application to rio de janeiro" *Engineering Geology* **69** 99–108

Guzzetti F, 2000 "Landslide fatalities and the evaluation of landslide risk in italy" *Engineering Geology* **58** 89–107

Guzzetti F, Cardinali M, Reichenbach P, Cipolla F, Sebastiani C, Galli M, Salvati P, 2004 "Landslides triggered by the 23 november 2000 rainfall event in the imperia province, western liguria, italy" *Engineering Geology* **73** 229–245

Guzzetti F, Carrara A, Cardinali M, Reichenbach P, 1999 "Landslide hazard evaluation: a review of current techniques and their application in a multi-scale study, central italy" *Geomorphology* **31** 181–216

Hammond C, Hall D, Miller S, Swetik P, 1992 "Level i stability analysis (lisa) documentation for version 2" *General Technical Report INT-285, USDA Forest Service Intermountain Research Station* **121**

Heimsath A, E. Dietrich W, Nishiizumi K, Finkel R, 1999 "Cosmogenic nuclides, topography, and the spatial variation of soil depth" *Geomorphology* **27** 151–172

Hillel D, 1982 "Introduction to soil physics" *New York*

Hsu M, 1994 *A grid-based model for predicting soil depth and shallow landslides* Ph.D. thesis University of California, Berkeley

Humbert M, 1977 "La cartographie zermos. modalités d'établissement des cartes des zones exposées à des risques liés aux mouvements du sol et du sous-sol" *BRGM Bull., Serie II, Sect. III* 5–8

Hungr O, 1996 "A model for the runout analysis of rapid flow slides, debris flows, and avalanches" *International Journal of Rock Mechanics and Mining Sciences and Geomechanics Abstracts* **33** 88A–88A

Hungr O, Evans S, Bovis M, Hutchinson J, 2001 "A review of the classification of landslides of the flow type" *Environmental and Engineering Geoscience* **7** 221

Hurley D, Pantelis G, 1985 "Unsaturated and saturated flow through a thin porous layer on a hillslope" *Water Resources Research* **21**

Innes J, 1983 "Debris flows" *Progress in Physical Geography* **7**

Iverson R, 1997 "The physics of debris flows" *Reviews of Geophysics* **35** 245–296

Iverson R, 2000 "Landslide triggering by rain infiltration" *Water Resources Research* **36** 1897–1910

Iverson R, LaHusen R, 1989 "Dynamic pore-pressure fluctuations in rapidly shearing granular materials" *Science* **246** 796–799

Iverson R, Reid M, Iverson N, LaHusen R, Logan M, Mann J, Brien D, 2000 "Acute sensitivity of landslide rates to initial soil porosity"

Iverson R, Reid M, LaHusen R, 1997 "Debris-flow mobilization from landslides 1" *Annual Reviews in Earth and Planetary Sciences* **25** 85–138

Janbu N, 1973 "Slope stability computations" *Embankment Dam Engineering: Casagrande Vol., John Wiley & Sons, New York* 47–86

Johnson A, Rodine J, 1984 "Debris flow" *Slope Instability* 257–361

Johnson K, Sitar N, 1990 "Hydrologic conditions leading to debris-flow initiation" *Canadian Geotechnical Journal* **27** 789–801

Keefer D, Wilson R, Mark R, Brabb E, Brown W, Ellen S, Harp E, Wieczorek G, Alger C, Zatkin R, 1987 "Real-time landslide warning during heavy rainfall" *Science* **238** 921–925

Kienholz H, 1978 "Maps of geomorphology and natural hazards of grindelwald, switzerland, scale 1: 10.000" *Arctic and Alpine Research* **10** 169–184

Kim J, Park S, Jeong S, 1998 "Effect of wetting front suction loss on stability of unsaturated soil slopes" in A S of Civil Engineers, ed., "Advances in Unsaturated Soil, Seepage, and Environmental Geotechnics (GEOTECHNICAL SPECIAL PUBLICATION)",

Krahn J, 2004 "Seepage modeling with seep/w" *Alberta: Geoslope*

Larsen M, Simon A, 1993 "A rainfall intensity-duration threshold for landslides in a humid-tropical environment, puerto rico" *Geografiska annaler. Series A. Physical geography* **75** 13–23

Lee S, Chwae U, Min K, 2002 "Landslide susceptibility mapping by correlation between topography and geological structure: the janghung area, korea" *Geomorphology* **46** 149–162

Lee S, Ryu J, Min K, Won J, 2003 "Landslide susceptibility analysis using gis and artificial neural network" *Earth Surface Processes and Landforms* **28** 1361–1376

Lee S, Ryu J, Won J, Park H, 2004 "Determination and application of the weights for landslide susceptibility mapping using an artificial neural network" *Engineering Geology* **71** 289–302

Lu N, ASCE M, Likos W, 2006 "Suction stress characteristic curve for unsaturated soil" *Journal of Geotechnical and Geoenvironmental Engineering* **132** 131

Mattiangeli L, 2007 "Le colate detritiche dell'isola di ischia del 30 aprile 2006: analisi geologico-tecnica e modellistica" *Università delgli Studi di Firenze, Tesi di Laurea*

Menardi-Noguera A, 1988 "Structural evolution of a briançonnais cover nappe, the caprauna–armetta unit (ligurian alps, italy)" *Journal of Structural Geology* **10** 625–637

Mercalli G, 1884 *L'Isola d'Ischia ed il terremoto del 28 luglio 1883* (Bernardoni di C. Rebeschini E C.)

Merizzi G, Seno S, 1991 "Deformation and gravity-driven translation of the s. remo-m. saccarello nappe (helminthoid flysch, ligurian alps)" *Bollettino della Società Geologica Italiana* **110** 757–770

Metternicht G, Hurni L, Gogu R, 2005 "Remote sensing of landslides: An analysis of the potential contribution to geo-spatial systems for hazard assessment in mountainous environments" *Remote Sensing of Environment* **98** 284–303

Mitchell J, Soga K, 2005 *Fundamentals of soil behavior.* (John Wiley & Sons Ltd Chichester, UK)

Montgomery D, Dietrich W, 1994 "A physically based model for the topographic control on shallow landsliding" *Water Resources Research* **30** 1153–1172

Montgomery D, Sullivan K, Greenberg H, 1998 "Regional test of a model for shallow landsliding" *HYDROLOGICAL PROCESSES* **12** 943–955

Montrasio L, Valentino R, 2003 "Experimental analysis on factors triggering soil slip" *Proceedings of int. conf. on fast slope movements prediction and prevention for risk mitigation, Patron Ed., Bologna* 371–378

Moore I, Gessler P, Nielsen G, Peterson G, 1993 "Soil attribute prediction using terrain analysis" *Soil Science Society of America Journal* **57** 443

Morgenstern N, Price V, 1965 "The analysis of the stability of general slip surfaces" *Geotechnique* **15** 79–93

Moser M, Hohensinn F, 1983 "Geotechnical aspects of soil slips in alpine regions" *Engineering Geology* 185–211

Neitsch S, Arnold J, Kiniry J, Williams J, King K, 2001 "Soil and water assessment tool theoretical documentation version 2000" *Grassland, Soil and Water Research Laboratory, Temple, Texas*

Okimura T, Ichikawa K, 1985 "A prediction method for surface failures by movements of infiltrated water in surface soil layer" *Nat. Disaster Sci.* **7** 41–51

O'Loughlin E, 1986 "Prediction of surface saturation zones in natural catchments by topographic analysis" *Water Resources Research* **22** 794–804

Pack R, Tarboton D, Goodwin C, 1998 "The sinmap approach to terrain stability mapping" in "8th Congress of the International Association of Engineering Geology, Vancouver, British Columbia, Canada",

Pack R, Tarboton D, Goodwin C, 2001 "Assessing terrain stability in a gis using sinmap" in "15th Annual GIS Conference, GIS",

Pareschi M, Santacroce R, Sulpizio R, Zanchetta G, 2002 "Volcaniclastic debris flows in the clanio valley (campania, italy): insights for the assessment of hazard potential" *Geomorphology* **43** 219–231

Perica S, Foufoula-Georgiou E, 1996 "Model for multiscale disaggregation of spatial rainfall based on coupling meteorological and scaling descriptions" *Journal of Geophysical Research. D. Atmospheres* **101** 26347–26361

Pierson T, 1980 "Piezometric response to rainstorms in forested hillslope drainage espressions" *Journal of Hydrology of New Zeland* **19** 1–10

Pierson T, 1983 "Soil pipes and slope stability" *gsqjegh* **16** 1–11

Pradel D, Raad G, 1993 "Effect of permeability on surficial stability of homogeneous slopes" *Journal of Geotechnical Engineering* **119** 315

Rebora N, Ferraris L, Von Hardenberg J, Provenzale A, 2006 "Rainfall downscaling and flood forecasting: a case study in the mediterranean area" *Natural Hazards and Earth System Sciences* **6** 611–619

Reid M, 1994 "A pore-pressure diffusion model for estimating landslide-inducing rainfall" *The Journal of Geology* **102** 709–717

Renau S, Dietrich W, 1997 "Size and location of colluvial landslides in a steep forested landscape" in R Beschta, T Blinn, G Grant, F Swanson, G Ice, eds., "Erosion and Sedimentation in the Pacific Rim", Number 165 (Int. Assoc. Hyd. Sci. Pub.) pp. 39–49

Richards L, 1931 "Capillary conduction of liquids through porous media" *Physics* **1** 318–333

Rigon R, Bertoldi G, Over T, 2006 "Geotop: A distributed hydrological model with coupled water and energy budgets" *Journal of Hydrometeorology* **7** 371–388

Ritter J, 2004 "Landslide and slope stability analysis: using an infinite slope model to delineate areas susceptible to translational sliding in the cincinnati, oh area, computational science module, dept. of geol" *Wittenberg U., Springfield, OH*

Rittmann A, Gottini V, 1980 "L'isola d'ischia-geologia" *Bollettino del Servizio* **101**

Rosso R, Rulli M, Vannucchi G, 2006 "A physically based model for the hydrologic control on shallow landsliding" *Water Resour. Res* **42**

Rulon J, Freeze R, 1985 "Multiple seepage faces on layered slopes and their implications for slope-stability analysis" *Canadian Geotechnical Journal*

Sagri M, 1980 "Le arenarie di bordighera: una conoide sottomarina nel bacino di sedimentazione del flysch ad elmintoidi di san remo (cretaceo superiore, liguria occidentale)" *Bollettino della Società Geologica Italiana* **98** 205–226

Sagri M, 1984 "Litologia, stratimetria e sedimentologia delle torbiditi di piana di bacino del flysch di san remo (cretaceo superiore, liguria occidentale)" *Mem. Soc. Geol. It* **28** 577–586

Salciarini D, Godt J, Savage W, Conversini P, Baum R, Michael J, 2006 "Modeling regional initiation of rainfall-induced shallow landslides in the eastern umbria region of central italy" *Landslides* **3** 181–194

Sassa K, 1984 "The mechanism starting liquefied landslides and debris flows" *Proceedings of 4 thInternational Symposium on Landslides, Toronto, June* **2** 349–354

Saulnier G, Beven K, Obled C, 1997 "Including spatially variable effective soil depths in topmodel" *Journal of Hydrology* **202** 158–172

Schmidt J, Turek G, Clark M, Uddstrom M, Dymond J, 2008 "Probabilistic forecasting of shallow, rainfall-triggered landslides using real-time numerical weather predictions" *Natural Hazards and Earth System Science* **8** 349–357

Schmugge T, Jackson T, McKim H, 1980 "Survey of methods for soil moisture determination" *Water Resources Research* **16**

Scott K, Pringle P, Vallance J, 1992 "Sedimentology, behavior, and hazards of debris flows at mount ranier, washington" *Available from Books and Open Files Reports Section, USGS Box 25425, Denver, CO 80225. USGS Open File Report 90-385, 1992. 106 p, 21 fig, 8 tab, 123 ref, 1 plate.*

Seggiani M, 2008 "Zonazione dell'innesco di frane superficiali nellisola di ischia" *Università delgli Studi di Firenze, Tesi di Laurea*

Segoni S, 2008 *Elaborazione ed applicazioni di un modella per la previsione dello spessore delle coperture superficiali* Ph.D. thesis Università degli Studi di Firenze

Segoni S, Catani F, 2008 "Modeling soil thickness to enhance slope stability analysis at catchment scale" *33rd International Geological Congress* **Oslo, Norway, 6-14 August**

Selby M, 1993 "Hillslope materials andprocesses"

Siccardi F, 1996 "Rainstorm hazards and related disasters in the western mediterranean region" *Remote Sens. Rev* **14** 5–21

Siccardi F, Boni G, Ferraris L, Rudari R, 2004 "A hydrometeorological approach for probabilistic flood forecast" *J. Geophys. Res* **110**

Sidle R, Swanston D, 1982 "Analysis of a small debris slide in coastal alaska" *Canadian Geotechnical Journal* **19** 167–174

Simoni S, Zanotti F, Bertoldi G, Rigon R, 2008 "Modelling the probability of occurrence of shallow landslides and channelized debris flows using geotop-fs" *HYDROLOGICAL PROCESSES* **22** 532

Skempton A, 1960 "Significance of terzaghi's concept of effective stress" *From theory to practice in soil mechanics* 42–53

Skempton A, DeLory F, 1957 "Stability of natural slopes in london clay" *Proceedings of the 4th International Conference on Soil Mechanics and Foundation Engineering* **2** 378–381

Soeters R, van Westen C, 1996 "Slope instability recognition, analysis and zonation" *Landslides Investigation and Mitigation* 129–177

Spencer E, 1967 "A method of analysis of the stability of embankments assuming parallel inter-slice forces" *Geotechnique* **17** 11–26

Takahashi T, 1978 "Mechanical characteristics of debris flow" *Journal of the Hydraulics Division* **104** 1153–1169

Takahashi T, 1981 "Debris flow" *Annual Reviews in Fluid Mechanics* **13** 57–77

Taylor G, Eggleton R, 2001 *Regolith Geology and Geomorphology* (Wiley)

Terzaghi K, 1936 "The shearing resistance of saturated soils and the angle between the planes of shear" *Proc. 1st Int. Conf. Soil Mech. Found. Engng, Cambridge, MA* **1** 54–56

Tofani V, Dapporto S, Vannocci P, Casagli N, 2006 "Infiltration, seepage and slope instability mechanisms during the 20–21 november 2000 rainstorm in tuscany, central italy" *Natural Hazards and Earth System Sciences* **6** 1025–1033

Tsai T, 2008 "The influence of rainstorm pattern on shallow landslide" *Environmental Geology* **53** 1563–1569

Tsai T, Chen H, Yang J, 2007 "Numerical modeling of rainstorm-induced shallow landslides in saturated and unsaturated soils" *Environmental Geology* 1–9

Tsai T, Yang J, 2006 "Modeling of rainfall-triggered shallow landslide" *Environmental Geology* **50** 525–534

USDA, 2006 "National soil survey characterization data" *Soil Survey Laboratory National Soil Survey Center, USDA-NRCS, Lincoln, NE*

Van Asch T, Buma J, Van Beek L, 1999 "A view on some hydrological triggering systems in landslides" *Geomorphology* **30** 25–32

Vanapalli S, Fredlund D, Pufahl D, Clifton A, 1996 "Model for the prediction of shear strength with respect to soil suction" *CANADIAN GEOTECHNICAL JOURNAL* **33** 379–392

Vanossi M, 1991 "Guide geologiche regionali-alpi liguri" *Soc. Geol. It., Milano*

Varnes D, 1978 "Slope movements: types and processes." *Landslide analysis and control* **Special Report** 11–33

Varnes D, 1984 "Iaeg commission on landslides (1984)." landslide hazard zonation: a review of principles and practice"

Wieczorek G, 1987 "Effect of rainfall intensity and duration on debris flows in central santa cruz mountains, california" *Debris Flows/Avalanches: Process, Recognition, and Mitigation* 93–104

Wieczorek G, 1996 "Landslide triggering mechanisms" *AK Turner and RL Schuster, op. cit* 76–90

Wu W, Sidle R, 1995 "A distributed slope stability model for steep forested basin" *Water Resources Research* **31** 2097–2110

Yin K, Yan T, 1988 "Statistical prediction models for slope instability of metamorphosed rocks" *Proceed* **5** 1269–1272

Zêzere J, Ferreira A, Rodrigues M, 1999 "Landslides in the north of lisbon region (portugal): Conditioning and triggering factors" *Physics and Chemistry of the Earth, Part A* **24** 925–934

Appendix A

C++ source code for the infinite slope model

Here follows the C++ source code of the infinite slope model developed during this thesis and used to calculate tha factor of safety for wide areas.

```
/*****************************************************************************

 *   Copyright (C) 2007 by Dipartimento di Scienze
    della Terra,,,   *
 *   dst@dst-linux   *
 *

    *
 *   This program is free software; you can
    redistribute it and/or modify  *
 *   it under the terms of the GNU General Public
    License as published by  *
 *   the Free Software Foundation; either version 2 of
     the License, or     *
 *   (at your option) any later version.
                                    *
 *

    *
 *   This program is distributed in the hope that it
    will be useful,       *
 *   but WITHOUT ANY WARRANTY; without even the
    implied warranty of        *
 *   MERCHANTABILITY or FITNESS FOR A PARTICULAR
    PURPOSE.  See the         *
 *   GNU General Public License for more details.
                           *
 *

    *
```

```
 *   You should have received a copy of the GNU
    General Public License     *
 *   along with this program; if not, write to the
                           *
 *   Free Software Foundation, Inc.,
                                          *
 *   59 Temple Place - Suite 330, Boston, MA
    02111-1307, USA.             *
 ************************************************************************


/*      SKEMPTON
        Linux kd version of SKEDEL code for computing
           Skempton&Delory's Factor of Safety
        L. Leoni DST-UNIFI, F.Catani DST-UNIFI
        Version kd1.0 Feb 2007

*/

#ifdef HAVE_CONFIG_H
#include <config.h>
#endif

#include <cstdlib>
#pragma hdrstop
#include <iostream.h>
#include <math.h>
#include <stdlib.h>
#include <fstream.h>
#include <exception>

#define PIGREEK 3.14159265358979
#define GAMMAW 9.81

//Global variables
   ------------------------------------------------------------

int nrows, ncols;
double cellsize;
int nodata_value;
double xllcorner, yllcorner;
double deg2rad;


//---------------------------------------------------------------------------

#pragma argsused
int main(int argc, char **argv)
{
```

```
ifstream Zfile, Cfile, PHIfile, SATfile, THETAfile
   , GAMMAfile;
ofstream outfile;
char buff[120];

if (argc < 8)
{
    cout << "Format: SKEMPTON <cohesion file> <
       friction file> <saturation file> <
       slopeangle file> <gammafile> <soildepth
       file> <outputfile>" << endl;
    exit (0);
}


Cfile.open(argv[1]);
PHIfile.open(argv[2]);
SATfile.open(argv[3]);
THETAfile.open(argv[4]);
GAMMAfile.open(argv[5]);
Zfile.open(argv[6]);


//reads the header of Cfile
Cfile >> buff;
Cfile >> ncols;
Cfile >> buff;
Cfile >> nrows;
Cfile >> buff;
Cfile >> xllcorner;
Cfile >> buff;
Cfile >> yllcorner;
Cfile >> buff;
Cfile >> cellsize;
Cfile >> buff;
Cfile >> nodata_value;

//reads the header of PHIfile
PHIfile >> buff;
PHIfile >> ncols;
PHIfile >> buff;
PHIfile >> nrows;
PHIfile >> buff;
PHIfile >> xllcorner;
PHIfile >> buff;
PHIfile >> yllcorner;
PHIfile >> buff;
PHIfile >> cellsize;
PHIfile >> buff;
PHIfile >> nodata_value;
```

```
//reads the header of THETAfile
THETAfile >> buff;
THETAfile >> ncols;
THETAfile >> buff;
THETAfile >> nrows;
THETAfile >> buff;
THETAfile >> xllcorner;
THETAfile >> buff;
THETAfile >> yllcorner;
THETAfile >> buff;
THETAfile >> cellsize;
THETAfile >> buff;
THETAfile >> nodata_value;

//reads the header of GAMMAfile
GAMMAfile >> buff;
GAMMAfile >> ncols;
GAMMAfile >> buff;
GAMMAfile >> nrows;
GAMMAfile >> buff;
GAMMAfile >> xllcorner;
GAMMAfile >> buff;
GAMMAfile >> yllcorner;
GAMMAfile >> buff;
GAMMAfile >> cellsize;
GAMMAfile >> buff;
GAMMAfile >> nodata_value;

//reads the header of Zfile
Zfile >> buff;
Zfile >> ncols;
Zfile >> buff;
Zfile >> nrows;
Zfile >> buff;
Zfile >> xllcorner;
Zfile >> buff;
Zfile >> yllcorner;
Zfile >> buff;
Zfile >> cellsize;
Zfile >> buff;
Zfile >> nodata_value;


//reads the header from the SATfile file and
   compare it with the header of
//the Cfile file in order to check for differences
int nc, nr, nodata; //control values from SATfile
   file
double cell, xll, yll;
```

```
SATfile >> buff;
SATfile >> nc;
SATfile >> buff;
SATfile >> nr;
SATfile >> buff;
SATfile >> xll;
SATfile >> buff;
SATfile >> yll;
SATfile >> buff;
SATfile >> cell;
SATfile >> buff;
SATfile >> nodata;

if (ncols!=nc || nrows!=nr || xllcorner!=xll ||
   yllcorner!=yll ||
        cellsize!=cell || nodata_value!=nodata)
{
    cout << "Saturation file is differently
       defined. Check it out!"
         << endl;
    exit (0);
}

//opens and write header in the output file
char stringxll[80]="";
char stringyll[80]="";
outfile.open(argv[7]);

int r = sprintf(stringxll, "%f", xllcorner);
r = sprintf(stringyll, "%f", yllcorner);

outfile << "ncols         " << ncols << endl;
outfile << "nrows         " << nrows << endl;
outfile << "xllcorner     " << stringxll << endl;
outfile << "yllcorner     " << stringyll << endl;
outfile << "cellsize      " << cellsize << endl;
outfile << "NODATA_value  " << nodata_value <<
   endl;

//after reading the dimension of the matrix
   dinamically declares
//double pointers to the bidimensional arrays
float **CArray = 0;   //initializes to 0 to avoid
   memory overlay problems
float **PHIArray = 0;
float **SATArray = 0;
float **THETAArray = 0;
float **GAMMAArray = 0;
float **ZArray = 0;
float **FSArray = 0;
```

```
int i,j,k;

//dinamic allocation of arrays (two phases: 1st:
   rows 2nd: columns)
try    //checks for memory exceptions during
   allocation
{
    CArray = new float*[nrows];
    for(j=0; j<nrows; j++)
        CArray[j] = new float[ncols];

    PHIArray = new float*[nrows];
    for(j=0; j<nrows; j++)
        PHIArray[j] = new float[ncols];

    SATArray = new float*[nrows];
    for(j=0; j<nrows; j++)
        SATArray[j] = new float[ncols];

    THETAArray = new float*[nrows];
    for(j=0; j<nrows; j++)
        THETAArray[j] = new float[ncols];

    GAMMAArray = new float*[nrows];
    for(j=0; j<nrows; j++)
        GAMMAArray[j] = new float[ncols];

    ZArray = new float*[nrows];
    for(j=0; j<nrows; j++)
        ZArray[j] = new float[ncols];

    FSArray = new float*[nrows];
    for(j=0; j<nrows; j++)
        FSArray[j] = new float[ncols];


}
catch(std::bad_alloc)  //only if bad_alloc error
   with the new operator...
{
    cout << "Could not allocate enough memory..."
       << endl
         << "Try close some applications or free
            some hard disk space..."
         << endl;
    exit (-1);
}

//reads from input files and fills arrays...
 for(i=0; i<nrows; i++)
```

```
{
   if(!((i+1)%10)) cout << "Processing COHESION
      file, line: " << (i+1) << endl;
   for(k=0; k<ncols; k++)
       Cfile >> CArray[i][k];
}

for(i=0; i<nrows; i++)
{
   if(!((i+1)%10)) cout << "Processing FRICTION
      ANGLE file, line: " << (i+1) << endl;
   for(k=0; k<ncols; k++)
       PHIfile >> PHIArray[i][k];
}

for(i=0; i<nrows; i++)
{
   if(!((i+1)%10)) cout << "Processing SATURATION
       file, line: " << (i+1) << endl;
   for(k=0; k<ncols; k++)
       SATfile >> SATArray[i][k];
}

for(i=0; i<nrows; i++)
{
   if(!((i+1)%10)) cout << "Processing SLOPE
      ANGLE file, line: " << (i+1) << endl;
   for(k=0; k<ncols; k++)
       THETAfile >> THETAArray[i][k];
}

for(i=0; i<nrows; i++)
{
   if(!((i+1)%10)) cout << "Processing GAMMA file
      , line: " << (i+1) << endl;
   for(k=0; k<ncols; k++)
       GAMMAfile >> GAMMAArray[i][k];
}

for(i=0; i<nrows; i++)
{
   if(!((i+1)%10)) cout << "Processing SOIL DEPTH
       file, line: " << (i+1) << endl;
   for(k=0; k<ncols; k++)
       Zfile >> ZArray[i][k];
}


//computes Skempton&Delory factor of safety for
   each grid cell...
```

```
int new_i, new_k, old_i, old_k;
float numer, denomin, ru;

deg2rad = 180 / PIGREEK;

//initializes FSArray[i][k] to zero
for (i=0; i<nrows; i++)
{
    for (k=0; k<ncols; k++)
    {
        FSArray[i][k]=0;
    }
}


for (i=0; i<nrows; i++)
{

    if(!((i+1)%10))
        cout << "Computing Factor of Safety...
           Line: " << (i+1) << endl;

    for (k=0; k<ncols; k++)
    {

        if(CArray[i][k]==nodata_value || PHIArray[
           i][k]==nodata_value || SATArray[i][k]==
           nodata_value
            || THETAArray[i][k]==nodata_value ||
               GAMMAArray[i][k]==nodata_value ||
               ZArray[i][k]==nodata_value)
        {
            FSArray[i][k]=nodata_value;
        }

        else
        {
                ru = (GAMMAW * SATArray[i][k]) / (
                   GAMMAArray[i][k] * ZArray[i][k
                   ]);
            numer = (CArray[i][k] / (GAMMAArray[i
               ][k] * ZArray[i][k])) + (cos(
               THETAArray[i][k] / deg2rad) * cos(
               THETAArray[i][k] / deg2rad) - ru) *
                tan(PHIArray[i][k] / deg2rad);
            denomin = sin(THETAArray[i][k]/deg2rad
               ) * cos(THETAArray[i][k]/deg2rad);
            FSArray[i][k] = numer / denomin;
        }
```

```
    }  //inner for cycle (k index, i.e. cols)

}  //outer for cycle (i index, i.e. rows)


//writes FSArray in outfile
for(i=0; i<nrows; i++)
{
    if(!((i+1)%10))
        cout << "Writing Factor of Safety values
           ... Line: " << (i+1) << endl;

    for(k=0; k<ncols; k++)
        outfile << FSArray[i][k] << "  ";
    outfile << endl;
}


//closes files and frees memory
Cfile.close();
PHIfile.close();
SATfile.close();
THETAfile.close();
GAMMAfile.close();
Zfile.close();
outfile.close();

for(i=0; i<nrows; i++)
{
    delete[] CArray[i];       //frees cols
    delete[] PHIArray[i];
    delete[] SATArray[i];
    delete[] THETAArray[i];
    delete[] GAMMAArray[i];
    delete[] ZArray[i];
    delete[] FSArray[i];
}
delete[] CArray;              //frees rows
CArray = 0;
delete[] PHIArray;
PHIArray = 0;
delete[] SATArray;
SATArray = 0;
delete[] THETAArray;
THETAArray = 0;
delete[] GAMMAArray;
GAMMAArray = 0;
delete[] ZArray;
ZArray = 0;
delete[] FSArray;
```

```
    FSArray = 0;


    return 0;
}
```

Appendix B

C++ source code for the modified Iverson model

Here follows the C++ source code of the modified Iverson model developed during this thesis and used to calculate tha factor of safety for wide areas.

```
/*************************************************************************

 *   Copyright (C) 2007 by Dipartimento di Scienze
    della Terra,,,   *
 *   dst@dst-linux   *
 *

    *
 *   This program is free software; you can
    redistribute it and/or modify  *
 *   it under the terms of the GNU General Public
    License as published by  *
 *   the Free Software Foundation; either version 2 of
     the License, or     *
 *   (at your option) any later version.
                                    *
 *

    *
 *   This program is distributed in the hope that it
    will be useful,       *
 *   but WITHOUT ANY WARRANTY; without even the
    implied warranty of        *
 *   MERCHANTABILITY or FITNESS FOR A PARTICULAR
    PURPOSE.  See the         *
 *   GNU General Public License for more details.
                           *
 *

    *
```

```
 *   You should have received a copy of the GNU
    General Public License     *
 *   along with this program; if not, write to the
                           *
 *   Free Software Foundation, Inc.,
                                          *
 *   59 Temple Place - Suite 330, Boston, MA
    02111-1307, USA.             *
 ************************************************************************


/*

        IVERSON_SF
        Linux version of Iverson_SF code for computing
            Iverson's Factor of Safety
        L. Leoni - dst_UNIFI,  G. Rossi - dst_UNIFI, F
           .Catani - dst_UNIFI
        Version 1.0 September 2008

*/

#ifdef HAVE_CONFIG_H
#include <config.h>
#endif

#include <cstdlib>
#pragma hdrstop
#include <iostream>
#include <cmath>
#include <fstream>
#include <exception>
#include <iostream>


using namespace std;

#define PIGREEK 3.14159265358979
#define GAMMAW 9810
#define layers 3
#define t_int 3600 //seconds in one hour
#define Diff_max 0.00001
//#define d 5 //initial depth (in meters) of the water
    table


//Global variables
   ------------------------------------------------------------

int nrows, ncols;
```

```
double cellsize;
int nodata_value;
double xllcorner, yllcorner;
double deg2rad;



//---------------------------------------------------------------------------

#pragma argsused
int main(int argc, char **argv)
{
    ifstream Zfile, Cfile, PHIfile, INTENSITYfile,
       THETAfile, GAMMAfile, CONDUCTIVITYfile,
       T_rain_old, press_distr_old, intensity_rec_old,
        press_zero_old;
    ofstream fs_outfile, T_rain_new, press_distr_new,
       intensity_rec_new, press_zero_new;
    char buff[120];

    if (argc < 16)
    {
        cout << "Format: IVERSON_SF\n <cohesion file>\
           n <friction file>\n <rainfall intensity
           file>\n <slopeangle file>\n <gammafile>\n <
           soildepth file>\n <hydro conductivity file
           >\n <T_rain_old>\n <T_rain_new>\n <
           fs_outputfile>\n <pressure_distribution_old
            file>\n <pressure_distribution_new file>\n
            <intensity_rec_old file>\n <
           intensity_rec_new file>\n <
           press_zero_old_file>\n <press_zero_new_file
           >\n" << endl;
        exit (0);
    }


//---------------------------------------------------------------------------

// Reads all the input files

    Cfile.open(argv[1]);
    PHIfile.open(argv[2]);
    INTENSITYfile.open(argv[3]);
    THETAfile.open(argv[4]);
    GAMMAfile.open(argv[5]);
    Zfile.open(argv[6]);
        CONDUCTIVITYfile.open(argv[7]);
        T_rain_old.open(argv[8]);
        press_distr_old.open(argv[11]);
```

```
        intensity_rec_old.open(argv[13]);
        press_zero_old.open(argv[15]);


    //reads the header of Cfile
    Cfile >> buff;
    Cfile >> ncols;
    Cfile >> buff;
    Cfile >> nrows;
    Cfile >> buff;
    Cfile >> xllcorner;
    Cfile >> buff;
    Cfile >> yllcorner;
    Cfile >> buff;
    Cfile >> cellsize;
    Cfile >> buff;
    Cfile >> nodata_value;

    //reads the header of PHIfile
    PHIfile >> buff;
    PHIfile >> ncols;
    PHIfile >> buff;
    PHIfile >> nrows;
    PHIfile >> buff;
    PHIfile >> xllcorner;
    PHIfile >> buff;
    PHIfile >> yllcorner;
    PHIfile >> buff;
    PHIfile >> cellsize;
    PHIfile >> buff;
    PHIfile >> nodata_value;

    //reads the header of THETAfile
    THETAfile >> buff;
    THETAfile >> ncols;
    THETAfile >> buff;
    THETAfile >> nrows;
    THETAfile >> buff;
    THETAfile >> xllcorner;
    THETAfile >> buff;
    THETAfile >> yllcorner;
    THETAfile >> buff;
    THETAfile >> cellsize;
    THETAfile >> buff;
    THETAfile >> nodata_value;

    //reads the header of GAMMAfile
    GAMMAfile >> buff;
    GAMMAfile >> ncols;
    GAMMAfile >> buff;
```

```
GAMMAfile >> nrows;
GAMMAfile >> buff;
GAMMAfile >> xllcorner;
GAMMAfile >> buff;
GAMMAfile >> yllcorner;
GAMMAfile >> buff;
GAMMAfile >> cellsize;
GAMMAfile >> buff;
GAMMAfile >> nodata_value;

//reads the header of Zfile
Zfile >> buff;
Zfile >> ncols;
Zfile >> buff;
Zfile >> nrows;
Zfile >> buff;
Zfile >> xllcorner;
Zfile >> buff;
Zfile >> yllcorner;
Zfile >> buff;
Zfile >> cellsize;
Zfile >> buff;
Zfile >> nodata_value;

    //reads the header of CONDUCTIVITYfile
CONDUCTIVITYfile >> buff;
CONDUCTIVITYfile >> ncols;
CONDUCTIVITYfile >> buff;
CONDUCTIVITYfile >> nrows;
CONDUCTIVITYfile >> buff;
CONDUCTIVITYfile >> xllcorner;
CONDUCTIVITYfile >> buff;
CONDUCTIVITYfile >> yllcorner;
CONDUCTIVITYfile >> buff;
CONDUCTIVITYfile >> cellsize;
CONDUCTIVITYfile >> buff;
CONDUCTIVITYfile >> nodata_value;


     //reads the header of T_rain_old file
T_rain_old >> buff;
T_rain_old >> ncols;
T_rain_old >> buff;
T_rain_old >> nrows;
T_rain_old >> buff;
T_rain_old >> xllcorner;
T_rain_old >> buff;
T_rain_old >> yllcorner;
T_rain_old >> buff;
T_rain_old >> cellsize;
```

```
T_rain_old >> buff;
T_rain_old >> nodata_value;

    //reads the header of pressure distribution
       old file
press_distr_old >> buff;
press_distr_old >> ncols;
press_distr_old >> buff;
press_distr_old >> nrows;
press_distr_old >> buff;
press_distr_old >> xllcorner;
press_distr_old >> buff;
press_distr_old >> yllcorner;
press_distr_old >> buff;
press_distr_old >> cellsize;
press_distr_old >> buff;
press_distr_old >> nodata_value;


    //reads the header of T_max_old file
intensity_rec_old >> buff;
intensity_rec_old >> ncols;
intensity_rec_old >> buff;
intensity_rec_old >> nrows;
intensity_rec_old >> buff;
intensity_rec_old >> xllcorner;
intensity_rec_old >> buff;
intensity_rec_old >> yllcorner;
intensity_rec_old >> buff;
intensity_rec_old >> cellsize;
intensity_rec_old >> buff;
intensity_rec_old >> nodata_value;

    //reads the header of press_zero file
press_zero_old >> buff;
press_zero_old >> ncols;
press_zero_old >> buff;
press_zero_old >> nrows;
press_zero_old >> buff;
press_zero_old >> xllcorner;
press_zero_old >> buff;
press_zero_old >> yllcorner;
press_zero_old >> buff;
press_zero_old >> cellsize;
press_zero_old >> buff;
press_zero_old >> nodata_value;


//reads the header from the INTENSITYfile file (
   and compare it with the header of
```

```
//the Cfile file in order to check for differences
   )
int nc, nr, nodata; //control values from SATfile
   file
double cell, xll, yll;
INTENSITYfile >> buff;
INTENSITYfile >> nc;
INTENSITYfile >> buff;
INTENSITYfile >> nr;
INTENSITYfile >> buff;
INTENSITYfile >> xll;
INTENSITYfile >> buff;
INTENSITYfile >> yll;
INTENSITYfile >> buff;
INTENSITYfile >> cell;
INTENSITYfile >> buff;
INTENSITYfile >> nodata;


    if (ncols!=nc || nrows!=nr || xllcorner!=xll
       || yllcorner!=yll ||
        cellsize!=cell || nodata_value!=nodata)
{
    cout << "Intensity file is differently defined
       . Check it out!"
         << endl;
    exit (0);
}


//opens and write header in the output file
char stringxll[80]="";
char stringyll[80]="";
fs_outfile.open(argv[10]);

int r = sprintf(stringxll, "%f", xllcorner);
r = sprintf(stringyll, "%f", yllcorner);

fs_outfile << "ncols         " << ncols << endl;
fs_outfile << "nrows         " << nrows << endl;
fs_outfile << "xllcorner     " << stringxll <<
   endl;
fs_outfile << "yllcorner     " << stringyll <<
   endl;
fs_outfile << "cellsize      " << cellsize << endl
   ;
fs_outfile << "NODATA_value  " << nodata_value <<
   endl;
```

```
T_rain_new.open(argv[9]);
r = sprintf(stringyll, "%f", yllcorner);

T_rain_new << "ncols         " << ncols << endl;
T_rain_new << "nrows         " << nrows << endl;
T_rain_new << "xllcorner     " << stringxll <<
   endl;
T_rain_new << "yllcorner     " << stringyll <<
   endl;
T_rain_new << "cellsize      " << cellsize << endl
   ;
T_rain_new << "NODATA_value  " << nodata_value <<
   endl;



press_distr_new.open(argv[12]);
r = sprintf(stringyll, "%f", yllcorner);

press_distr_new << "ncols         " << ncols <<
   endl;
press_distr_new << "nrows         " << nrows <<
   endl;
press_distr_new << "xllcorner     " << stringxll
   << endl;
press_distr_new << "yllcorner     " << stringyll
   << endl;
press_distr_new << "cellsize      " << cellsize <<
    endl;
press_distr_new << "NODATA_value  " <<
   nodata_value << endl;



    intensity_rec_new.open(argv[14]);
r = sprintf(stringyll, "%f", yllcorner);

intensity_rec_new << "ncols         " << ncols <<
   endl;
intensity_rec_new << "nrows         " << nrows <<
   endl;
intensity_rec_new << "xllcorner     " << stringxll
    << endl;
intensity_rec_new << "yllcorner     " << stringyll
    << endl;
intensity_rec_new << "cellsize      " << cellsize
   << endl;
intensity_rec_new << "NODATA_value  " <<
   nodata_value << endl;
```

```
    press_zero_new.open(argv[16]);
r = sprintf(stringyll, "%f", yllcorner);

press_zero_new << "ncols         " << ncols <<
   endl;
press_zero_new << "nrows         " << nrows <<
   endl;
press_zero_new << "xllcorner     " << stringxll <<
    endl;
press_zero_new << "yllcorner     " << stringyll <<
    endl;
press_zero_new << "cellsize      " << cellsize <<
   endl;
press_zero_new << "NODATA_value  " << nodata_value
    << endl;


//after reading the dimension of the matrix
   dinamically declares
//double pointers to the bidimensional arrays
float **CArray = 0;   //initializes to 0 to avoid
   memory overlay problems
float **PHIArray = 0;
float **INTENSITYArray = 0;
float **THETAArray = 0;
float **GAMMAArray = 0;
float **ZArray = 0;
    float **CONDUCTIVITYarray = 0;
float **FSArray = 0;
    float **T_rain_old_array = 0;
    float **T_rain_new_array = 0;
    float **press_distr_old_array = 0;
    float **press_distr_new_array = 0;
    float **Diff_ch = 0;
    float **Distr_ss = 0;
    float **t_norm = 0;
    float **intensity_rec_old_array = 0;
    float **intensity_rec_new_array = 0;
    float **d_array =0;
    float **press_zero_old_array = 0;
    float **press_zero_new_array = 0;
    float **fs_min_array = 0;
int i,j,k,z;

//dinamic allocation of arrays (two phases: 1st:
   rows 2nd: columns)
try    //checks for memory exceptions during
   allocation
```

```
{
    CArray = new float*[nrows];
    for(j=0; j<nrows; j++)
        CArray[j] = new float[ncols];

    PHIArray = new float*[nrows];
    for(j=0; j<nrows; j++)
        PHIArray[j] = new float[ncols];

    INTENSITYArray = new float*[nrows];
    for(j=0; j<nrows; j++)
        INTENSITYArray[j] = new float[ncols];

    THETAArray = new float*[nrows];
    for(j=0; j<nrows; j++)
        THETAArray[j] = new float[ncols];

    GAMMAArray = new float*[nrows];
    for(j=0; j<nrows; j++)
        GAMMAArray[j] = new float[ncols];

    ZArray = new float*[nrows];
    for(j=0; j<nrows; j++)
        ZArray[j] = new float[ncols];

        CONDUCTIVITYarray = new float*[nrows];
        for(j=0; j<nrows; j++)
                CONDUCTIVITYarray[j] = new
                   float[ncols];

    FSArray = new float*[nrows * layers];
    for(j=0; j<nrows * layers; j++)
        FSArray[j] = new float[ncols];

        T_rain_old_array = new float*[nrows];
    for(j=0; j<nrows; j++)
        T_rain_old_array[j] = new float[ncols];

        T_rain_new_array = new float*[nrows];
    for(j=0; j<nrows; j++)
        T_rain_new_array[j] = new float[ncols];

        press_distr_old_array = new float*[
           nrows * layers];
    for(j=0; j<nrows * layers; j++)
        press_distr_old_array[j] = new float[ncols
           ];

        press_distr_new_array = new float*[
           nrows * layers];
```

```
    for(j=0; j<nrows * layers; j++)
        press_distr_new_array[j] = new float[ncols
           ];

            Diff_ch = new float*[nrows];
            for(j=0; j<nrows; j++)
                    Diff_ch[j] = new float[ncols];

            Distr_ss = new float*[nrows];
            for(j=0; j<nrows; j++)
                    Distr_ss[j] = new float[ncols
                       ];

            t_norm = new float*[nrows];
            for(j=0; j<nrows; j++)
                    t_norm[j] = new float[ncols];

            intensity_rec_old_array = new float*[
               nrows];
    for(j=0; j<nrows; j++)
        intensity_rec_old_array[j] = new float[
           ncols];

            intensity_rec_new_array = new float*[
               nrows];
    for(j=0; j<nrows; j++)
        intensity_rec_new_array[j] = new float[
           ncols];

            d_array = new float*[nrows];
    for(j=0; j<nrows; j++)
        d_array[j] = new float[ncols];

            press_zero_old_array = new float*[
               nrows];
    for(j=0; j<nrows; j++)
        press_zero_old_array[j] = new float[ncols
           ];

            press_zero_new_array = new float*[
               nrows];
    for(j=0; j<nrows; j++)
        press_zero_new_array[j] = new float[ncols
           ];

            fs_min_array = new float*[nrows];
    for(j=0; j<nrows; j++)
        fs_min_array[j] = new float[ncols];

}
```

```
catch(std::bad_alloc)  //only if bad_alloc error
   with the new operator...
{
    cout << "Could not allocate enough memory..."
       << endl
         << "Try close some applications or free
            some hard disk space..."
         << endl;
    exit (-1);
}

//reads from input files and fills arrays...
 for(i=0; i<nrows; i++)
 {
    if(!((i+1)%10)) cout << "Processing COHESION
       file, line: " << (i+1) << endl;
    for(k=0; k<ncols; k++)
        Cfile >> CArray[i][k];
 }

 for(i=0; i<nrows; i++)
 {
    if(!((i+1)%10)) cout << "Processing FRICTION
       ANGLE file, line: " << (i+1) << endl;
    for(k=0; k<ncols; k++)
        PHIfile >> PHIArray[i][k];
 }

 for(i=0; i<nrows; i++)
 {
    if(!((i+1)%10)) cout << "Processing RAINFALL
       INTENSITY file, line: " << (i+1) << endl;
    for(k=0; k<ncols; k++)
        INTENSITYfile >> INTENSITYArray[i][k];
 }


     //Divide for 3600000
     //conversion from mm/h to m/s

     for(i=0; i<nrows; i++)
 {
    for(k=0; k<ncols; k++)
                    if (INTENSITYArray[i][k] ==
                       nodata_value ||
                       INTENSITYArray[i][k] == 0 )
                            INTENSITYArray[i][k] =
                                 0;
                    else
```

```
                                INTENSITYArray[i][k] =
                                     INTENSITYArray[i
                                   ][k]/3600000;
}



for(i=0; i<nrows; i++)
{
   if(!((i+1)%10)) cout << "Processing SLOPE
      ANGLE file, line: " << (i+1) << endl;
   for(k=0; k<ncols; k++)
       THETAfile >> THETAArray[i][k];
}

for(i=0; i<nrows; i++)
{
   if(!((i+1)%10)) cout << "Processing GAMMA file
      , line: " << (i+1) << endl;
   for(k=0; k<ncols; k++)
       GAMMAfile >> GAMMAArray[i][k];
}

for(i=0; i<nrows; i++)
{
   if(!((i+1)%10)) cout << "Processing SOIL DEPTH
       file, line: " << (i+1) << endl;
   for(k=0; k<ncols; k++)
       Zfile >> ZArray[i][k];
}

    for(i=0; i<nrows; i++)
{
   if(!((i+1)%10)) cout << "Processing
      CONDUCTIVITY file, line: " << (i+1) << endl
      ;
   for(k=0; k<ncols; k++)
       CONDUCTIVITYfile >> CONDUCTIVITYarray[i][k
          ];
}

    for(i=0; i<nrows; i++)
{
   if(!((i+1)%10)) cout << "Processing T_rain_old
       file, line: " << (i+1) << endl;
   for(k=0; k<ncols; k++)
       T_rain_old >> T_rain_old_array[i][k];
}
```

```
         for(i=0; i<nrows * layers; i++)
         {
        if(!((i+1)%10)) cout << "Processing
           press_distr_old file, line: " << (i+1) <<
           endl;
        for(k=0; k<ncols; k++)
            press_distr_old >> press_distr_old_array[i
               ][k];
     }


         for(i=0; i<nrows; i++)
         {
        if(!((i+1)%10)) cout << "Processing
           intensity_rec_old file, line: " << (i+1) <<
            endl;
        for(k=0; k<ncols; k++)
            intensity_rec_old >>
               intensity_rec_old_array[i][k];
     }

         for(i=0; i<nrows; i++)
         {
        if(!((i+1)%10)) cout << "Processing
           press_zero_old file, line: " << (i+1) <<
           endl;
        for(k=0; k<ncols; k++)
            press_zero_old >> press_zero_old_array[i][
               k];
     }

//-------------------------------------------------------------------------


        //Hydrologic model
        //Computes transient pressure distribution
           using the Iverson's form of the Richards
           equation for each grid cell...

        //initializes T_rain_new_array[i][k] to zero
    for (i=0; i<nrows; i++)
    {
        for (k=0; k<ncols; k++)
        {
            T_rain_new_array[i][k]=0;
        }
    }


    for (i=0; i<nrows; i++)
```

```
{

    if(!((i+1)%10))
        cout << "Computing T_rain_new... Line: "
           << (i+1) << endl;

    for (k=0; k<ncols; k++)
    {

        if(CArray[i][k]==nodata_value || PHIArray[
           i][k]==nodata_value
            || THETAArray[i][k]==nodata_value ||
               GAMMAArray[i][k]==nodata_value ||
               ZArray[i][k]==nodata_value)
        {
            T_rain_new_array[i][k] = nodata_value;
        }

                    else if(INTENSITYArray[i][k
                       ]==0)
                    {
                            T_rain_new_array[i][k]
                                = T_rain_old_array
                               [i][k] + t_int;
                    }


                    else if(INTENSITYArray[i][k
                       ]!=0)
                    {
                            T_rain_new_array[i][k]
                                = t_int;
                    }


    }  //inner for cycle (k index, i.e. cols)

}  //outer for cycle (i index, i.e. rows)


    //writes T_rain_new in outfile
for(i=0; i<nrows; i++)
{
    if(!((i+1)%10))
        cout << "Writing T_rain_new values... Line
           : " << (i+1) << endl;

    for(k=0; k<ncols; k++)
        T_rain_new << T_rain_new_array[i][k] << "
            ";
```

```
        T_rain_new << endl;
    }

//End of T_rain_new computation



        deg2rad = 180 / PIGREEK;



//Compute the intensity_rec_new

        //initializes intensity_rec_new_array[i][k] to
            zero
        for (i=0; i<nrows; i++)
    {
        for (k=0; k<ncols; k++)
        {
            intensity_rec_new_array[i][k]=0;
        }
    }


        for (i=0; i<nrows; i++)
    {

        if(!((i+1)%10))
            cout << "Computing intensity_rec_new...
               Line: " << (i+1) << endl;

        for (k=0; k<ncols; k++)
        {

            if(CArray[i][k]==nodata_value || PHIArray[
               i][k]==nodata_value
       || THETAArray[i][k]==nodata_value || GAMMAArray
          [i][k]==nodata_value || ZArray[i][k]==
          nodata_value || INTENSITYArray[i][k]==
          nodata_value || intensity_rec_old_array[i][k
          ]==nodata_value )
          {
          intensity_rec_new_array[i][k] = 0;
          }

          else if(INTENSITYArray[i][k]==0)//it doesn't
              rain, case t>T
          {
```

```
      intensity_rec_new_array[i][k] =
         intensity_rec_old_array[i][k];
      }

      else if(INTENSITYArray[i][k]!=0 ||
         T_rain_old_array[i][k]==t_int)//it's
         raining, case t<T, and before it was
         already raining
      {
      intensity_rec_new_array[i][k] = (
         intensity_rec_old_array[i][k] +
         INTENSITYArray[i][k])/ (
         press_zero_old_array[i][k]+1 ) ;
      }

      else if(INTENSITYArray[i][k]!=0 ||
         T_rain_old_array[i][k]>t_int)//it's
         raining, case t<T, and before it was not
         raining
      {
      intensity_rec_new_array[i][k] =
         INTENSITYArray[i][k] ;
      }


    }  //inner for cycle (k index, i.e. cols)

}  //outer for cycle (i index, i.e.




    //writes intensity_rec_new in outfile
    for(i=0; i<nrows; i++)
{
    if(!((i+1)%10))
        cout << "Writing intensity_rec_new values
           ... Line: " << (i+1) << endl;

    for(k=0; k<ncols; k++)
        intensity_rec_new <<
           intensity_rec_new_array[i][k] << "  ";
    intensity_rec_new << endl;
}
```

```
//Compute the effective hydraulic diffusivity and
   normalized t and T

        for (i=0; i<nrows; i++)
    {
        for (k=0; k<ncols; k++)
        {
            Diff_ch[i][k] = 0;
        }
    }


        for (i=0; i<nrows; i++)
    {
        for (k=0; k<ncols; k++)
        {
        Diff_ch[i][k] = 4 * Diff_max * cos(THETAArray[
           i][k]/deg2rad); //"Diff_max" is the maximum
            characteristic diffusivity governing
           transmission of preassure head
        }
    }




//Depth d using the last preassure haed:

        //float d = 3;

        for (i=0; i<nrows; i++)
    {
        for (k=0; k<ncols; k++)
        {
            d_array[i][k]=0;
        }
    }

        for (i=0; i<nrows; i++)
    {
        for (k=0; k<ncols; k++)
        {
  d_array[i][k] = ZArray[i][k] - (
     press_distr_old_array[i][k] / (cos(THETAArray[i][
     k]/deg2rad) - ((intensity_rec_old_array[i][k
     ]+0.000000000001)/CONDUCTIVITYarray[i][k]) ) );
        }
    }
```

```
//Compute the steady, background pressure head
   distribution:

        for (i=0; i<nrows; i++)
    {
        for (k=0; k<ncols; k++)
        {
            Distr_ss[i][k] = 0;
        }
    }



        for (i=0; i<nrows; i++)
    {
        for (k=0; k<ncols; k++)
        {
  Distr_ss[i][k] = (ZArray[i][k] - d_array[i][k]) * (
     cos(THETAArray[i][k]/deg2rad)*cos(THETAArray[i][k
     ]/deg2rad));// - 1); //((INTENSITYArray[i][k
     ]+0.00001)/CONDUCTIVITYarray[i][k]));
     intensity_rec_new_array[i][k]
        }
    }




    for (i=0; i<nrows; i++)
    {
       for (k=0; k<ncols; k++)
      {
      if (T_rain_new_array[i][k]>t_int)//it doesn't
         rain
      {
   t_norm[i][k] = (T_rain_new_array[i][k]) / (((ZArray
      [i][k]/cos(THETAArray[i][k]/deg2rad)) * (ZArray[
      i][k]/cos(THETAArray[i][k]/deg2rad))) / Diff_ch[
      i][k]);
      }

      else //it's raining
      {
      t_norm[i][k] = t_int / (((ZArray[i][k]/cos(
         THETAArray[i][k]/deg2rad)) * (ZArray[i][k]/
```

```
          cos(THETAArray[i][k]/deg2rad))) / Diff_ch[i][
          k]);
    }
    }
    }



//initializes press_distr_new_array[i][k] to zero
//the preassure distribution is computed on n layers (
   each layer is at different depth)

    for (i=0; i<nrows * layers; i++)
    {
        for (k=0; k<ncols; k++)
        {
            press_distr_new_array[i][k]=0;
        }
    }


     for (z=0; z<layers; z++)
     {
     for (i=0; i<nrows; i++)
     {

     if(!((i+1)%10))
     cout << "Computing New Pressure Distribution...
        Line: " << (i+1) << endl;// Y = Y(n-1) - Y(0,
        computed with d_array) + Y(n, computed with d)

     for (k=0; k<ncols; k++)
     {
     if(CArray[i][k]==nodata_value || PHIArray[i][k]==
        nodata_value
     || THETAArray[i][k]==nodata_value || GAMMAArray[i
        ][k]==nodata_value || ZArray[i][k]==
        nodata_value )
     {
     press_distr_new_array[i + z * nrows][k] =
        nodata_value;
     }

     else if(ZArray[i][k]<=0)
     {
     press_distr_new_array[i + z * nrows][k] =
        nodata_value;
     }
```

```
   /*else if(INTENSITYArray[i][k]==nodata_value)
   {
press_distr_new_array[i + z * nrows][k] =
   press_distr_old_array[i + z * nrows][k] -  ((
   ZArray[i][k] - d_array[i][k]) * (cos(THETAArray[i
   ][k]/deg2rad))*(cos(THETAArray[i][k]/deg2rad))) +
    ((cos(THETAArray[i][k]/deg2rad) * cos(THETAArray
   [i][k]/deg2rad)) - (((0.000000000001)/
   CONDUCTIVITYarray[i][k]) * cos(THETAArray[i][k]/
   deg2rad))) * (((ZArray[i][k]/(z+1))/cos(
   THETAArray[i][k]/deg2rad))-d_array[i][k]) + (((
   ZArray[i][k]/(z+1))/cos(THETAArray[i][k]/deg2rad)
   ) * ((0.000000000001)/CONDUCTIVITYarray[i][k])) *
    ((   (sqrt (fabs (t_norm[i][k])/PIGREEK) * exp
   (-1/ fabs (t_norm[i][k])) - ( erfc (t_norm[i][k])
     ))) - (sqrt ((fabs (t_norm[i][k]-T_norm[i][k]))
   /PIGREEK) * exp (-1/(fabs (t_norm[i][k]-T_norm[i
   ][k])))) - ( erfc (t_norm[i][k]-T_norm[i][k])))  )
    ;
   }*/



  else if(T_rain_new_array[i][k]>t_int &&
     INTENSITYArray[i][k]<CONDUCTIVITYarray[i][k])
     //It has not been raining for the last n time-
     steps; case t>T
   {
  press_distr_new_array[i + z * nrows][k] = (   ((
     ZArray[i][k]/(z+1)) - 2) * (cos(THETAArray[i][k
     ]/deg2rad)*cos(THETAArray[i][k]/deg2rad))   ) +
      (((ZArray[i][k]/(z+1))/cos(THETAArray[i][k]/
     deg2rad)) * ((intensity_rec_new_array[i][k
     ]+0.000000000001)/CONDUCTIVITYarray[i][k])) *
     ((   (sqrt (((t_int + T_rain_new_array[i][k]) /
      (((ZArray[i][k]/cos(THETAArray[i][k]/deg2rad))
      * (ZArray[i][k]/cos(THETAArray[i][k]/deg2rad))
     ) / Diff_ch[i][k]))/PIGREEK) * exp (-1/ ((t_int
      + T_rain_new_array[i][k]) / (((ZArray[i][k]/
     cos(THETAArray[i][k]/deg2rad)) * (ZArray[i][k]/
     cos(THETAArray[i][k]/deg2rad))) / Diff_ch[i][k
     ])))) - ( erfc ((t_int + T_rain_new_array[i][k])
      / (((ZArray[i][k]/cos(THETAArray[i][k]/deg2rad
     )) * (ZArray[i][k]/cos(THETAArray[i][k]/deg2rad
     ))) / Diff_ch[i][k]))  ))) - (sqrt ((t_norm[i][
     k])/PIGREEK) * exp (-1/(t_norm[i][k])) - ( erfc
      (t_norm[i][k])))  ) ;
   }
```

```
else if(T_rain_new_array[i][k]>t_int &&
   intensity_rec_new_array[i][k]>=CONDUCTIVITYarray
   [i][k]) //It has not been raining for the last n
    time-steps; case t>T
 {
press_distr_new_array[i + z * nrows][k] =  (   ((
   ZArray[i][k]/(z+1)) - 2) * (cos(THETAArray[i][k
   ]/deg2rad)*cos(THETAArray[i][k]/deg2rad))   ) +
   (((ZArray[i][k]/(z+1))/cos(THETAArray[i][k]/
   deg2rad)) * 1 ) * ((   (sqrt (((t_int +
   T_rain_new_array[i][k]) / (((ZArray[i][k]/cos(
   THETAArray[i][k]/deg2rad)) * (ZArray[i][k]/cos(
   THETAArray[i][k]/deg2rad))) / Diff_ch[i][k]))/
   PIGREEK) * exp (-1/ ((t_int + T_rain_new_array[i
   ][k]) / (((ZArray[i][k]/cos(THETAArray[i][k]/
   deg2rad)) * (ZArray[i][k]/cos(THETAArray[i][k]/
   deg2rad))) / Diff_ch[i][k]))) - ( erfc ((t_int +
    T_rain_new_array[i][k]) / (((ZArray[i][k]/cos(
   THETAArray[i][k]/deg2rad)) * (ZArray[i][k]/cos(
   THETAArray[i][k]/deg2rad))) / Diff_ch[i][k]))  )
   )) - (sqrt ((t_norm[i][k])/PIGREEK) * exp (-1/(
   t_norm[i][k])) - ( erfc (t_norm[i][k]))  ) ;
 }



 else if(T_rain_new_array[i][k]=t_int &&
    INTENSITYArray[i][k]<CONDUCTIVITYarray[i][k])
    //It has been raining for the last n time_steps
    ; case t<T
 {
press_distr_new_array[i + z * nrows][k] =
   press_distr_old_array[i + z * nrows][k] + (((
   ZArray[i][k]/(z+1))/cos(THETAArray[i][k]/deg2rad
   )) * ((INTENSITYArray[i][k]+0.000000000001)/
   CONDUCTIVITYarray[i][k])) * (   (sqrt (fabs (
   t_norm[i][k])/PIGREEK) * exp (-1/ fabs (t_norm[i
   ][k])) - ( erfc (t_norm[i][k])  ))  ) ;
 }

   else if(T_rain_new_array[i][k]=t_int &&
      INTENSITYArray[i][k]>=CONDUCTIVITYarray[i][k
      ]) //It has been raining for the last n
      time_steps; case t<T
 {
  press_distr_new_array[i + z * nrows][k] =
     press_distr_old_array[i + z * nrows][k] + (((
     ZArray[i][k]/(z+1))/cos(THETAArray[i][k]/
```

```
    deg2rad)) * 1) * (   (sqrt (fabs (t_norm[i][k
    ])/PIGREEK) * exp (-1/ fabs (t_norm[i][k])) -
    ( erfc (t_norm[i][k])  ))  ) ;
}



}  //inner for cycle (k index, i.e. cols)
           }

}  //outer for cycle (i index, i.e. rows)



for (z=0; z<layers; z++)
{
for (i=0; i<nrows; i++)
{

for (k=0; k<ncols; k++)
{
 if (press_distr_new_array[i][k] > (ZArray[i][k]/(
    z+1)) * (cos(THETAArray[i][k]/deg2rad))   )//
    saturated conditions, beta-line correction (
    physically unrealistic)
 {
    press_distr_new_array[i + z * nrows][k] = (
       ZArray[i][k]/(z+1)) * (cos(THETAArray[i][k
       ]/deg2rad)) ;
    }
    else
    {
    press_distr_new_array[i + z * nrows][k] =
       press_distr_new_array[i + z * nrows][k];
    }

  }  //inner for cycle (k index, i.e. cols)
}

}  //outer for cycle (i index, i.e. rows)



    //writes press_distr_new in outfile
for(i=0; i<nrows * layers; i++)
{
    if(!((i+1)%10))
        cout << "Writing press_distr_new values...
            Line: " << (i+1) << endl;
```

```
        for(k=0; k<ncols; k++)
            press_distr_new << press_distr_new_array[i
               ][k] << "  ";
        press_distr_new << endl;
    }



//-------------------------------------------------------------------------


    //Slope stability model:
    //computes Iverson factor of safety for each grid
       cell...




    //initializes FSArray[i][k] to zero
    for (i=0; i<nrows * layers; i++)
    {
        for (k=0; k<ncols; k++)
        {
            FSArray[i][k]=0;
        }
    }




    for (z=0; z<layers; z++)
    {
    for (i=0; i<nrows; i++)
    {

    if(!((i+1)%10))
    cout << "Computing Factor of Safety... Line: " <<
       (i+1) << endl;

    for (k=0; k<ncols; k++)
    {

   if(CArray[i][k]==nodata_value || PHIArray[i][k]==
      nodata_value
   || THETAArray[i][k]==nodata_value || GAMMAArray[i][
      k]==nodata_value || ZArray[i][k]==nodata_value)
                                {
   FSArray[i + z * nrows][k]=nodata_value;
   }
```

```
 else if(THETAArray[i][k]<=5)
 {
 FSArray[i + z * nrows][k] = 30;
 }

 else if(ZArray[i][k]<=0)
 {
 FSArray[i + z * nrows][k] = nodata_value;
 }

 else if(press_distr_new_array[i + z * nrows][k]<=0)
    //when the groundwater preassure head is
    negative the soil is unsaturated!
  {
FSArray[i + z * nrows][k] = (tan(PHIArray[i][k]/
   deg2rad)/tan(THETAArray[i][k]/deg2rad)) + ((
   CArray[i][k]+((-press_distr_new_array[i + z *
   nrows][k]*GAMMAW)*tan(PHIArray[i][k]/deg2rad)*(
   ((((press_distr_new_array[i + z * nrows][k]*
   GAMMAW)*(0.0011)+0.4464)/0.4328) - 10) / 90   )))
   /(GAMMAArray[i][k] * (ZArray[i][k]/(z+1)) * sin(
   THETAArray[i][k]/deg2rad) )) - (  (
   press_distr_new_array[i + z * nrows][k] * GAMMAW
   * tan(PHIArray[i][k]/deg2rad))/(GAMMAArray[i][k]
   * (ZArray[i][k]/(z+1)) * sin(THETAArray[i][k]/
   deg2rad))  ) ;
  }

  else
  {
  FSArray[i + z * nrows][k] = (tan(PHIArray[i][k]/
     deg2rad)/tan(THETAArray[i][k]/deg2rad)) + (
     CArray[i][k]/(GAMMAArray[i][k] * (ZArray[i][k
     ]/(z+1)) * sin(THETAArray[i][k]/deg2rad) )) - (
       (press_distr_new_array[i + z * nrows][k] *
     GAMMAW * tan(PHIArray[i][k]/deg2rad))/(
     GAMMAArray[i][k] * (ZArray[i][k]/(z+1)) * sin(
     THETAArray[i][k]/deg2rad))  ) ;
  }


  }  //inner for cycle (k index, i.e. cols)

  }  //outer for cycle (i index, i.e. rows)
  }



      //assign minimum value of FSArray to the
         output file
```

```
        for (i=0; i<nrows; i++)
    {
        for (k=0; k<ncols; k++)
        {
           fs_min_array[i][k] = 0;
        }
    }



    for(k=0; k<ncols; k++)
    {
    for(i=0; i<nrows; i++)
    {

    fs_min_array[i][k] = FSArray[i][k];

    for(z=1; z<layers-1; z++)
      {
      if ( FSArray[i + z * nrows][k] < FSArray[i][k] )
      fs_min_array[i][k] = FSArray[i + z * nrows][k];
      else
      fs_min_array[i][k] = FSArray[i][k];
      }
    }

    }


    //writes FSArray in outfile
    for(i=0; i<nrows; i++)
    {
        if(!((i+1)%10))
            cout << "Writing Factor of Safety values
               ... Line: " << (i+1) << endl;

        for(k=0; k<ncols; k++)

            fs_outfile << fs_min_array[i][k] << "  ";

        fs_outfile << endl;
    }



//Update the press_zero_new


//initializes press_zero_new[i][k] to zero
```

```
for (i=0; i<nrows; i++)
{
    for (k=0; k<ncols; k++)
    {
       press_zero_new_array[i][k]=0;
    }
}



for (i=0; i<nrows; i++)
{

if(!((i+1)%10))
cout << "Computing press_zero_new... Line: " << (i
   +1) << endl;

for (k=0; k<ncols; k++)
{

if(CArray[i][k]==nodata_value || PHIArray[i][k]==
   nodata_value
|| THETAArray[i][k]==nodata_value || GAMMAArray[i
   ][k]==nodata_value || ZArray[i][k]==
   nodata_value )
                              {
press_zero_new_array[i][k]=nodata_value;
                              }

else if(INTENSITYArray[i][k]>0 || T_rain_old_array
   [i][k]== t_int ) //piove e pioveva anche prima
{
press_zero_new_array[i][k] = press_zero_old_array[
   i][k] + 1 ;
}

else if(INTENSITYArray[i][k]==0 )
{
press_zero_new_array[i][k] = press_zero_old_array[
   i][k];
}

else if(INTENSITYArray[i][k]>0 || T_rain_old_array
   [i][k]>t_int ) // piove, prima non pioveva
{
press_zero_new_array[i][k] =  1 ;
}

}  //inner for cycle (k index, i.e. cols)
```

```
} //outer for cycle (i index, i.e. rows)



//writes press_zero_new_array in outfile
for(i=0; i<nrows; i++)
{
    if(!((i+1)%10))
        cout << "Writing press_zero_new_file...
           Line: " << (i+1) << endl;

    for(k=0; k<ncols; k++)
                    //if (FSArray[i][k]<=0 &&
                       FSArray[i][k]!=-9999)
                    //fs_outfile << 0.1;
                    //else
        press_zero_new << press_zero_new_array[i][
           k] << "  ";
    press_zero_new << endl;
}



//closes files and frees memory
Cfile.close();
PHIfile.close();
INTENSITYfile.close();
THETAfile.close();
GAMMAfile.close();
Zfile.close();
    CONDUCTIVITYfile.close();
    T_rain_new.close();
    T_rain_old.close();
    press_distr_new.close();
    press_distr_old.close();
fs_outfile.close();
    intensity_rec_old.close();
    intensity_rec_new.close();
    press_zero_old.close();
    press_zero_new.close();


for(i=0; i<nrows; i++)
{
    delete[] CArray[i];       //frees cols
    delete[] PHIArray[i];
    delete[] INTENSITYArray[i];
    delete[] THETAArray[i];
    delete[] GAMMAArray[i];
```

```
            delete[] ZArray[i];
            delete[] CONDUCTIVITYarray[i];
            delete[] T_rain_new_array[i];
            delete[] T_rain_old_array[i];
            delete[] Diff_ch[i];
            delete[] Distr_ss[i];
            delete[] t_norm[i];
            delete[] intensity_rec_old_array[i];
            delete[] intensity_rec_new_array[i];
            delete[] press_zero_old_array[i];
            delete[] press_zero_new_array[i];
}
delete[] CArray;              //frees rows
CArray = 0;
delete[] PHIArray;
PHIArray = 0;
delete[] INTENSITYArray;
INTENSITYArray = 0;
delete[] THETAArray;
THETAArray = 0;
delete[] GAMMAArray;
GAMMAArray = 0;
delete[] ZArray;
ZArray = 0;
    delete[] CONDUCTIVITYarray;
    CONDUCTIVITYarray = 0;
    delete[] T_rain_new_array;
    T_rain_new_array = 0;
    delete[] T_rain_old_array;
    T_rain_old_array = 0;
    delete[] Diff_ch;
Diff_ch = 0;
    delete[] Distr_ss;
Distr_ss = 0;
    delete[] t_norm;
t_norm = 0;
    delete[] intensity_rec_old_array;
    intensity_rec_old_array = 0;
    delete[] intensity_rec_new_array;
    intensity_rec_new_array = 0;
    delete[] press_zero_old_array[i];
    press_zero_old_array[i];
    delete[] press_zero_new_array[i];
    press_zero_new_array[i];

    for(i=0; i<nrows * layers; i++)
    {
            delete[] press_distr_new_array[i];
            delete[] press_distr_old_array[i];
            delete[] FSArray[i];
```

```
        }
        delete[] press_distr_new_array;
        press_distr_new_array = 0;
        delete[] press_distr_old_array;
        press_distr_old_array = 0;
    delete[] FSArray;
        FSArray = 0;
        delete[] press_zero_old_array[i];
        press_zero_old_array[i];
        delete[] press_zero_new_array[i];
        press_zero_new_array[i];

    return 0;
}
```